TU/e EINDHOVEN UNIVERSITY OF TECHNOLOGY

Integration of microwave heating with continuously operated milli-reactors for fine chemical synthesis

Citation for published version (APA):
Patil, N. G. (2012). *Integration of microwave heating with continuously operated milli-reactors for fine chemical synthesis*. [Phd Thesis 1 (Research TU/e / Graduation TU/e), Chemical Engineering and Chemistry]. Technische Universiteit Eindhoven. https://doi.org/10.6100/IR735446

DOI:
10.6100/IR735446

Document status and date:
Published: 01/01/2012

Document Version:
Publisher's PDF, also known as Version of Record (includes final page, issue and volume numbers)

Please check the document version of this publication:

• A submitted manuscript is the version of the article upon submission and before peer-review. There can be important differences between the submitted version and the official published version of record. People interested in the research are advised to contact the author for the final version of the publication, or visit the DOI to the publisher's website.
• The final author version and the galley proof are versions of the publication after peer review.
• The final published version features the final layout of the paper including the volume, issue and page numbers.

Link to publication

General rights
Copyright and moral rights for the publications made accessible in the public portal are retained by the authors and/or other copyright owners and it is a condition of accessing publications that users recognise and abide by the legal requirements associated with these rights.

• Users may download and print one copy of any publication from the public portal for the purpose of private study or research.
• You may not further distribute the material or use it for any profit-making activity or commercial gain
• You may freely distribute the URL identifying the publication in the public portal.

If the publication is distributed under the terms of Article 25fa of the Dutch Copyright Act, indicated by the "Taverne" license above, please follow below link for the End User Agreement:

www.tue.nl/taverne

Take down policy
If you believe that this document breaches copyright please contact us at:

openaccess@tue.nl

providing details and we will investigate your claim.

Download date: 16. Nov. 2023

Integration of microwave heating with continuously operated milli-reactors for fine chemical synthesis

PROEFSCHRIFT

ter verkrijging van de graad van doctor aan de
Technische Universiteit Eindhoven, op gezag van de
rector magnificus, prof.dr.ir. C.J. van Duijn, voor een
commissie aangewezen door het College voor
Promoties in het openbaar te verdedigen
op woensdag 26 september 2012 om 16.00 uur

door

Narendra Gambhirrao Patil

geboren te Bhokne, India

Dit proefschrift is goedgekeurd door de promotoren:

prof.dr.ir. J.C. Schouten
en
prof.dr. J. Meuldijk

Co-promotor:
prof.dr. L.A. Hulshof

Eindhoven University of Technology, 2012
A catalogue record is available from the Eindhoven University of Technology Library
Patil, Narendra G.
Integration of microwave heating with continuously operated milli-reactors for fine chemical synthesis
ISBN: 978-90-386-3220-9

Table of Contents

Summary

Integration of microwave heating with continuously operated milli-reactors for fine chemical synthesis

Major efforts in the research field of microwave assisted organic synthesis have demonstrated the specific benefits associated with the use of microwave irradiation such as selective and rapid heating of the reaction mixture. In many case studies, these benefits eventually lead to a significant enhancement in the production rates. Therefore, microwave assisted flow synthesis can be an interesting alternative for fine chemical production in conventionally heated batch reactors. However, realization of microwave assisted flow synthesis at kilogram scale requires a proper design of tubular reactors integrated with the microwave heating source, *i.e.* the cavity. The design of these reactors should primarily be able to overcome the limitations by the penetration depth of the microwaves, *i.e.* ~0.013 m. Moreover, operation based on microwave heating should allow accurate temperature control by precise tuning and quantification of the microwave energy distribution. Therefore, being case specific, design efforts are necessary for the microwave setup as well as for the reactor configuration.

Heating in monomode microwave equipment is energy efficient and fast in comparison to heating in multimode microwave equipment. State-of-the-art microwave cavities, however, lack in providing important functionalities, such as a predictable electric field pattern, tuning facility, detailed energy distribution and possibilities for modular scale-up. A waveguide type monomode microwave cavity in combination with the short circuit, stub tuners, and isolators can provide the aforementioned functionalities for continuously operated reactors. This type of microwave setup allows an accurate elaboration of energy balances for efficient and uniform heating. Additionally the use of multiple cavities connected to a single microwave generator via a main waveguide permits modular scale-up.

The dielectric properties (*i.e.* dielectric constant and dielectric loss) of a microwave absorbing load (*e.g.* reaction mixture/solvent) are significantly dependent on temperature. As a consequence, microwave absorption, which involves interaction of the electromagnetic field with the applied load, is a recurring process. Therefore, detailed understanding of the dielectric property change with temperature is a prerequisite for a proper design of the load to be used under stop-flow (batch) and continuous-flow conditions. For stop-flow conditions, the highest heating efficiency (70 %) is observed for a load diameter equal to and larger than half of the wavelength of the microwaves in the liquid medium. For continuous-flow conditions, the heating efficiency increases linearly with the load diameter. However, microwave leakage above the propagation diameter (*i.e.* half wavelength) limits further increase of the load diameter in continuous operation.

The high energy intensity of the focused electromagnetic field in case of waveguide type microwave cavities makes an efficient and controlled continuous operation difficult, especially when a strong microwave absorbing load (*e.g.* ethanol) is present. In cases, such as the reaction of ethanol and acetic acid to produce ethyl acetate over a strong acid ion-exchange resin, a milli reactor-heat exchanger combination with a co-current flow of a microwave transparent solvent (coolant) can be a solution. Here, rapid volumetric heating to the reaction temperature can be achieved by microwaves before the reaction mixture enters into the catalyst bed. Additionally, the coolant not only limits overheating of the reaction mixture but also permits heat integration, resulting in extended reactor lengths and efficient heating (*i.e.* 96 %). However, stagnancy in the flow of the microwave absorbing load results in a poor convective heat transport. As a consequence, stagnant layer formation caused either by any insertion (of system components, such as fiber optic sensors) or at the reactor walls, yields higher temperatures and lower microwave energy dissipation regions.

One of the promising approaches for scaling microwave assisted flow synthesis is numbering up. The numbering up approach is based on parallelization of tubular structured reactors with a channel diameter in the millimeter range. The performance of such a configuration is evaluated by a multi-tubular milli-

reactor/heat exchanger system with a thin Cu film on the inner walls of the reactor tubes. The thin Cu film provides uniform microwave absorption and it improves the production rate by acting as a heated catalytically active surface, as demonstrated in the synthesis of 1,3-diphenyl-2-propynyl-piperidine from benzaldehyde, piperidine, and phenylacetylene. Controlled selective heating of the thin Cu film is achievable by using a counter-current flow of a microwave transparent coolant (toluene). The coolant flow avoids Cu burning and reduces leaching, consequently improving the steady state catalytic performance of the Cu coated reactor tubes. Higher temperatures, *i.e.* at least 100 K higher than the bulk liquid, are achievable at the locus of the reaction, *i.e.* the catalyst surface, purely due to selective microwave heating.

Another approach to realize higher production rates is utilization of multiple microwave cavities in series. In this approach, the process stream is taken from one cavity to the next where the process efficiency is well optimized over each consecutive cavity. Transient operation through each optimized cavity and utilization of multiple cavities in series increases conversion and consequently results in higher production rate. Additionally, known kinetics allows estimation of the production rate for each additional cavity in the series. This approach of scale-up is possible at minimized grid to applicator losses by connecting multiple cavities to a single microwave generator via a main waveguide.

Scale-up approaches based on parallelization of tubular structured reactors as well as on utilization of multiple microwave cavities in series were found to be successful. Application of microwaves as a process intensification tool, especially in the case of organic synthesis, is very attractive for liquid-solid reactions, where the solid is the selectively (microwave) heated catalyst.

1

Introduction

1.1 Microwave heating; a process intensification tool

Field interaction with materials is a vast area of science and engineering. A large number of applications such as communications,[1] remote sensing,[2-4] navigation,[5,6] power/heating,[7] and spectroscopy,[8,9] operate in a relatively small, but important, part of the electromagnetic spectrum between 300 MHz to 300 GHz corresponding to wavelengths of 1 m to 1 mm, respectively (Figure 1.1).[10] This part of the spectrum is referred to as microwave part. The commonly used frequency for heating is 2.45 GHz.[11] At this microwave frequency the electromagnetic waves can induce molecular rotations (Figure 1.1). However, other frequencies are explored more regularly nowadays.[12]

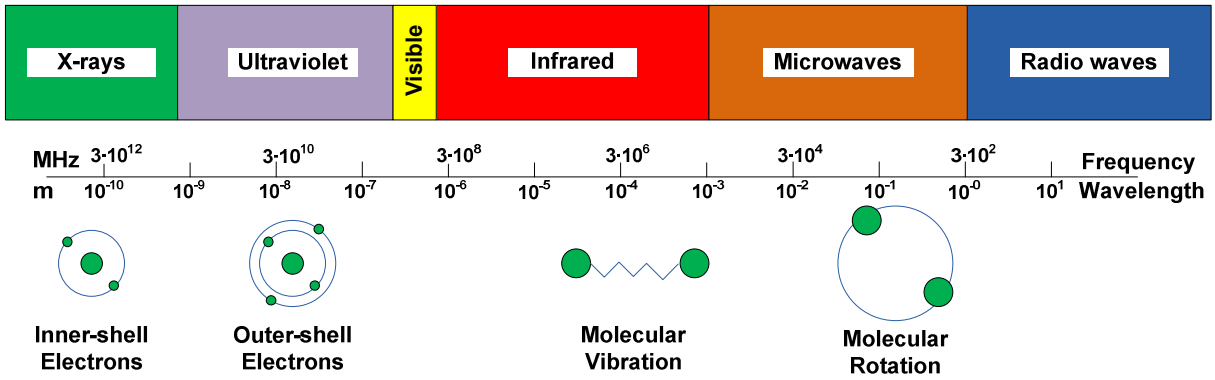

Figure 1.1: The electromagnetic spectrum. Wavelength, frequency and corresponding energies

Knowledge of field-material interactions is critical to the design of the high-frequency applicators, because the electrical properties of the material of interest is

a part of the device' functioning and process control. This part is a unique feature of these devices, which sets them apart from conventional heating devices. For example, in the design of a conventional furnace, it is of little importance what material is to be heated, but the dielectric properties of a material being processed by a microwave applicator are of great importance in the design of the devise.

In liquids, the electric component of the electromagnetic field causes heating by two possible mechanisms, *i.e.* dipolar polarization and/or ionic conduction (Figure 1.2).[7,10,13] Existing or induced dipoles and/or ions try to orient themselves in the direction of the electric field vector of the microwaves. However, the time constant for electric field oscillations is much smaller than the time constant for molecular or ionic orientation in the field direction. This difference in time constants leads to repetitive movement and results ultimately in heating via friction.

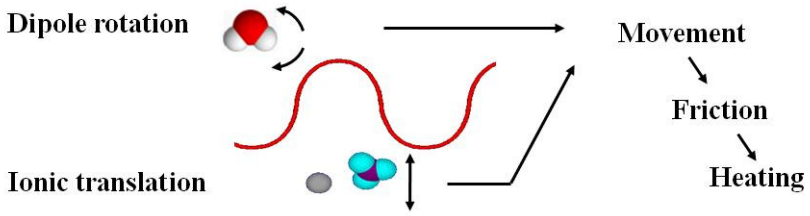

Figure 1.2: Microwave heating mechanisms

The extent of coupling and the conversion of electromagnetic energy into heat depends on the permittivity of the medium ($\varepsilon = \varepsilon' - j\varepsilon''$), having real and imaginary parts which are also referred to as the dielectric constant (ε') and the dielectric loss (ε''), respectively. ε' is a measure of the interaction of the electric field with the medium, while ε'' is a measure for the dissipation of this interaction energy into heat. ε' as well as ε'' are a strong function of temperature. The ratio of ε'' to ε', also called the loss tangent ($tan\delta = \varepsilon''/\varepsilon'$), demonstrates the ability of any liquid to convert microwave energy into heat. In general, organic solvents can be classified based on this ability as high ($tan\,\delta > 0.5$), medium ($tan\,\delta = 0.1 - 0.5$), and low ($tan\,\delta < 0.1$) microwave absorbing fluids.[14] Heating at the molecular level, *i.e.* volumetric heating, makes microwaves a desirable option for organic synthesis. However, microwaves have a limited penetration depth (D_P) and it depends on the dielectric properties of a solvent ($D_P = \lambda\sqrt{\varepsilon'}/2\,\pi\varepsilon''$). The penetration depth, at 2.45

GHz, is in the order of millimeters for organic solvents, *e.g.* at room temperature it is 13 mm for water. The energy gets depleted to 1/3 of its capacity over a single penetration depth ($P(D_P)/P(0) = 1/e = 0.37$), thus jeopardizing the basic benefit of volumetric heating.

Microwave cavities can be of many shapes and forms, and in essence they are voids that are enclosed by high conductivity metal walls or grids.[10,11,14] The main frequency coupled into the cavity will set up standing waves only if the frequency matches one of natural resonant frequencies of the cavity. Each natural resonant frequency represents a "mode", with its own field configuration. In a single mode cavity, the material under processing (load) is preferably placed in locations of highest field intensity node for the mode of interest. This is in contrast to multimode cavities, where the placement of the load is random, and interacts with nodes of multiple resonance modes. The addition of a material load to a cavity modifies the field configuration to varying degrees depending on the size and material properties of the load. Furthermore the field can be disturbed due to the openings in the cavity for loading the material (reactor). Waveguide-based cavity applicators are important, particularly in laboratory research of chemical synthesis, because they can be conveniently manufactured in a rectangular shape and shorted at one end using a short-plunger, and fed from the other side through a microwave iris.[15]

1.2 Microwave assisted organic synthesis

Since its first application in 1986 by Gedye[16] and Giguere[17], microwave heating is becoming a popular method for synthetic organic chemists day by day. There are many examples in a number of reviews[14,18-21] and books[10,11,22-24] demonstrating the benefits associated with the use of microwave heating. Most of the examples report a reduction in reaction times due to selective and/or rapid heating, resulting in a considerable increase in production rates as compared with conventionally heated systems. Although this fetched a lot of attention towards replacing the conventional, *i.e.* oil bath, heating methodology, it also brought up claims of specific (non-thermal) microwave effects.[25] These specific microwave effects later

on faded away after interdisciplinary research, providing a proper understanding of microwave heating.[13] Additionally, accurate temperature measurements allowed a proper and reliable comparison of conventional heating with microwave heating.[26-29] For limited scales, it can also be said that batch synthesis is useful only to get preliminary evidence of microwave heating (thermal) benefits unless production is limited to laboratory scales.

Several authors presented their continuously operating microwave integrated reactor setups for performing a diversity of chemical reactions.[30-40] They reported an increase in yield,[30] the presence of hot spots,[31-33] an increase of the reaction rate,[34] efficiency of microwave heating,[35,36,40] and specific designs for optimal continuous operations.[37-39] Most of the articles discovered the enhancement in reaction rate or yields due to selective nature of microwave heating. However several of these articles described indirect methods for temperature measurements such as infrared detectors.[37-40] This limited the quantification and control of microwave heating benefits without direct temperature measurement by fiber optic sensors.[33-35]

The efficiency of microwave heating, raised as an important issue for scaling up, was investigated by several authors.[35,36,40] They reported that the efficiency of microwave heating is better for the monomode type microwaves than for the conventional multimode type relatively large microwave cavities. The high energy intensity of the focused microwaves in the case of monomode cavities, however, makes an efficient and controlled operation impossible, especially when a strong microwave absorbing component is present.[30] Some of the proposed flow reactor systems suggested the use of a dead load to extract the excess of microwave energy to avoid runaways.[37,38] Beneficial use of the extracted excess energy has, however, not been discussed. Additionally, ignoring the heat losses to the surroundings did not permit establishment of comprehensive energy balances for precise reactor design.

The possibility of utilizing micro-flow reactors has also been investigated by many researchers.[41-48] In these studies the benefit of wall coated capillary tubes,[42-44,47] parallelization,[41] and specific microreactor design[45,46,48] is discussed in detail.

Catalytically active metallic coatings on the inner wall of capillary tubes have shown an extraordinary increase in reaction rate resulting in high temperatures at the coated surface. To the best of our knowledge, the controlled and sustainable application of these coatings has, although, not been discussed. Although parallelization is introduced for the library synthesis, it can also be utilized for scale up without limitation of the penetration depth. The designs of micro-reactors demonstrated additional temperature control by forced cooling, but the possibility of a modular scale up under microwave heating conditions has not been explored.

1.3 Scale up of microwave assisted processing for the production of fine-chemicals

After rigorous application of the microwave heating technology over a period of two decades, researchers have been able to successfully perform batch-wise chemical synthesis at multi-gram scales.[49] However, the illusive target of reaching kilogram scales still remains. This is especially due to the penetration depth limitations of microwaves. The idea of scaling up batch procedures of very small volumes (5 ml) by increasing reaction volumes (liters) almost never works.[50-59] The reasons are simple. Firstly, microwave heating is selective in nature and this is not understood explicitly for most of the case studies before approaching the scale up. Secondly, almost in all the case studies, the process is developed in a monomode type microwave cavities and then shifted to multimode microwave cavities for scaling. However, few of the papers look into the possibility of designing a microwave setup which satisfies the requirements of large batch processes assuring homogeneous heating.[51,58,59]

One of the options for scale up is to switch from batch operation to continuous operation at early stages in the process development. Scale up studies on continuous operation reveal evaluations of commercially available continuous flow microwave reactors,[60-62] of micro-reactors[63] and of process specific microwave integrated reactor setups[64]. However, most of the researchers try to replicate standardized batch recipes in continuous flow. This approach not only leads to

questionable underperformance but also jeopardizes the application of microwave heating in general.[65,66] Usually recipe modifications such as solvent changes (*i.e.* highly microwave absorbing/transparent solvent) and catalyst modifications (for selective microwave absorption and/or immobilization) should help improve the process performance. Additionally, most of the scale-up (batch as well as continuous) related studies assume a proper performance of state-of-the-art microwave setups and standard reactors therein, while the process demands specific microwave integrated reactor setup designs.

1.4 Research objectives and outline of the thesis

Major efforts in the research field of microwave assisted organic synthesis have demonstrated the specific benefits associated with the use of the microwave heating, *e.g.* selective heating, resulting in a substantial reduction of reaction times. Therefore, microwave assisted flow synthesis can be an interesting alternative for conventionally heated, multi-step production of fine-chemicals in batch reactors. However, realization of microwave assisted flow synthesis at an industrial scale requires a proper design of multi-tubular reactors integrated with microwave heating. Proper design of multi-tubular reactors should primarily overcome the penetration depth limitation of the microwaves (~0.013 m). Moreover, operation under microwave heating should also allow accurate temperature control by precise tuning and quantification of the microwave energy distribution. So being case specific, design efforts were necessary for the microwave system, the reactor configuration and, if applicable, the catalytic system.

As a part of our stepwise approach towards designing a microwave-heated continuous fine-chemicals production plant, a feasibility study of state-of-the-art multi- and mono-mode microwave cavities (2.45 GHz) is reported in **chapter 2**. The feasibility of multi- as well as mono-mode types was investigated based on the dependence of heating uniformity and efficiency on *i)* sample position, *ii)* sample volume, and *iii)* sample geometry, respectively. Design rules were formulated for microwave heated reactor-heat exchanger combinations for continuous fine-chemicals production. The feasibility study resulted in important functionalities

necessary in a microwave setup for continuous fine-chemicals synthesis which were then used to design a microwave setup with all the required flexibility and applicability. Finally, the realized microwave setup was evaluated for its heating performance.

In **chapter 3** the effect of the load diameter and loss tangent of the medium on the efficiency of microwave heating (2.45 GHz) is discussed. Experimentally observed temperature profiles of ethylene glycol as a load are reported for stop-flow (*i.e.* stagnant liquid) and continuous-flow conditions. Results are explained in terms of dielectric properties and load geometry.

In **chapter 4**, an integrated reactor-heat exchanger system for efficient and controlled flow processing of highly microwave absorbing reaction media is presented. Esterification of ethanol and acetic acid catalyzed by a strong acid ion exchange resin to produce ethyl acetate was chosen as a model reaction. Toluene, being a microwave transparent solvent, was used as coolant. To achieve insight into the temperature profiles, the reactor-heat exchanger system was divided into two parts, *i.e.* a microwave cavity for heating and a fixed bed reactor downstream the cavity. Convective heat transfer concepts were used to describe the temperature profiles for the reaction mixture and the coolant in the cavity and the reactor section. Predictions based on theoretical calculation were validated with experiments.

The interactions of the oscillating electric field and the hydrodynamics of microwave absorbing fluids in a microwave integrated reactor-heat exchanger are reported in **chapter 5**. In this chapter, we take a closer look at the influence of liquid velocity profiles on the axial and radial temperature profiles in a tubular microwave integrated milli-reactor combined with a heat exchanger. The effect of coolant flow (microwave transparent), system component (such as a fiber optic sensor), and geometry orientation (gravitational effect) on microwave energy dissipation and temperature distribution are discussed. Model predictions were also validated with experiments in this case.

Chapter 6 reports the scale up of a microwave assisted continuous fine-chemicals synthesis by using a multi-tubular milli-reactor/heat exchanger (MTMR) to the

commercially interesting capacity of 1 kg/day. This is achieved, amongst others, by providing a uniform temperature distribution in all parallel tubes of the MTMR assembly. The performance of thin Cu films deposited on the inner wall of the reactor tubes, acting as a catalyst and as a microwave absorbing material, is reported for the formation of 1,3-diphenyl-2-propynyl-piperidine from benzaldehyde, piperidine, and phenylacetylene. Experimental results are discussed in terms of temperature dependent kinetics of the Cu-catalyzed reaction and heat balances.

In **chapter 7**, the concept of modular scale up is presented where energy utilization and reactor performance are optimized at the single cavity level and then scaled out by transient operation through cavities in series. The productivity increase with each additional cavity in series is reported for two different types of reactors, namely a packed bed reactor and a wall-coated tubular reactor for the chemical processes, as discussed in chapters 4 and 6, respectively. Calculated productivities were then validated for the case of an esterification reaction in a packed bed reactor.

Chapter 8 gives the overall conclusions of this work and the outlook based on these conclusions.

References

1. Kizer, G. M. Microwave Communication, Iowa State University Press, Ames, Iowa, 1990.
2. Vrieling, A. Satellite remote sensing for water erosion assessment: A review. *CATENA* 2006, *65*, 2.
3. Evans, D. L.; Alpers, W.; Cazenave, A.; Elachi, C.; Farr, T.; Glackin, D.; Holt, B.; Jones, L.; Liu, W. T.; McCandless, W.; Menard, Y.; Moore, R.; Njoku, E. Seasat: A 25-year legacy of success. *Remote Sens. Environ.* **2005**, *94*, 384.
4. Payan, S.; De La Noe, J.; Hauchecorne, A.; Camy-Peyret, C. A review of remote sensing techniques and related spectroscopy problems. *C. R. Phys.* **2005**, *6*, 825.
5. Haynes, S. K.; Jackson, W. J. The Physics of Radar. *Am. J. Phys.* **1946**, *14*, 143.
6. Haynes, S. K.; Jackson, W. J. The Physics of Radar (Continued). *Am. J. Phys.* **1946**, *14*, 403.
7. Meredith, R. Engineers Handbook of Industrial Microwave Heating, the Institution of Electrical Engineers, 1998.
8. Meckenstock, R. Three-dimensional hydrodynamic focusing in a microfluidic Coulter counter. *Rev. Sci. Instrum.* **2008**, *79*.

9. Towness, C. H.; Schawlow, A. L. Microwave Spectroscopy, Dover Publications Inc, New York, 1975.
10. Metaxas, A. C.; Meredith, R. J. Industrial microwave heating, Peter peregrines Ltd, London, 1983.
11. Hayes, B. L.; Microwave synthesis: chemistry at the speed of light (*1st edition*), CEM publishing, Matthews NC, 2002.
12. Horikoshi, S.; Hamamura, T.; Kajitani, M.; Yoshizawa-Fujita, M.; Serpone, N. Green Chemistry with a Novel 5.8-GHz Microwave Apparatus. Prompt One-Pot Solvent-Free Synthesis of a Major Ionic Liquid: The 1-Butyl-3-methylimidazolium Tetrafluoroborate System. *Org. Process Res. Dev.* **2008,** *12,* 1089.
13. Gabriel, C.; Gabriel, S.; Grant, E. H.; Ben, S. J.; Halstead, B. S. J.; Mingos, D. M. P. Dielectric parameters relevant to microwave dielectric heating. *Chem. Soc. Rev.* **1998,** *27,* 213.
14. C.O. Kappe, Controlled Microwave Heating in Modern Organic Synthesis, *Angew. Chem., Int. Ed.* **2004,** *43,* 6250.
15. Toukoniitty, B.; Mikkola, J. -P.; Era¨nen, K.; Salmi, T.; Murzin, D. Yu. Esterification of propionic acid under microwave irradiation over an ion-exchange resin. *Cat. Today.* **2005,** *100,* 431.
16. Gedye, R.; Smith, F.; Westaway, K.; Ali, H.; Baldisera, L.; Laberge, L.; Rousell, J. The use of microwave ovens for rapid organic synthesis. *Tetrahedron Lett.* **1986**, *27*, 279.
17. Giguere, R. J.; Bray, T. L.; Duncan, S. M. Application of commercial microwave ovens to organic synthesis. *Tetrahedron Lett.* **1986**, *27*, 4945.
18. Michael, D.; Mingos, P.; Baghurst, D. R. Applications of microwave dielectric heating effects to synthetic problems in chemistry. *Chem. Soc. Rev*. **1991**, *20*, 1.
19. Kappe, C. O. Microwave dielectric heating in synthetic organic chemistry. *Chem. Soc. Rev.* **2008**, *37*, 1127.
20. Nüchter, M.; Ondruschka, B.; Bonrath, W.; Gum, A. Microwave assisted synthesis – a critical technology overview. *Green chem*. **2004**, *6*, 128.
21. Lidstrom, P.; Tierney, J.; Wathey, B.; Westman, J. Microwave assisted organic synthesis – a review. *Tetrahedron.* **2001**, *57*, 9225.
22. Lidstrom P. Microwave assisted organic synthesis (*1st edition*), Blackwell, Oxford, 2004.
23. Kappe C. O. Microwaves in organic and Medicinal chemistry (*1st edition*), Wiley-VCH, Weinheim, 2005.
24. Larhed, M.; Olofsson, K. Microwave methods in organic synthesis (*1st edition*). Springer, Berlin, 2006.
25. Loupy, A. Microwaves in organic synthesis (*2nd edition*), Wiley-VCH, Weinheim, 2006.
26. Hosseini, M.; Stiasni, N.; Barbieri, V.; Kappe, C. O. Microwave-assisted asymmetric organocatalysis: a probe for nonthermal microwave effects and the concept of simultaneous cooling. *J. Org. Chem.* **2007**, *72*, 1417.
27. Herrero, M. A.; Kremsner, J. M.; Kappe, C. O. Nonthermal microwave effects revisited: on the importance of internal temperature monitoring and agitation in microwave chemistry. *J. Org. Chem.* **2008**, *73*, 36.
28. Dressen, M. H. C. L. Microwave heating in fine chemical applications: role of heterogeneity. PhD thesis, Eindhoven University of Technology, 2009. *ISBN: 978-90-386-1821-0.*

29. Van de Kruijs B. H. P. Microwave-matter effects in metal (oxide)-mediated chemistry and in drying. PhD thesis, Eindhoven University of Technology, 2010. *ISBN: 978-90-386-2178-4.*
30. Chemat, F.; Poux, M.; Di Martino, J. L.; Berlan, J. A new continuous-flow recycle microwave reactor for homogeneous and heterogeneous chemical reactions. *Chem. Eng. Technol.* **1996,** *19*, 420.
31. Chemat, F.; Esveld, E.; Poux, M.; Di-Martino, L. J. The role of selective heating in the microwave activation of heterogeneous catalysis reactions using a continuous microwave reactor. *J. microwave power EE.* **1998,** *33,* 88.
32. Baxendale, I. R.; Griffiths-Jones, M. C.; Ley, V. S.; Tranmer, K. G. Microwave-assisted Suzuki coupling reactions with an encapsulated palladium catalyst for batch and continuous-flow transformations. *Chem. Eur. J.* **2006,** *12*, 4407.
33. Cecilia, R.; Kunz, U.; Turek, T. Possibilities of process intensification using microwaves applied to catalytic microreactors. *Chem. Eng. Process.* **2007,** *46*, 870.
34. Roberts, A. B.; Strauss, R. C. Towards rapid, 'green' predictable microwave-assisted synthesis. *Acc. Chem. Res.* **2005,** *38*, 653.
35. Esveld, E.; Chemat, F.; van Haveren, J. Pilot scale continuous microwave dry-media reactor - Part 1: design and modeling. *Chem. Eng. Technol.* **2000,** *23*, 279.
36. Esveld, E.; Chemat, F.; van Haveren, J. Pilot Scale Continuous Microwave Dry-Media Reactor - Part II: Application to waxy ester production. *Chem. Eng. Technol.* **2000,** *23*, 429.
37. Plazl, I.; Pipus, G.; Koloini, T. Microwave heating of the continuous flow catalytic reactor in a nonuniform electric field. *AIChE J.* **1997,** *43,* 754.
38. Pipus, G.; Plazl, I.; Koloini, T. Esterification of benzoic acid in microwave tubular flow reactor. *Chem. Eng. J.* **2000,** *76,* 239.
39. Wilson, S. N.; Sarko, R. C.; Roth, P. G.; Development and applications of a practical continuous flow microwave cell. *Org. Process Res. Dev.* **2004**, *8*, 535.
40. Hoogenboom, R.; Wilms, A. F. T.; Schubert, S. U. Microwave irradiation – a closer look at heating efficiencies. *Aust. J. Chem.* **2009,** *62*, 236.
41. Comer, E.; Organ, M. G. A Microcapillary System for Simultaneous, Parallel Microwave-Assisted Synthesis, *Chem. Eur. J.* **2005**, *11*, 7223.
42. Comer, E.; Organ, M. G.; A microreactor for microwave-assisted capillary (continuous flow) organic synthesis. *J. Am. Chem. Soc.* **2005**, *127*, 8160.
43. Shore, G.; Morin, S.; Organ, M. G. Catalysis in Capillaries by Pd Thin Films Using Microwave-Assisted Continuous-Flow Organic Synthesis (MACOS). *Angew. Chem.* **2006**,*118*, 2827.
44. Shore, G.; Yoo, W.; Li, C.; Organ, M. G. Propargyl Amine Synthesis Catalysed by Gold and Copper Thin Films by Using Microwave-Assisted Continuous-Flow Organic Synthesis (MACOS). *Chem. Eur. J.* **2010,** *16*, 126.
45. He, P.; Haswell, S. J.; Fletcher, P. D. I. Microwave heating of heterogeneously catalysed Suzuki reactions in a micro reactor. *Lab Chip.* **2004**, *4*, 38.
46. He, P.; Haswell, S. J.; Fletcher, P. D. I.; Kelly, S. M.; Mansfield, A. Scaling up of continuous-flow, microwave-assisted, organic reaction by varying the size of Pd-functionalized catalytic monoliths. *Appl. Catal. A.* **2004,** *274,* 111.

47. He, P.; Haswell, S. J.; Fletcher, P. D. I. Efficiency, monitoring and control of microwave heating within a continuous flow capillary reactor. *Sensors and Actuators B.* **2005**, *105*, 516.
48. Jachuck, R. J. J.; Selvaraja, D. K.; Varma, R. S. Process intensification: oxidation of benzyl alcohol using a continuous isothermal reactor under microwave irradiation. *Green Chem.* **2006**, *8*, 29.
49. Moseley, J. D.; Lenden, P.; Lockwood, M.; Ruda, K.; Sherlock, J. -P.; Thomson, A. D.; Gilday, J. P. A Comparison of Commercial Microwave Reactors for Scale-Up within Process Chemistry. *Org. Process Res. Dev.* **2008**, *12,* 30.
50. Amore, K. M.; Leadbeater, N. E. Microwave-Promoted Esterification Reactions: Optimization and Scale-Up. *Macromol. Rapid Commun.* **2007**, *28*, 473.
51. Feher, L. E.; Thumm, M. K. Microwave Innovation for Industrial Composite Fabrication—The HEPHAISTOS Technology. *IEEE Trans. Plasma Sci.* **2004**, *32*, 73.
52. Lehmann, H.; LaVecchia, L. Scale-Up of Organic Reactions in a Pharmaceutical Kilo-Lab Using a Commercial Microwave Reactor. *Org. Process Res. Dev.* **2010**, *14,* 650.
53. Nakamura, T.; Nagahata, R.; Kunii, K.; Soga, H.; Sugimoto, S.; Takeuchi, K. Large-Scale Polycondensation of Lactic Acid Using Microwave Batch Reactors. *Org. Process Res. Dev.* **2010**, *14,* 781.
54. Moseley, J. D.; Woodman, E. K. Scaling-Out Pharmaceutical Reactions in an Automated Stop-Flow Microwave Reactor. *Org. Process Res. Dev.* **2008**, *12,* 967.
55. Bowman, M. D.; Schmink, J. R.; McGowan, C. M.; Kormos, C. M.; Leadbeater, N. E. Scale-Up of Microwave-Promoted Reactions to the Multigram Level Using a Sealed-Vessel Microwave Apparatus. *Org. Process Res. Dev.* **2008**, *12,* 1078.
56. Marafie, J. A.; Moseley, J. D.; The application of stop-flow microwave technology to scaling-out SNAr reactions using a soluble organic base. *Org. Biomol. Chem.*, **2010**, *8*, 2219.
57. Bowman, M. D.; Holcomb, J. L.; Kormos, C. M.; Leadbeater, N. E.; Williams, V. A. Approaches for Scale-Up of Microwave-Promoted Reactions. *Org. Process Res. Dev.* **2008**, *12,* 41.
58. Schmink, J. R.; Kormos, C. M.; Devine, W. G.; Leadbeater, N. E. Exploring the Scope for Scale-Up of Organic Chemistry Using a Large Batch Microwave Reactor. *Org. Process Res. Dev.* **2010**, *14,* 205.
59. SAIREM SAS Labotron Extraction & Synthesis 2450 MHz. available at: http://www.sairem.com/gb/equipements/equipements_chimie/synthese_sous_micro_ondes.html **2010,** Accessed 14.05.2012.
60. Moseley, J. D.; Lawton, S. J. Initial results from a commercial continuous flow microwave reactor for scale-up. *Chem. Today*. **2007**, *25*, 16.
61. Bergamelli, F.; Iannelli, M.; Marafie, J. A.; Moseley, J. D. A Commercial Continuous Flow Microwave Reactor Evaluated for Scale-Up. *Org. Process Res. Dev.* **2010**, *14*, 926.
62. Bagley, M. C.; Fusillo, V.; Jenkins, R. L.; Lubinu, M. C.; Mason, C. Continuous flow processing from microreactors to mesoscale: the Bohlmann–Rahtz cyclodehydration reaction. *Org. Biomol. Chem.* **2010**, *8*, 2245.
63. Bierbaum, R.; Nuchter, M.; Ondruschka, B. Microwave–assisted reaction engineering: Microwave apparatus at mini plant scale with online analysis. *Chem. Engg. Technol.* **2005**, *28*, 427.

64. Matsuzawa, M.; Togashi, S.; Hasebe, S.; Basic Examination of a Pilot Plant for Continuous Flow Microwave-Assisted Chemical Reaction Combined with Microreactors. *J. Thermal Sci. Tech.* **2011**, *6*, 69.
65. Leadbeater, N. E. Microwave heating as a tool for sustainable chemistry. CRC press Taylor and Francis group. 2010.
66. Kremsner, J. M.; Stadler, A.; Kappe, C. O. The Scale-Up of microwave-Assisted Organic Synthesis. *Top. Curr. Chem*. **2006**, *266*, 233.

2

Microwave setup design for continuous fine-chemicals synthesis

This chapter will be submitted as:
Patil, N. G.; Benaskar, F.; Rebrov, E. V.; Meuldijk, J.; Hulshof, L. A.; Hessel, V.; Schouten, J. C.; Microwave setup design for continuous fine-chemicals synthesis. *Chem. Eng. Technol.* **2012,** *In preparation.*

Abstract

A feasibility study in state-of-the-art multi- and mono-mode microwave cavities (2.45 GHz) was conducted to outline important functionalities necessary in a microwave setup for continuous fine-chemicals synthesis. Keeping in mind the reactor-heat exchanger scales, several water filled cylindrical load volumes ($2.5 \cdot 10^{-6}$ - $4 \cdot 10^{-5}$ m^3; diameter: $7 \cdot 10^{-3}$ - $4 \cdot 10^{-2}$ m) were used during the experiments. These loads were exposed to a fixed microwave power (20 or 50 W) and temperature profiles were measured for 300 s to determine the heating rates. The heating efficiency was then calculated as the ratio of the energy absorbed by the load (including heat losses by natural convection) and the energy released by the microwave irradiation. For a $1 \cdot 10^{-5}$ m^3 load volume, heating efficiencies of 18 and 40 % were obtained for multi- and mono-mode operation, respectively. For multimode operation, the heating efficiency depends on the position as well as on the volume distribution of the load. For monomode operation, the heating efficiency does not depend on the axial position and has a maximum (of 97 %) with respect to the load diameter. Based on the feasibility study, a microwave setup consisting of four cavities was designed and constructed. The setup provided a defined microwave field pattern and allowed focusing of the microwave power permitting comprehensive energy balances for precise reactor design. A near-uniform distribution of microwave energy in all four cavities of the setup was achieved at reduced grid to applicator losses.

2.1 Introduction

Since its first application in 1986 by Gedye[1] and Giguere[2], microwave heating is becoming a popular method for synthetic chemists day by day. There is a large number of reviews[3-7] and books[8-11] written in the area of microwave assisted organic synthesis (MAOS). The popularity of using microwave heating lies in its clean and fast supply of heat to reaction media. Microwave heating also permits instantaneous switching on and off of the power and thus heat supply to the reaction system. This possibility makes the operation inherently safe. Although this fetched a lot of attention towards replacing the conventional, *i.e.* oil bath, heating methodology, it also brought up claims of specific (non-thermal) microwave effects.[12] These specific microwave effects, however, seemed to fade away after interdisciplinary research, providing a proper understanding of microwave heating.[13] Additionally, the accurate temperature measurements allowed straight comparison of conventional heating with microwave heating.[14-17]

After rigorous application of the microwave heating technology over a period of two decades, researchers have been able to successfully perform batch-wise chemical synthesis at multi-gram scales. The current challenge of this new heating technology is its application together with continuous flow systems for the production of high added value organic specialties on a kilogram scale. There have been many modest attempts of applying microwave heating in continuous flow systems.[18] However, most of this research work faces the limitation of penetration depth (*e.g.* ~ 0.012 m) of microwave irradiation to find microwave heating as efficient, uniform and predictable as conventional heating for continuous flow systems. Therefore, combining two emerging technologies namely micro-reactors and microwave heating has been a topic of on-going discussions in the literature.

The literature on the combined concept of micro-reactors and microwave irradiation highlights many important possibilities such as application of coated capillaries for heterogeneously catalyzed organic reactions, parallelization of these capillaries for parallel library synthesis,[19-21] metal coating of external surface of capillaries for enhanced microwave absorption in a micro-reactor,[22-24] application of isothermal micro-reactor operation to justify rate enhancements under microwave irradiation,[25]

etc. However, many important aspects necessary for the development of microwave integrated continuous flow reactors cannot be found in this literature. These aspects are the choice of the mode (multi/mono) of microwave operation, reliable energy balances, providing comparable efficiencies with conventional heating, and uniformity of volumetric microwave heating, giving the possibility of predicting temperature profiles in well-defined samples, *i.e.* size, geometry, dielectric properties etc.

As a part of our stepwise effort towards designing a microwave-heated continuous fine-chemicals production plant, the suitability of two state-of-the-art, mono- and multi-mode, microwave equipment types, available in the market will be elucidated in this chapter. The suitability of both types was investigated based on the dependence of heating uniformity and efficiency on, *i)* sample position, *ii)* sample volume, and *iii)* sample geometry, respectively. These criteria were defined based on the possible degree of freedom that can be achieved in designing the continuous flow reactor-heat exchanger. Finally, a conceptual design of a microwave setup with all the required flexibility and applicability was realized and evaluated for its heating performance.

2.2 Experimental Section

2.2.1 Equipment

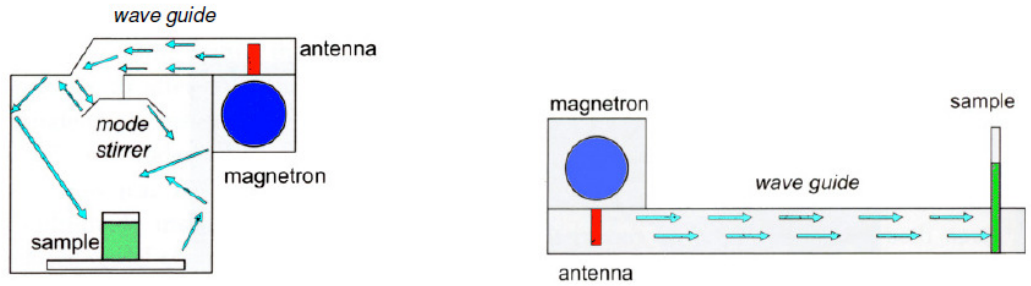

(a) ***(b)***

Figure 2.1: Schematic of multimode (a) and monomode (b) microwave cavities, depicting microwave pattern and respective cavity design. Length of arrows represents the microwave modes.

The multimode type of microwaves usually consists of a big cubic cavity (0.34 m) allowing scales of up to $1 \cdot 10^{-3}$ m^3 of the load (Figure 2.1a). The cavity is supplied with a maximum of 1000 W power by one or multiple magnetrons (in the case of two: 500 W each) placed at the back of the cavity. This cavity is called a multimode cavity because all the modes (transverse electric (TE), transverse magnetic (TM), and transverse electric and magnetic (TEM)) of microwaves exist at all times inside the cavity. The homogeneity of the electromagnetic field inside such a microwave cavity is maintained by a mode mixture on top of the cavity.

The monomode type of microwaves usually consists of a small cylindrical cavity, providing enough space to work up to a scale of $5 \cdot 10^{-5}$ m^3 of the load (Figure 2.1b). The cavity is supplied with a maximum of 300 W power by a magnetron placed at one end of the cavity. This cavity is called monomode system because only one mode (TE) of microwaves exists at all times inside the cavity. This type of cavities uses special holders, which allow the placement of the load only in the axially centric position of a cylindrical cavity. Both mono- and multi-mode microwave power equipment types are compared in Table 2.1.

Table 2.1: Parametric comparison of multi- and mono-mode microwave cavities

Parameter	Multimode	Monomode
Modes	TE, TM, TEM (All)	TE (only one mode)
Powers	Up to 1000 W	Up to 300 W
Cavity type	Rectangular	Cylindrical
Cavity size	Big (0.34 x 0.34 m)	Small (0.075 x 0.09 m)
Processing volume	Large (up to $1 \cdot 10^{-3}$ m^3)	Small (up to $5 \cdot 10^{-5}$ m^3)

(a) ***(b)***

Figure 2.2: Images of (a) a multimode microwave cavity MicroSYNTH, manufactured by Milestone s. r. l., and (b) a monomode microwave cavity Voyager by the CEM Corporation.

A microSYNTH microwave (Milestone s.r.l.) was used for multimode experiments (Figure 2.2a). A voyager microwave (CEM Corporation) was used for monomode

experiments (Figure 2.2b). Build-in fiber-optic sensors were directly inserted in the sample/load to record the temperatures during the experiments.

2.2.2 Experimental procedures

All experiments were performed batch-wise without stirring and water was used as a liquid. Keeping in mind the reactor-heat exchanger scales, the sample volume was varied from $2.5 \cdot 10^{-6}$ to $4 \cdot 10^{-5}$ m^3 with a tube diameter varying from $7 \cdot 10^{-3}$ to $4 \cdot 10^{-2}$ m. These samples were exposed to a fixed amount of power of either 20 or 50 W. Several temperature profiles were collected for 300 s by using a fiber-optic sensor. The sensor position was always maintained at the bottom of the sample during temperature measurement. In each case either the sample position or its size was varied. Details of these variations can be found in the figure caption hereafter.

2.2.3 Heating efficiency calculation

The heating efficiency (η, %) was calculated as the ratio of the amount of energy absorbed by the sample (P_a) and the set point of the microwave power input (P_{in}):

$$\eta = \frac{P_a}{P_{in}} \times 100 \tag{2.1}$$

P_a was calculated as the sum of the enthalpy change of the sample and the energy transferred to the surroundings during the experiment.

$$P_a = P_{heat} + P_{loss} \tag{2.2}$$

$$P_{heat} = mC_p \frac{\Delta T_s}{\Delta t} \tag{2.3}$$

$$P_{loss} = \bar{h}A(T_s - T_u) \tag{2.4}$$

where m is the loaded fluid mass, C_p is the fluid heat capacity, A is the heat transfer area, T_s and T_u are the temperatures of the sample and surroundings, respectively. The average convective heat transfer coefficient ($\bar{h}$) was calculated by Eq. 2.5:

$$Nu = \frac{\bar{h}L}{k} \tag{2.5}$$

where L is the characteristic length of a heat transfer surface, *i.e.* the height of the cylindrical load and k is the thermal conductivity of the surrounding air.

The Nusselt number (*Nu*) was calculated by Eq. 2.6, assuming natural convection around a vertical cylinder being the only mechanism for heat transfer:[26]

$$Nu = \left\{ 0.825 + \left(\frac{0.387(Gr \cdot \mathrm{Pr})^{1/6}}{[1+(0.492/\mathrm{Pr})^{9/16}]^{8/27}} \right) \right\}^2 \tag{2.6}$$

The Grashof (*Gr*) and Prandtl (*Pr*) numbers were calculated according to Eq. 2.7 and 8:

$$Gr = \frac{L^3 g \alpha \Delta T \rho^2}{\mu^2} \tag{2.7}$$

$$Pr = \frac{C_p \mu}{k} \tag{2.8}$$

where g is the acceleration due to gravity and α, ρ, μ, k, and C_p are the thermal expansion coefficient, density, viscosity, thermal conductivity, and the heat capacity of the coolant (air), respectively. The physical properties of air are listed in Table 2.2.[26] These physical properties were assumed to be temperature independent in the range of the temperatures studied. The heat capacity of water (C_p= 4200 J/kg·K) was also assumed to be temperature independent in the whole range of the temperatures studied.[27]

Table 2.2: Physical properties of coolant (air)

Property	Air
Viscosity (μ, Pa.s)	$1.8 \cdot 10^{-5}$
Density (ρ, kg/m^3)	$1.2 \cdot 10^{0}$
Heat capacity (C_p, J/kg/K)	$1.0 \cdot 10^{3}$
Thermal conductivity (k, W/m/K)	$2.6 \cdot 10^{-2}$
Thermal expansion coefficient (α, 1/K)	$3.3 \cdot 10^{-3}$

A heat transfer in series model, where the resistance in the bulk liquid, solid (glass), and surrounding air are combined, could be used for the heat transfer calculations.[28] However, since most of the resistance was found to be in surrounding air, the calculations were simplified by ignoring the resistances in the bulk liquid and the solid.

2.3 Results and Discussion

2.3.1 Multimode microwave cavity

A multimode microwave cavity is more attractive with the possibility of applying a high microwave power and placing a larger reactor-heat exchanger inside (Table 1.1). Therefore, this feasibility study of microwave heating was started with a state-of-the-art cubical multimode microwave cavity.

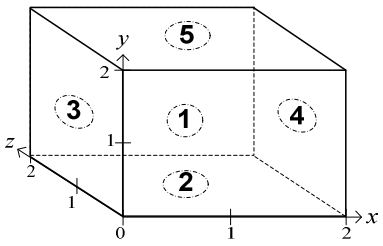

Sample position	
No	Co-ordinates
1	(1,1,1)
2	(1,0,1)
3	(0,1,1)
4	(2,1,1)
5	(1,2,1)

(a)

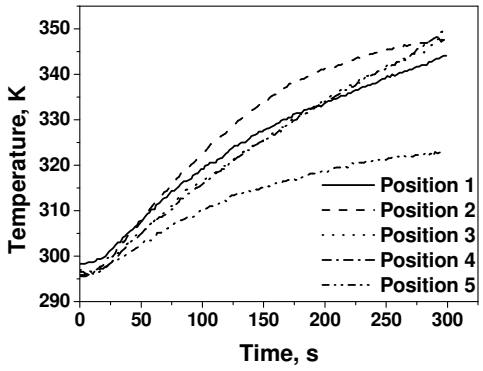

(b)

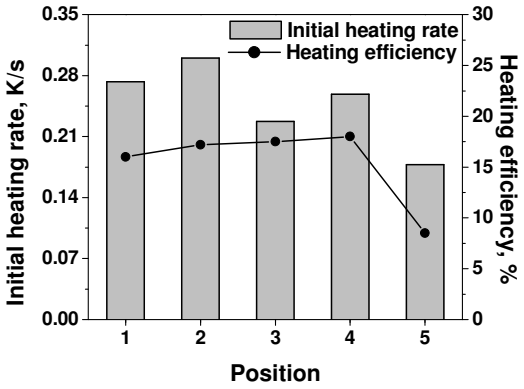

(c)

Figure 2.3: a) Schematic view of the multimode microwave oven with different sample positions inside the cavity; b) Temperature-time histories of a sample at different positions inside the multimode microwave cavity; c) Initial heating rates and heating efficiencies at the respective positions. Same volume of the sample (and its distribution) was placed at all 5 positions. Adjustable Teflon stand was used to support sample at positions 1 to 5 except position 2. Supplied power: 50 W constant; sample volume: $1 \cdot 10^{-5}$ m^3; solvent: water.

Figure 2.3 shows the heating profiles at different positions inside the cubical multimode cavity. A sample volume of $1 \cdot 10^{-5}$ m^3 was placed at various positions (Figure 2.3a) inside the multimode cavity and the temperature profiles were collected for 300 s (Figure 2.3b). The sample volume was restricted to $1 \cdot 10^{-5}$ m^3 to envisage a reactor volume that can be processed in a multimode microwave integrated micro-flow reactor-heat exchanger. The average heating efficiency inside the multimode microwave cavity (Figure 2.3c) was quite low, *i.e.* 17 %. Although

the heating efficiency did not vary much between the sample positions 1 to 4, it dropped drastically at position 5 at the top of the cavity. This could be due to the design of the multimode type cavities for relatively large batch synthesis ($1 \cdot 10^{-3}$ m^3) thus making it not very efficient for low processing volumes. The heating rate on the other hand strongly varied with the sample position (Figure 2.3c). Although slightly visible, it can be categorized in 3 regions. First region with the highest heating rate was at position 1 and 2. Second region with the moderate heating rate was at position 3 and 4. The third region with the lowest heating rate was observed at position 5. These variations in the heating rates pointed to a non-uniform microwave field inside the cavity.

Further on, the dependency of the heating rate and heating efficiency on the sample volume was investigated. Figure 2.4a shows the temperature profiles for different sample volumes placed at position 2 (Figure 2.3a).

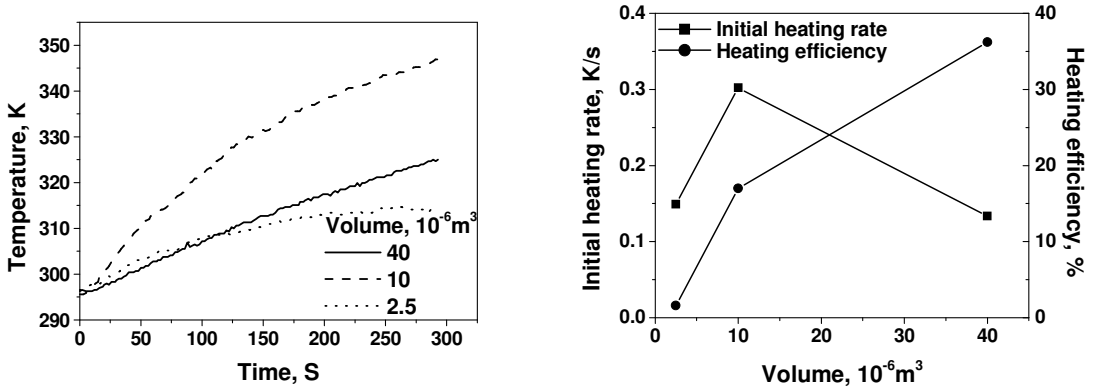

(a) *(b)*

Figure 2.4: a) Temperature-time histories of the sample with different volumes inside the multimode microwave cavity; b) Initial heating rates and heating efficiencies as functions of the sample volume. Sample position: 2 (Figure 2.3a); supplied power: 50 W constant; solvent: water.

While the heating efficiency increased with an increasing sample volume, the heating rate did not show any particular trend with respect to the sample volume (Figure 2.4b). This indicated the possible dependence of the heating rate on the sample distribution, *i.e.* geometry. This was verified by performing an experiment in which both samples had same volumes, but different geometries, *i.e.* different distribution in radial and axial directions (Figure 2.5).

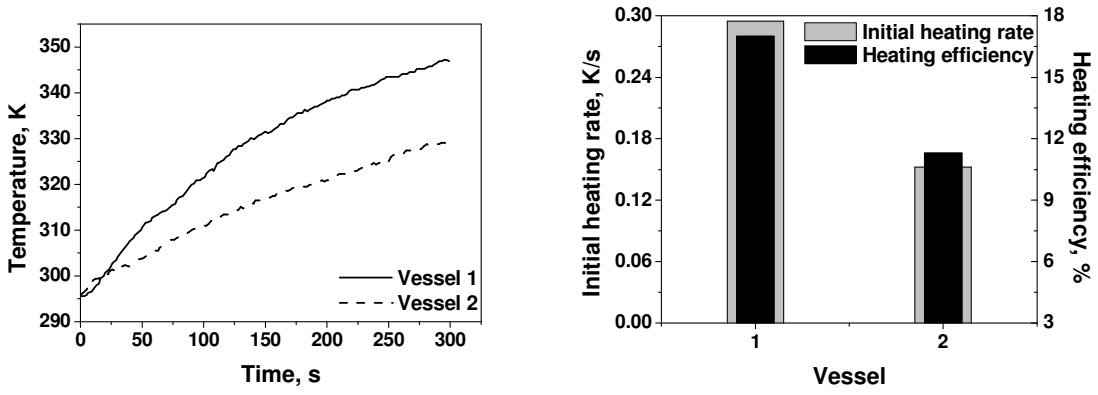

(a) *(b)*

Figure 2.5: a) Temperature-time histories for the sample with different distributions inside the multimode microwave cavity; b) Initial heating rates and heating efficiencies in the case of both the samples. Sample sizes, vessel 1: 0.024 x 0.024 m^2; vessel 2: 0.014 x 0.073 m^2. Sample volume: $1 \cdot 10^{-5}$ m^3; sample position: 2 (Figure 2.3a); supplied power: 50 W constant; solvent: water.

A cylindrical vessel with a ratio of diameter to the height of 1 (0.024 x 0.024 m^2) gave a higher heating rate as well as a better efficiency than an elongated vessel of 0.014 x 0.073 m^2 (Figure 2.5b) demonstrating that the heating rate depends on the space distribution of the sample. Thus the suitability study demonstrated an overall dependence on sample position, volume and space distribution inside a multimode microwave cavity. Additionally, the heating efficiency of a large multimode type microwave cavity was found to be fairly low (≈17 %).

2.3.2 Monomode microwave cavity

The feasibility study was continued with a state-of-the-art monomode microwave cavity. In this cavity, the sample position can only be changed in the axial direction. A schematic view of different axial sample positions and the corresponding temperature profiles is shown in Figure 2.6. Identical sample volumes were employed at all axial positions. It can be seen that no significant differences were observed in the heating rate and the heating efficiency with respect to the axial position of the sample (Figure 2.6c). However, the average heating efficiency obtained during the experiment in the monomode cavity, *i.e.* 45 % was more than twice the average efficiency obtained with that of the multimode cavity (17 %, Figure 2.3). The high heating efficiency found in monomode microwave cavity was in line with the previously reported studies.[29,30]

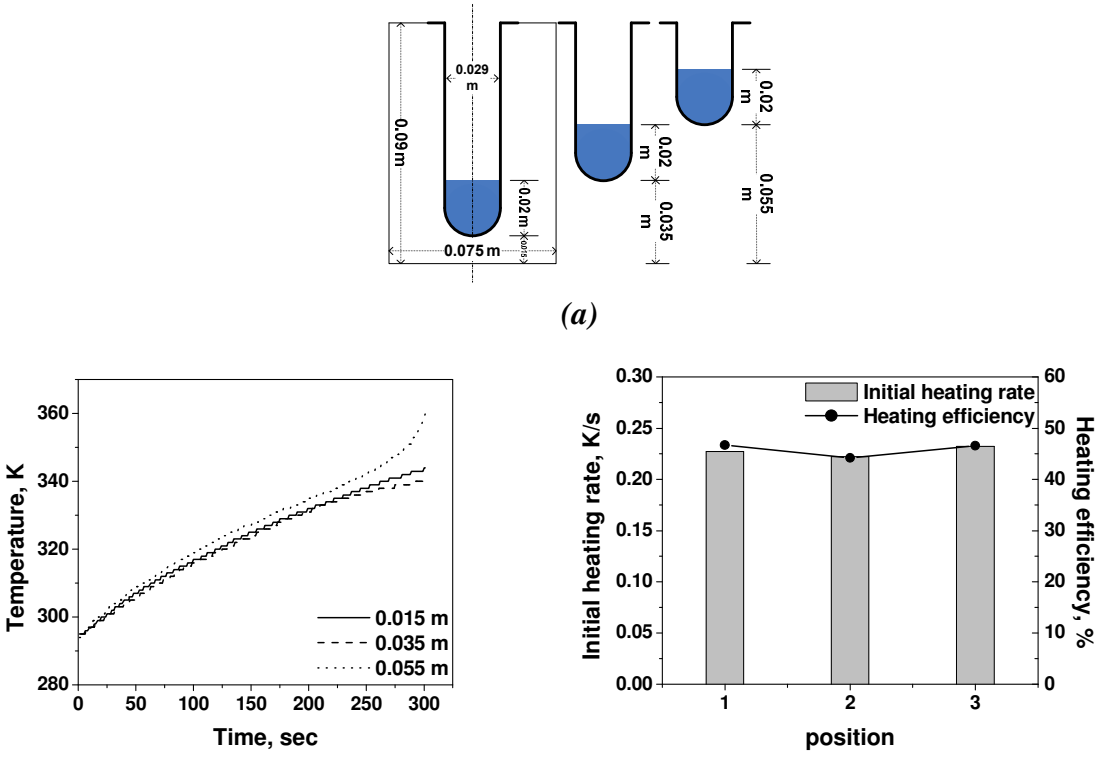

Figure 2.6: (a) Schematic view of the sample with different axial positions and cavity sizes; (b) Temperature-time histories of the sample with different axial positions inside the monomode microwave cavity; (c) Initial heating rates and heating efficiencies as functions of the axial position. Supplied power: 20 W constant; solvent: water; sample volume: $1 \cdot 10^{-5} m^3$.

The heating rate dependence on the sample volume was further verified. Figure 2.7 gives a schematic view of different sample volumes inside the cavity (Figure 2.7a), and the observed temperature profiles (Figure 2.7b).

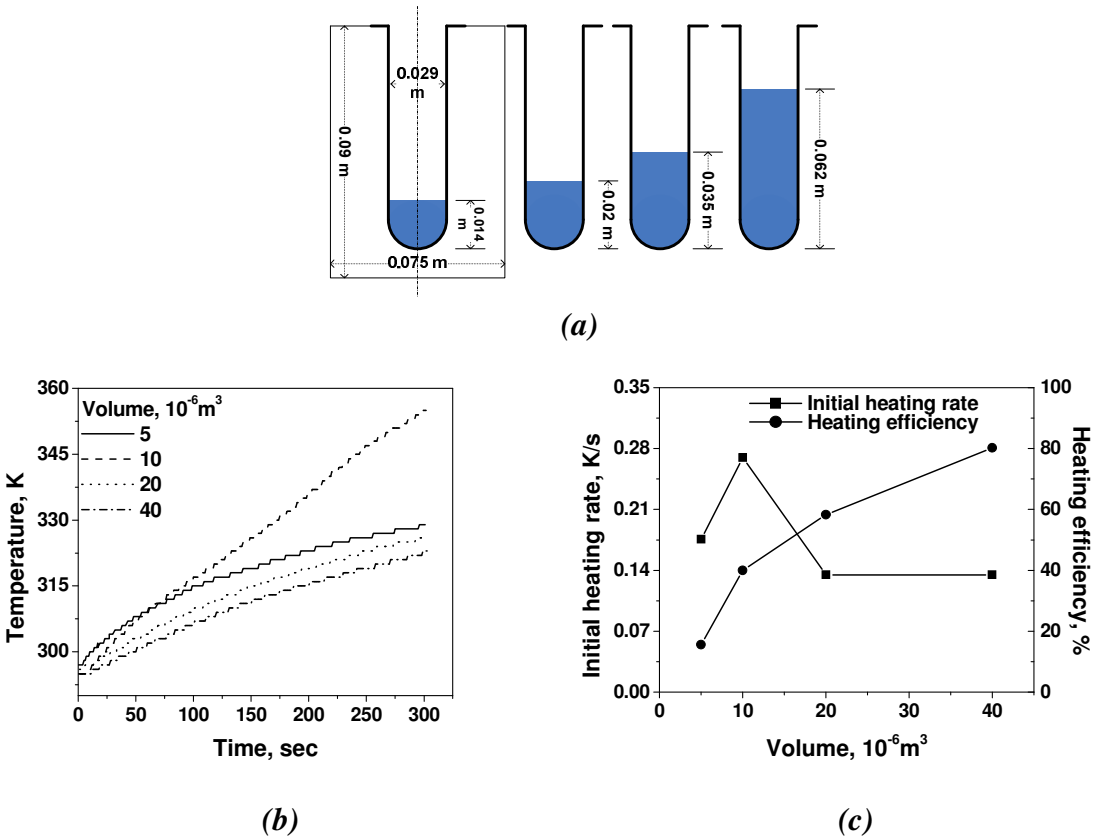

Figure 2.7: (a) Schematic view of the sample with different volumes and cavity sizes; (b) Temperature-time histories of the sample with different volumes inside the monomode microwave cavity; (c) Initial heating rates and heating efficiencies as functions of the sample volume. Supplied power: 20 W constant; solvent: water.

Similar to the multimode cavity, the heating efficiency increased with an increasing sample volume and the heating rate did not show any particular trend with respect to sample volume (Figure 2.7c). Independence from axial position (Figure 2.6), but strong influence of the sample volume (Figure 2.7) indicated uniformity of the microwave field in the axial direction of the microwave cavity. Therefore, the radial distribution effect was further verified.

Figure 2.8 gives a schematic view of different sample sizes, *i.e.* different diameters ($8 \cdot 10^{-3}$ to $16 \cdot 10^{-3}$ m), inside the cavity (Figure 2.8a), together with the obtained temperature profiles (Figure 2.8b) in the samples that gave highest, moderate and lowest heating rates. The heating rate and efficiency both passed through a

maximum at a diameter of $1.3 \cdot 10^{-2}$ m, showing a clear dependence on the sample diameter (Figure 2.8c). This effect will be discussed in the next chapter.

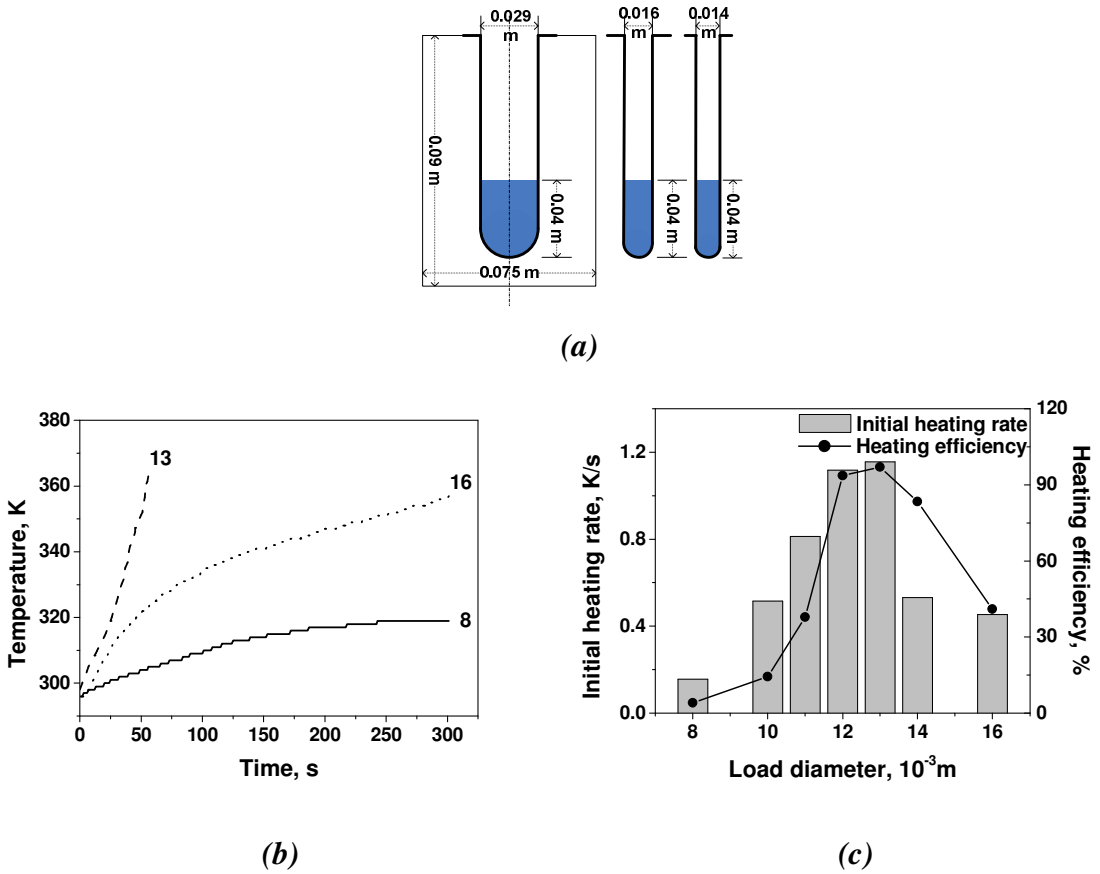

Figure 2.8: (a) Schematic view of the sample with different load diameters and cavity sizes; (b) Temperature-time histories of the sample with different diameters inside the monomode microwave cavity. The samples providing the highest (dashed line), moderate (dotted line) and lowest (solid line) heating rates are shown. The labels represent sample diameters in millimeters (different than shown in Figure 2.8a); (c) Initial heating rates and heating efficiencies as functions of the sample diameter. Supplied power: 20W constant; Solvent: water.

2.3.3 Novel microwave setup designed for intensified flow synthesis

For the design of a microwave integrated micro-flow reactor-heat exchanger, the monomode cavity is more attractive, considering the field uniformity at least in one direction and the higher heating efficiencies for similar volumes. However, state-of-the-art monomode microwave lacks in providing important details such as the electric field pattern.[31] To the best of our knowledge, microwave focusing is not provided in these devices.[32] Knowledge of electric field pattern and its possible focusing is mandatory to obtain desired heating rates at optimal energy efficiencies

for a microwave-heated (continuous) reactor setup. The amount of reflected energy should be known to produce energy balances and, by that, the correct design equations for reactor-heat exchanger equipment. However the measurements of the reflected power are not possible in commercial monomode microwaves. The scale-up by numbering up of individual reactors in series or parallel is also limited for commercial monomode microwaves.[33] Therefore, a novel monomode microwave applicator (capacity 2 kW), having all of the abovementioned functionalities, has been built with the help of Frick und Mallah GMbH for further study. The design concept of four cavities on a single main waveguide (single magnetron) was realized to minimize the grid to applicator losses (conversion of electrical power into microwave power), while providing the possibility of unitized scale-up going consecutively from one cavity to another (Figure 2.9). For detailed technical information of the setup please see Appendix A.

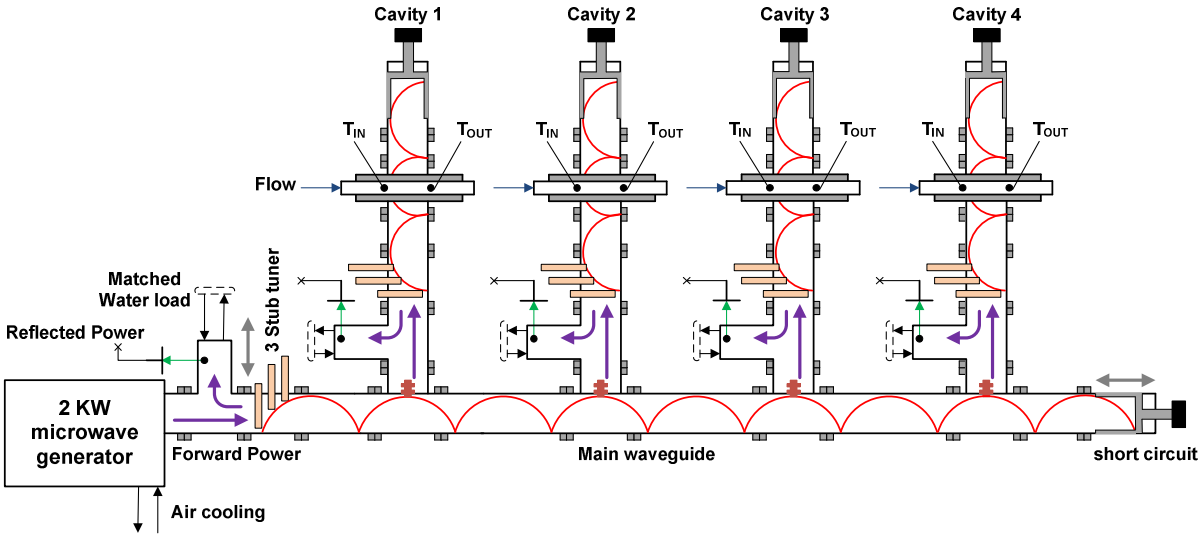

Figure 2.9: Schematic view of a dedicated microwave setup (with labeling of all the parts) designed for continuous flow fine-chemicals synthesis and multiphase flow handling. Red lines designate field pattern. Arrows signify flow of energy (purple), signals (green), and liquids (blue), and movement of stub tuner, short circuit (grey). Design: TU/e; Manufacturer: Frick und Mallah GMbH, Germany.

The microwave setup consists of a 2 kW microwave generator, providing the main waveguide with resonant standing electromagnetic waves. Four individual cavities are coaxially coupled with this main waveguide, allowing variable energy inputs (0-500 W). Each cavity can be tuned to match the impedance with the inserted load

(*i.e.* reactor tube). The tuning is possible with the use of a short circuit and stub tuners available on each individual cavity. All cavities and the main waveguide are equipped with isolators in combination with detector diodes to measure the reflected powers.

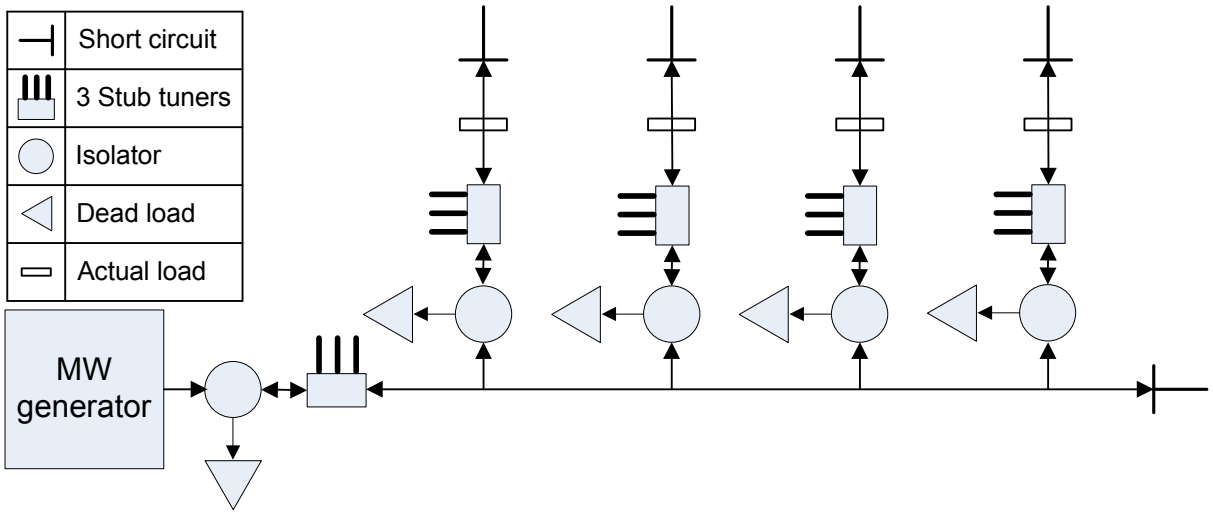

Figure 2.10: Schematic depiction of the microwave energy flow with microwave resonance in the microwave setup. Arrows show the propagation direction for the microwaves.

The energy flow diagram of the setup describes the resonance of microwaves in the main waveguide as well as in an individual cavity (Figure 2.10). The microwaves can enter in the main waveguide and in each individual cavity, but the back-flow of the microwaves is restricted by the isolators as they transferred the microwaves to the dead loads at all positions. Thus the isolators protect the magnetron, and maintain a consistent field pattern in the main waveguide which provides (at least theoretically) a near uniform distribution of microwave energy in all four cavities.

The microwave setup was calibrated for reflected power measurements at all 5 positions in the applied microwave power range of 300 to 1600 W. A water flow of $3.33 \cdot 10^{-6}$ to $6.66 \cdot 10^{-6}$ m^3/s was used as a load to limit the temperature rise to 10 K and to ignore the heat losses to the surroundings. Figure 2.11 shows experimentally determined overall energy distribution in the microwave setup. The energy balance was closed with 90% of the input power in the whole range of applied powers (Figure 2.11a). Although it was expected that the energy distribution would be the same in all four cavities, it was found to vary from cavity to cavity (Figure 2.11b).

The fourth cavity withdrew a slightly larger amount of energy from the main waveguide.

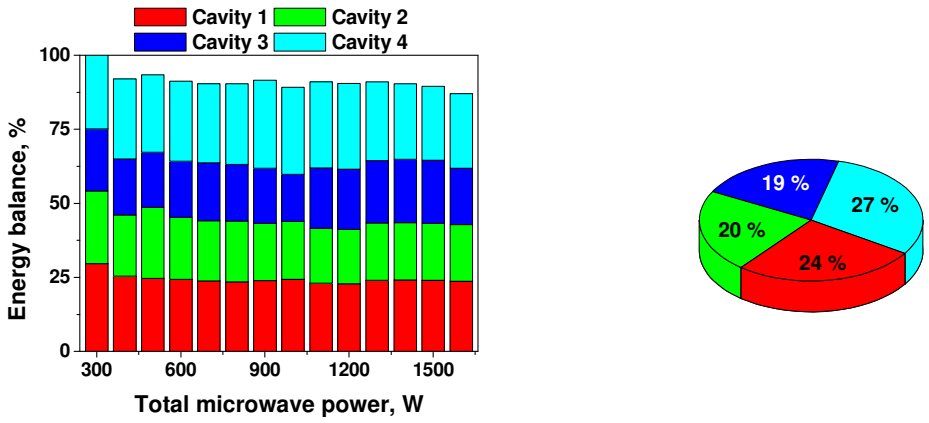

(a) *(b)*

Figure 2.11: (a) Overall energy balance in the microwave setup at various applied microwave powers in the range of 300 to 1600 W; (b) Average energy distribution in all four cavities of the microwave setup. Solvent: water, flow rate: $3.33 \cdot 10^{-6}$ to $6.66 \cdot 10^{-6}$ m^3/s.

The differences were, however, relatively small and could be a result of electromagnetic energy built-up at the short circuit and stub tuners of the main waveguide (Figure 2.9). These deviations are expected not to affect scale-up as long as the energy requirements of the process do not exceed the highest possible microwave power available for one individual cavity, *i.e.* 380 W.

2.4 Conclusions

State-of-the-art multi- and mono-mode microwave cavities were tested for their suitability in designing a microwave integrated micro-flow reactor-heat exchanger. Multimode cavity, although having advantage of large cavity size and higher microwave powers, proved to be essentially inferior to monomode microwave cavity by giving very limited heating efficiencies (≈ 17 %). Additionally, the heating rate and the heating efficiency showed dependence on the position as well as the geometry of the sample. In the case of monomode microwave cavities the higher heating efficiency (≈ 45 %) made it a more desirable option for (continuous) reactor-heat exchanger design. This mode of microwave operation gave almost twice as high efficiencies when compared to multimode microwave operations. Furthermore, the monomode microwave cavity had independence from sample

position as long as the sample stayed in the axially centric position of the cylindrical cavity. Nevertheless, this mode of operation also showed dependence on the radial distribution of the sample *i.e.* diameter of the sample. The heating rate and the heating efficiency were found to be going through a maximum with respect to the diameter of the sample. However, state-of-the-art monomode microwave cavities lacked in providing following important functionalities:

- a predictable electric field pattern,
- a tunable cavity,
- reflected power measurements and
- unitized scale-up

Considering the importance of abovementioned functionalities, an alternative microwave setup was designed, providing these features (Figures 9 and 10). This novel monomode microwave setup not only allowed proper formulation of complete energy balances, but also more or less equal distribution of this microwave energy in all four cavities at reduced grid to applicator losses (single magnetron) for unitized scale-up.

Nomenclature

Symbol	**Description**
A	heat transfer area, m^2
C_p	heat capacity, J/kg.K
Gr	Grashof number
g	acceleration due to gravity, m/s^2
$\overline{h}$	heat transfer coefficient, $W/m^2 \cdot K$
L	length of the cylindrical load, m
m	mass of the sample, kg
Nu	Nusselt number
P_a	absorbed energy, W
P_{in}	microwave set energy input, W
P_{heat}	Energy gained by the liquid, W
P_{loss}	energy lost to the surrounding, W
Pr	Prandtl number
T_s	temperature of the sample, K
T_u	temperature of the surrounding, K
ΔT_s	temperature change over time, K
Δt	time interval, s

$tan\ \delta$	loss tangent

Greek symbols

ε'	dielectric constant
ε''	dielectric loss
λ	wavelength of the electromagnetic field in a liquid, m
λ_0	wavelength of the electromagnetic field in free space, m
η	heating efficiency, %
k	thermal conductivity of liquids, W/m·K
α	thermal expansion coefficient,1/K
ρ	Density, kg/m^3
μ	Viscosity, Pa.s

Appendix 2.A

Technical information of the Frick und Mallah microwave setup

Table 2A.3: Operating details for the microwave setup

Component	Type/capacity
Main supply voltage	3L/N/PE AC 50 Hz 400 V~
Main power consumption	max. 12 kVA
Anode Voltage	-4000 V
Microwave frequency	2450 MHz ± 15 MHz
Cooling water flow	min. $8.33 \cdot 10^{-5}$ m^3/s at 293 K (inlet)

Table 2A.4: Technical information for the components of the microwave setup

Component	Model number/ Material of construction	Size/capacity
Generator: Magnetron Transformer	ML2000 NLL- BV:019/0842-0	2 kW at 2.45 GHz
Isolator	D09020 2722 162 13431	2.425 – 2.475 GHz
3 Stub tuner	Brass	Up to 2 kW
Short Circuit	COD CE 83634 DD52R FR-001 00-S-AR	Up to 2 kW
Waveguide	WR 340/Aluminum	0.0472 x 0.0 902 m
Cavity	WR 340/Aluminum	0.0472 x 0.0 902 m
Reactor opening	Aluminum (Circular)	Diameter = $1.4 \cdot 10^{-2}$ m

References

1. Gedye, R.; Smith, F.; Westaway, K.; Ali, H.; Baldisera, L.; Laberge, L.; Rousell, J. The use of microwave ovens for rapid organic synthesis. *Tetrahedron Lett.* **1986**, *27*, 279.
2. Giguere, R. J.; Bray, T. L.; Duncan, S. M. Application of commercial microwave ovens to organic synthesis. *Tetrahedron Lett.* **1986**, *27*, 4945.
3. Kappe, C. O. Controlled microwave heating in modern organic synthesis. *Angew. Chem. Int. Ed.* **2004**, *43*, 6250.
4. Michael,D.; Mingos, P.; Baghurst, D. R. Applications of microwave dielectric heating effects to synthetic problems in chemistry. *Chem. Soc. Rev*. **1991**, *20*, 1.

5. Kappe, C. O. Microwave dielectric heating in synthetic organic chemistry. *Chem. Soc. Rev.* **2008**, *37*, 1127.
6. Nüchter, M.; Ondruschka, B.; Bonrath, W.; Gum, A. Microwave assisted synthesis – a critical technology overview. *Green chem*. **2004**, *6*, 128.
7. Lidstrom, P.; Tierney, J.; Wathey, B.; Westman, J. Microwave assisted organic synthesis – a review. *Tetrahedron.* **2001**, *57*, 9225.
8. Hayes, B. L.; Microwave synthesis: chemistry at the speed of light (*1st edition*), CEM publishing, Matthews NC, 2002.
9. Lidstrom P. Microwave assisted organic synthesis (*1st edition*), Blackwell, Oxford, 2004.
10. Kappe C. O. Microwaves in organic and Medicinal chemistry (*1st edition*), Wiley-VCH, Weinheim, 2005.
11. Larhed, M.; Olofsson, K. Microwave methods in organic synthesis (*1st edition*). Springer, Berlin, 2006.
12. Loupy, A. Microwaves in organic synthesis (*2nd edition*), Wiley-VCH, Weinheim, 2006.
13. Gabriel, C.; Gabriel, S.; Grant, E. H.; Ben S. J.; Halstead, B. S. J.; Mingos, D. M. P. Dielectric parameters relevant to microwave dielectric heating. *Chem. Soc. Rev.* **1998**, *27*, 213.
14. Hosseini, M.; Stiasni, N.; Barbieri, V.; Kappe, C. O. Microwave-assisted asymmetric organocatalysis: a probe for nonthermal microwave effects and the concept of simultaneous cooling. *J. Org. Chem.* **2007**, *72*, 1417.
15. Herrero, M. A.; Kremsner, J. M.; Kappe, C. O. Nonthermal microwave effects revisited: on the importance of internal temperature monitoring and agitation in microwave chemistry. *J. Org. Chem.* **2008**, *73*, 36.
16. PhD thesis, Dressen, M. H. C. L. Eindhoven University of Technology, 2009. *ISBN: 978-90-386-1821-0.*
17. PhD thesis, Van de Kruijs B. H. P. Eindhoven University of Technology, 2010. *ISBN: 978-90-386-2178-4.*
18. Glasnov, N. T.; Kappe, O. C. Microwave-assisted synthesis under continuous-flow conditions. *Macromol. Rap. Com.* **2007**, *28,*395.
19. Comer, E.; Organ, M. G.; A microreactor for microwave-assisted capillary (continuous flow) organic synthesis. *J. Am. Chem. Soc.* **2005**, *127*, 8160.
20. Comer, E.; Organ, M. G. A microcapillary system for simultaneous, parallel microwave-assisted synthesis, *Chem. Eur. J.* **2005**, *11*, 7223.
21. Shore, G.; Morin, S.; Organ, M. G. Catalysis in capillaries by Pd thin films using microwave-assisted continuous-flow organic synthesis (MACOS). *Angew. Chem. Int. Ed.* **2006**, *45*, 2761.
22. He, P.; Haswell, S. J.; Fletcher, P. D. I. Microwave heating of heterogeneously catalysed Suzuki reactions in a micro reactor. *Lab Chip.* **2004**, *4*, 38.
23. He, P.; Haswell,S. J.; Fletcher, P. D. I.; Kelly, S. M.; Mansfield, A. Scaling up of continuous-flow, microwave-assisted, organic reactions by varying the size of Pd-functionalized catalytic monoliths. *Appl. Catal. A.* **2004**, *274*, 111.
24. He, P.; Haswell, S. J.; Fletcher, P. D. I. Efficiency, monitoring and control of microwave heating within a continuous flow capillary reactor. *Sensors and Actuators B.* **2005**, *105*, 516.

25. Jachuck, R. J. J.; Selvaraja, D. K.; Varma, R. S. Process intensification: oxidation of benzyl alcohol using a continuous isothermal reactor under microwave irradiation. *Green Chem.*, **2006**, *8*, 29.
26. Welty, J. R.; Wicks, C. E.; Wilson, R. E. Fundamentals of momentum, heat, and mass transfer, John Wiley & Sons, New York, 1984.
27. D.R. Lide, CRC Handbook of Chemistry and Physics, Taylor & Francis group, Boca Raton 2000.
28. Delsman, E.R.; Croon, M.H.J.M. de; Kramer, G.J.; Cobden, P.D.; Hofmann, C.; Cominos, V.; Schouten, J.C. Experiments and modelling of an integrated preferential oxidation–heat exchanger microdevice. *Chem. Eng. J.* **2004,** 101, 123.
29. Robinson, J.; Kingman, S.; Irvine, D.; Licence, P.; Smith, A.; Dimitrakis, G.; Obermayer, D.; Kappe, C. O. Understanding microwave heating effects in single mode type cavities — theory and experiment. *Phys. Chem. Chem. Phys.* **2010,** *12,* 4750.
30. Hoogenboom, R.; Wilms, A. F. T.; Schubert, S. U. Microwave irradiation – a closer look at heating efficiencies. *Aust. J. Chem.* **2009,** *62*, 236.
31. Toukoniitty, B.; Mikkola, J. –P.; Eranen, K.; Salmi, T.; Murzin, D. Y. Esterification of propionic acid under microwave irradiation over an ion-exchange resin. *Catal Today.* **2005**, *100*, 431.
32. Marquié, J.; Salmoria, G.; Poux, M.; Laporterie, A.; Dubac, J.; Roques, N. Acylation and Related Reactions under microwaves. 5. Development to large laboratory scale with a continuous-flow process. *Ind. Eng. Chem. Res.* **2001**, *40,* 4485.
33. Matsuzawa, M.; Togashi, S.; Hasebe, S. Basic examination of a pilot plant for continuous flow microwave-assisted chemical reaction combined with microreactors. *J. Thermal Sci. Tech*. **2011**, *6*, 69.

3

Effect of load size on the efficiency of microwave heating under stop-flow and continuous-flow conditions

This chapter is published as:
Patil, N. G.; Rebrov, E. V.; Esveld, E.; Eränen, K.; Benaskar, F.; Meuldijk, J.; Mikkola, J. -P.; Hessel, V.; Hulshof, L. A.; Murzin, D.Y.; Schouten, J. C. Effect of the load size on the efficiency of microwave heating under stop-flow and continuous-flow conditions. *J. Microwave Power EE*. **2012,** 46(2), 83-92.

Abstract

A novel heating efficiency analysis of the microwave heated stop-flow (*i.e.* stagnant liquid) and continuous-flow reactors has been presented. The thermal losses to the surrounding air by natural convection have been taken into account for heating efficiency calculation of the microwave heating process. The effect of the load diameter in the range of $4 \cdot 10^{-3}$ – $2.9 \cdot 10^{-2}$ m on the heating efficiency of ethylene glycol was studied in a monomode microwave cavity under continuous-flow and stop-flow conditions. The variation of the microwave absorbing properties of the load with temperature was estimated. Under stop-flow conditions, the heating efficiency depends on the load diameter. The highest heating efficiency has been observed at the load diameter close to the half wavelength of the electromagnetic field in the corresponding medium. Under continuous-flow conditions, the heating efficiency increased linearly. However, microwave leakage above the propagation diameter restricted further experimentation at higher load diameters. Contrary to the stop-flow conditions, the load temperature did not raise monotonously from the inlet to outlet under continuous-flow conditions. This was due to the combined effect of lagging convective heat fluxes in comparison to volumetric heating. This severely disturbs the uniformity of the electromagnetic field in the axial direction and creates areas of high and low field intensity along the load length decreasing the heating efficiency as compared to stop-flow conditions.

3.1 Introduction

Interest in applying microwave heating to chemical synthesis has been intensively pursued over the last several decades since dielectric heating provides an elegant and fast heat transfer to reaction media.[1-4] The shortened reaction times and expanded range of reaction conditions due to fast volumetric heating is one of the primary motivations why to apply microwaves in organic synthesis.[5-7] There is also growing interest to use microwave-assisted organic synthesis beyond the laboratory scale, *i.e.* at a process chemistry level for pilot and production campaigns.[8] Numbering-up into many small-heated batch units has been suggested as a suitable solution by Stadler *et al.*[9]

The majority of such industrial applications employs a multimode cavity in which numerous standing-wave resonant modes exist simultaneously in a given frequency range.[10-12] Although this cavity provides the possibility of relatively large-scale operations (up to $1 \cdot 10^{-3}$ m^3) and high power inputs, the existence of multiple standing modes leads to an uneven electromagnetic field distribution causing non-uniform heating at different locations inside the cavity.[13] On the contrary, a monomode cavity has uniform electric field intensity in one direction but the loads are limited approximately to $5 \cdot 10^{-5}$ m^3 in volume.[14,15]

The important characteristic of the microwave reactor is the efficiency of transformation of the microwave energy into heat of the reactants. In most cases, the amount of electromagnetic energy absorbed by the reactants is lower than the input power in a microwave cavity. Furthermore, if the physical properties of the reactants change in the course of heating, the volumetric heating rate changes together with microwave pattern. This makes it difficult to estimate the efficiency of microwave heating as required engineering correlations are still not well documented. In order to emphasize the scale-up methodology for microwave equipment, it is important to compute the actual energy consumption under microwave heating.

There are several experimental studies devoted to the heating efficiency of a solvent (often called as load) under microwave heating[16-20] as well as theoretical studies devoted to the development of physical models describing electromagnetic

interactions with the medium.[10-15,20-23] However, experimental studies validating a theoretical approach are scarce in the literature. Recently, Robinson *et al.*[24] performed an experimental study to verify their modeling approach explaining the effect of dielectric properties, the load volume and its distribution in the microwave cavity. However, the heat losses to the environment were not considered in their approach providing no information on the energy efficiency of the system.

The size of the load has a great influence on the heating efficiency during microwave heating under stop-flow conditions.[13] Under continuous-flow, the load temperature should monotonously increase from the inlet to outlet as a result of volumetric heating and convection. However, the change of electromagnetic properties of the load along the flow direction disturbs the symmetry of the electromagnetic (EM) field which might result in local minima and maxima of intensity. In this study, the effect of the load diameter and loss tangent of the medium on the efficiency of microwave heating and the existence of local minima and maxima due to changing dielectric properties have been investigated in a monomode microwave cavity under stop-flow and continuous-flow conditions.

3.2 Experimental

Following sub-sections give the experimental details for stop-flow experiments, continuous-flow experiments, heating efficiency calculations and dielectric property measurements.

3.2.1 Stop-flow experiments

A microwave transparent cylindrical quartz load filled with ethylene glycol (>99 wt. %, Sigma Aldrich) was positioned along the centerline in the microwave applicator in such a way that a length of $4 \cdot 10^{-2}$ m was exposed to microwave irradiation with an input power of 20 W. The microwave applicator (CEM corporation, model: Discover) had a cylindrical shape with a diameter of $7.5 \cdot 10^{-2}$ m and a height of $9 \cdot 10^{-2}$ m. Multiple cylindrical loads with inner diameter varying from $4 \cdot 10^{-3}$ to $2.9 \cdot 10^{-2}$ m were used in the stop-flow experiments. The temperature was measured by an inbuilt fiber optic sensor (Fiso Technologies). The liquid was

allowed to be completely stagnant (*i.e.* stop-flow) in the microwave cavity and the temperature was recorded until the boiling point or the time scale of 300 s. The initial temperature was 298 K in the stop-flow experiments.

3.2.2 Continuous-flow experiments

The monomode microwave set-up with an auto tuner operated at 2.45 GHz (Sairem, France) was used for the continuous-flow experiments (Figure 3.1). The short and the stubs/iris were automatically moved by the auto tuner for the maximum of the standing wave on the applied load. The continuous-flow experiments were conducted at the input power range from 100 to 500 W and a flow rate range from $2.5 \cdot 10^{-7}$ to $1.66 \cdot 10^{-6}$ m^3/s. The load inner diameter was varied from $4 \cdot 10^{-3}$ to $1.1 \cdot 10^{-2}$ m. The temperature was measured by a fiber optic sensor (Fiso Technologies). The temperature profile was recorded at six different positions by simultaneously moving two fiber optic sensors which stayed at a distance of $3 \cdot 10^{-2}$ m from each other along the axial direction. The distance between sensors allowed maintaining the empty volume of the load in the microwave irradiation zone. The inlet temperature was kept at 298 K.

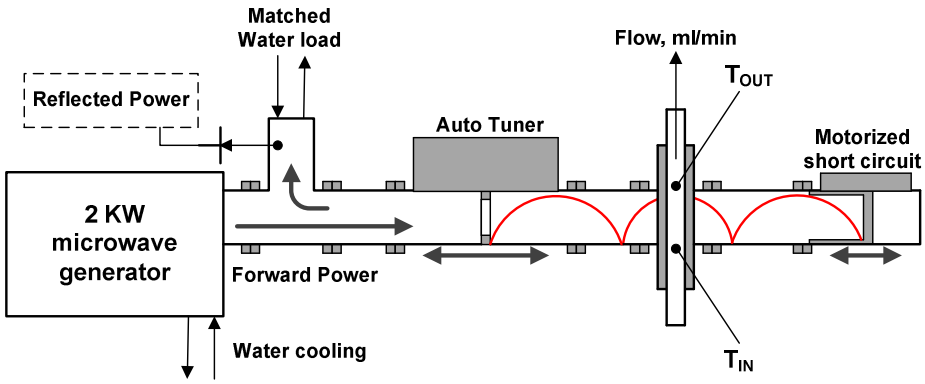

Figure 3.1: Microwave set-up used for continuous-flow experiments.

In both cases, *i.e.* stop-flow and continuous-flow experiments, Ethylene glycol was chosen firstly because it is a polar solvent which interacts very strongly with microwave s and secondly because it has a high boiling point. For both studies, the temperature profiles were recorded and averaged over three runs under otherwise identical experimental conditions.

3.2.3 Heating efficiency

The heating efficiency (η) was calculated as the ratio of the amount of energy absorbed by the load (P_a) to the microwave input power (P_{in}):

$$\eta = \frac{P_a}{P_{in}} \times 100 \tag{3.1}$$

The energy absorbed by the load (P_a) was calculated as the sum of the enthalpy change of the load and the energy transferred to the surroundings during the experiment.

$$P_a = P_{heat} + P_{loss} \tag{3.2}$$

$$P_{heat} = mC_p \frac{\Delta T_1}{\Delta t} \quad \text{(for stop flow)} \tag{3.3a}$$

$$= \dot{m} C_p \Delta T_2 \quad \text{(for continuous flow)} \tag{3.3b}$$

$$P_{loss} = \bar{h} A \Delta T \tag{3.4}$$

where m is the liquid weight, $\dot{m}$ is mass flow rate, C_p is the liquid heat capacity, ΔT_1 is the temperature change over time Δt, ΔT_2 is the difference between the outlet and inlet liquid temperature in continuous-flow, and A is the heat transfer area. Radial distribution of temperature was neglected at both; stop-flow and continuous-flow; conditions. The recorded temperatures were considered as average temperatures over the cross sections. The average convective heat transfer coefficient ($\bar{h}$) was calculated from the Nusselt number (Eq. 3.5) assuming natural convection around a vertical cylinder as the only mechanism for heat transfer[25]:

$$Nu = \frac{\bar{h}L}{k}, \; Nu = \left\{ 0.825 + \left(\frac{0.387(Gr \cdot \mathrm{Pr})^{1/6}}{[1 + (0.492/\mathrm{Pr})^{9/16}]^{8/27}} \right) \right\}^2 \tag{3.5}$$

where L is the length of the cylindrical load, k is the thermal conductivity of the surrounding air, Gr and Pr are the Grashof and Prandtl numbers:

$$Gr = \frac{L^3 g \alpha \Delta T \rho^2}{\mu^2} \tag{3.6}$$

$$Pr = \frac{C_p \mu}{k} \tag{3.7}$$

where α is the thermal expansion coefficient, ρ is the density, μ is the viscosity, k is the thermal conductivity and C_p is the heat capacity of air and g is the acceleration due to gravity. The physical properties of the air were taken from Welty *et al.*[25] (Table 3.1). The heat capacity of ethylene glycol (C_p= $2.4 \cdot 10^3$ J/kg·K), taken from Lide *et al.*[26], was assumed to be temperature independent in the whole range of the temperatures studied. The heat transfer calculations could be performed by using heat transfer in series model where the resistance in bulk liquid, solid (glass), and surrounding air could be combined. However since most of the resistance was found to be in surrounding air, the calculations were simplified by ignoring resistances in bulk liquid and solid as well as at the liquid-solid and solid-gas interfaces.

Table 3.1: Physical properties of coolant (air)

Property	Air
Viscosity (μ, Pa.s)	$1.8 \cdot 10^{-5}$
Density (ρ, kg/m^3)	$1.2 \cdot 10^{0}$
Heat capacity (C_p, J/kg/K)	$1.0 \cdot 10^{3}$
Thermal conductivity (k, W/m/K)	$2.6 \cdot 10^{-2}$
Thermal expansion coefficient (α, 1/K)	$3.3 \cdot 10^{-3}$

3.2.4 Dielectric property measurements

A high temperature dielectric probe kit (85070D, Agilent) and a network analyzer (NWA E5062A, Agilent) were used for the measurements of the dielectric constant (ε') and the dielectric loss (ε'') of different liquids at a frequency of 2.45 GHz. The measurements of the batch sample at different temperatures were repeated and averaged over three runs. Oil bath was used to maintain the temperature. Then, the loss tangent ($\tan\delta$) was calculated[27]:

$$\tan\delta = \frac{\varepsilon''}{\varepsilon'} \tag{3.8}$$

Assuming the permeability of unity for all liquids, the wavelength of the EM field in the liquids was calculated as a function of temperature[27]:

$$\lambda = \frac{\lambda_0}{\sqrt{\varepsilon'}} \tag{3.9}$$

where $\lambda_0 = 1.224 \cdot 10^{-1}$ m is the wavelength in free space; air. Under continuous operation, an axial temperature gradient exists in the load, therefore the propagation diameter, which is half the wavelength of electromagnetic field in the liquid (½λ), was calculated as a function of temperature.

3.3 Results and Discussion

The change of the dielectric properties with temperature influences the standing wave pattern inside the cavity and thus the microwave absorption. Consequently, the change in dielectric constant (ε') and dielectric loss (ε'') of ethylene glycol were measured in the temperature range from 298 to 428 K (Figure 3.2). Both the ε' and ε'' have a maximum due to a shift in rotation correlation time in Debye relaxation at 343 and 313 K, respectively.[2, 28]

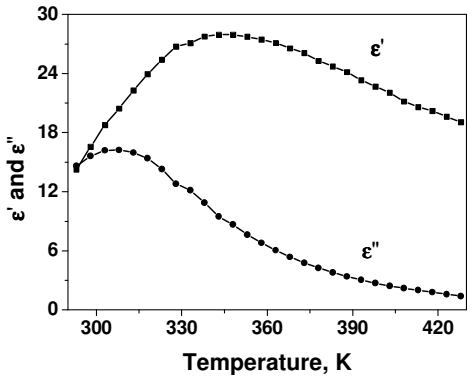

Figure 3.2: Real (ε') and imaginary (ε'') parts of the permittivity of ethylene glycol as a function of temperature at 2.45 GHz.

3.3.1 Heating under stop-flow conditions

The effect of the load diameter on the heating rate is shown in Figure 3.3a at the highest, mean and slowest heating rates, respectively at stop-flow conditions. Surprisingly, the heating rate was found to be independent of the load size (*i.e.* higher heating rate for $1.3 \cdot 10^{-2}$ m than $1.8 \cdot 10^{-2}$ m load diameter, Figure 3.3a). This can be due to the stagnancy of the applied load (*i.e.* stop-flow conditions) and thus, resonance occurring only at multiple of half wavelengths (½λ). In this particular case, the half wavelength varied between $1.2 \cdot 10^{-2}$ to $1.6 \cdot 10^{-2}$ m depending upon the

measured dielectric permittivity of the load in a particular temperature range (Figure 3.3b).

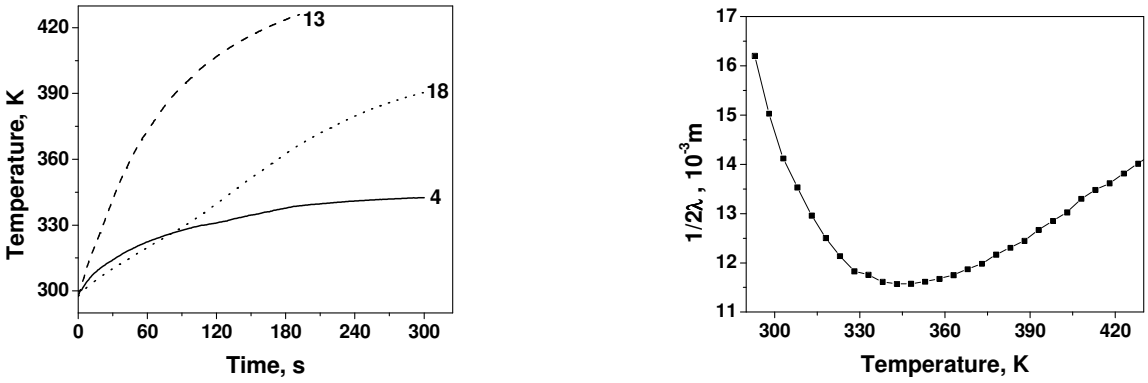

(a) *(b)*

Figure 3.3: a) Temperature as a function of time for ethylene glycol as a load at stop-flow conditions. The loads providing the highest (dashed line), moderate (dotted line) and lowest (solid line) heating rate are shown. The labels represent the load diameters in millimeter. Microwave irradiation at 2.45 GHz and at constant power of 20 W; b) Change in half wavelength with temperature as derived from the measurement of dielectric permittivity.

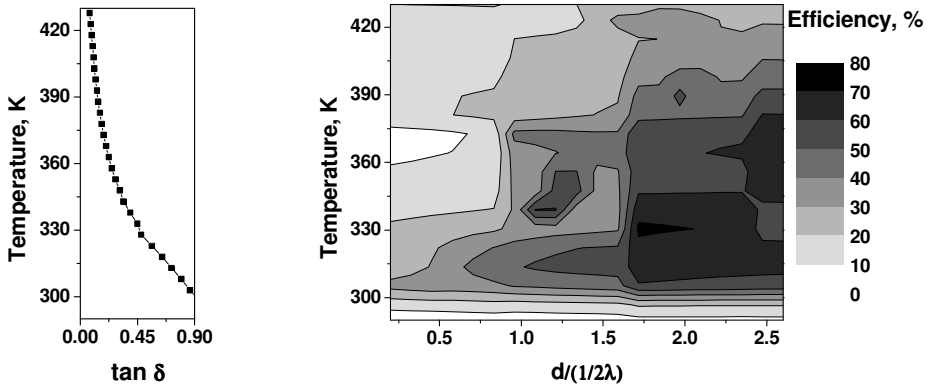

(a) *(b)*

Figure 3.4: a) Loss tangent and b) heating efficiency as a function of temperature and d/(½λ) (ratio of load diameter over half wavelength) for ethylene glycol at stop-flow conditions. The loss tangent monotonously decreases with temperature from 0.90 to 0.05.

Therefore, the heating efficiency as a function of the load diameter was calculated at several temperature intervals and compared with the loss tangent (Figure 3.4). The maximum heating efficiency of 70 % was observed at a load diameter equal to and above the half wavelength of the EM field (Figure 3.4b). It is known that the resonance in a dielectric surrounded by air occurs at the whole number of half wavelengths (½λ).[27] The heating rate decreases as the temperature increases (Figure

3.3a) therefore the heating efficiency decreased at higher temperatures. This was also due to the monotonous decrease of loss tangent with increasing temperature (Figure 3.4a).

3.3.2 Heating under continuous-flow conditions

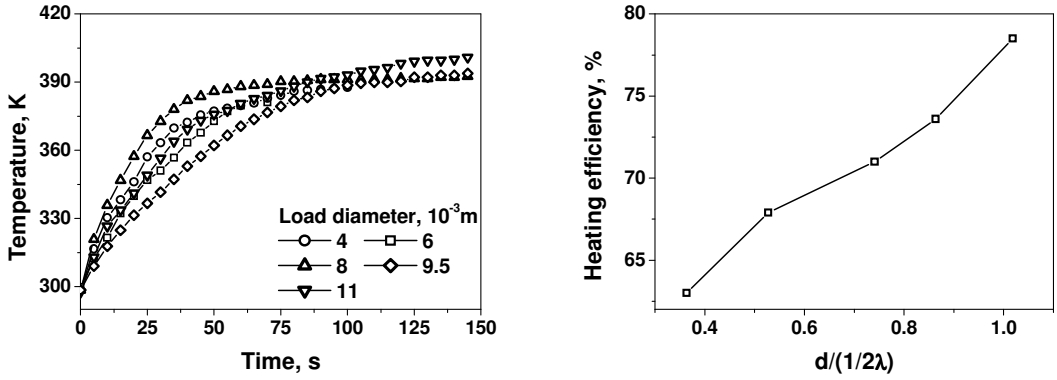

(a) *(b)*

Figure 3.5: a) Temperature as a function of time and b) heating efficiency dependence on d/(½λ) (ratio of load diameter over half wavelength) in case of ethylene glycol at continuous-flow conditions. Flow rate: $2.5 \cdot 10^{-7}$ m^3/s. Microwave irradiation at 2.45 GHz and constant applied power of 100 W. Temperature measurements at the outlet of the cavity (T_{OUT} in Figure 3.1)

The temperature profiles ($T_{OUT,}$ Figure 3.1) during load start-up and corresponding heating efficiency as a function of the load diameter are shown in Figure 3.5 under continuous-flow conditions. Although the initial heating rate was similar for all load diameters, higher steady state temperatures were observed for larger load diameters (Figure 3.5a). The heat flux to the surroundings (Eq. 3.4) increased from 200 to 1000 W/m^2 at higher temperatures and it amounts up to 30 % of the absorbed energy. These losses can be minimized by implementing a co-current tube and shell heat-exchanger assembly where a microwave transparent liquid flowing through the shell side is used for energy recovery. However, this is beyond the scope of the present paper. At a load diameter of $1.2 \cdot 10^{-2}$ m, microwave leakage from the cavity was observed via the flowing liquid therefore the largest diameter studied was limited to $1.1 \cdot 10^{-2}$ m. The heating efficiency monotonously increased with the load diameter reaching to a maximum of 78 % at the load diameter equal

to the half wavelength of EM-field in the liquid (Eq. 3.9). The heating rate in this case was similar to that under stop-flow conditions.

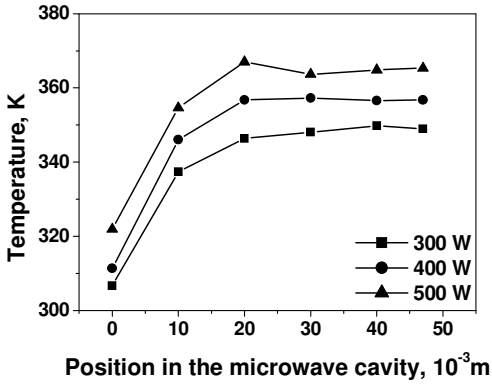

Figure 3.6: Steady state temperatures along the axial direction of the load at continuous-flow conditions at different applied microwave powers. Flow rate: $4.16 \cdot 10^{-7}$ - $1.66 \cdot 10^{-6}$ m^3/s, load diameter: $4 \cdot 10^{-3}$ m. The steady state temperatures were recorded at six different positions by simultaneously moving two fiber optic sensors which stayed at a distance of $3 \cdot 10^{-2}$ m from each other along the axial direction.

The steady state temperature profiles were recorded for a load diameter of $4 \cdot 10^{-3}$ m at liquid flow rates from $4.16 \cdot 10^{-7}$ to $1.66 \cdot 10^{-6}$ m^3/s (Figure 3.6). In these experiments the applied power was increased proportionally to the flow rate in order to get comparable heating rates. A clear temperature profile emerged till $2 \cdot 10^{-2}$ m from the inlet while leveling off was observed in the 2nd half of the of the cavity length. The flowing liquid can create a temperature gradient in the direction of the flow as a combination of volumetric heating and convective mass flux. As a result of this gradient, both the dielectric constant and dielectric loss of ethylene glycol will change and result in a non-uniform intensity of the EM field along the flow direction. Thus, there may exist regions with higher and lower intensities of the EM field. It can be said that the higher intensity region is up to a distance of $2 \cdot 10^{-2}$ m from the inlet based on the presence of a high initial heating rates in this region. On the contrary, the region near the outlet ($2 \cdot 10^{-2}$ - $4.7 \cdot 10^{-2}$ m) may have a lower intensity of the EM field. This can be concluded from the fact that the volumetric heat generation is lower than the heat losses to the surroundings which resulted in flat temperature profiles in the $2 \cdot 10^{-2}$ - $4.7 \cdot 10^{-2}$ m interval. It should also be mentioned that the steady state heating efficiency is lower as compared to that observed during the start-up intervals (Figure 3.5a) due to a non-inform field

intensity and a possibility of multiple reflections at the air/glass interface which further reduced the heating efficiency. Because the steady state temperature distribution in the load depends on the EM field distribution and the field distribution in turn depends on the temperature gradient in the load, the procedure to describe spatial distribution of both the parameters inside the cavity requires 3D numerical simulations of the EM field with temperature dependant properties which were obtained in this study. Such simulations should provide a useful insight into specific distribution of the volumetric heating as a function of the flow rate and temperature, which can be used for more optimal reactor design.

3.4 Conclusions

The effect of the load diameter and loss tangent on the heating efficiency of ethylene glycol was determined in a monomode microwave cavity under stop-flow and continuous-flow conditions. Newly developed heating efficiency analysis of the microwave heated stop-flow and continuous-flow reactors took into account the thermal losses to the surrounding air. Under stop-flow conditions, the highest heating efficiency of 70 % was observed at the load diameter equal to and above the half wavelength of the electromagnetic field in the liquid. It decreased at higher temperatures due to a decreasing heating rate and a monotonous drop in loss tangent with increasing temperature. The heating efficiency, at continuous-flow conditions increased linearly with the load diameter reaching to a maximum of 78%. However, microwave leakage above the propagation diameter restricted further experimentation at higher load diameters. The heat flux to the surrounding increased from 200 to 1000 W/m^2 at higher temperatures and it amounted up to 30 % of the absorbed energy. Under continuous-flow conditions, the steady state load temperature did not raise monotonously along the axial direction of the load, suggesting the existence of high and low field intensities of the EM field. In this case, the heating efficiency dropped due to a non-inform field intensity and a possibility of multiple reflections at the air/glass interface.

Nomenclature

Symbol	Description
A	heat transfer area, m^2
C_p	heat capacity, J/kg.K
Gr	Grashof number
g	acceleration due to gravity, m/s^2
$\bar{h}$	heat transfer coefficient, $W/m^2 \cdot K$
L	length of the cylindrical load, m
m	mass of the sample, kg
$\dot{m}$	mass flow rate, kg/s
Nu	Nusselt number
P_a	absorbed energy, W
P_{in}	microwave set energy input, W
P_{heat}	Energy gained by the liquid, W
P_{loss}	energy lost to the surrounding, W
Pr	Prandtl number
ΔT_1	temperature change over time, K
ΔT_2	difference between the outlet and inlet liquid temperature, K
Δt	time interval, s
$tan\ \delta$	loss tangent
Greek symbols	
ε'	dielectric constant
ε''	dielectric loss
λ	wavelength of the electromagnetic field in a liquid, m
λ_0	wavelength of the electromagnetic field in free space, m
η	heating efficiency, %
k	thermal conductivity of liquids, $W/m \cdot K$
α	thermal expansion coefficient,1/K
ρ	Density, kg/m^3
μ	Viscosity, Pa.s

References

1. Kappe, C. O. Controlled microwave heating in modern organic synthesis. *Angew. Chem. Int. Ed.* **2004,** *43,* 6250.
2. Mingos, D. M. P.; Baghurst, D. R. Applications of microwave dielectric heating effects to synthetic problems in chemistry. *Chem. Soc. Rev.* **1991,** *20,* 1.
3. Nuchter, M.; Ondruschka, B.; Bonrath, W.; Gum, A. Microwave-assisted synthesis – a critical technology overview. *Green Chem.* **2004,** *6,* 128.
4. Lidstrom, P.; Tierney, J.; Wathey, B.; Westman, J. Microwave assisted organic synthesis – a review *Tetrahedron.* **2001,** *57,* 9225.
5. Hayes B. L. Microwave synthesis: chemistry at the speed of light. CEM publishing, Matthews NC. 2002.

6. Lidstrom, P.; Tierney, J. P. Microwave-assisted organic synthesis. Blackwell, Oxford. 2004.
7. Larhed, M.; Olofsson, K. Microwave methods in organic synthesis. Springer, Berlin. 2006.
8. Moseley, J. D.; Lawton, S. J. Initial results from a commercial continuous-flow microwave reactor for scale-up. *Chem. Today*. **2007,** *25,* 16.
9. Stadler, A.; Yousefi, B. H.; Dallinger, D.; Walla, P.; Van der Eycken, E.; Kaval, N.; Kappe, C. O. Scalability of microwave-assisted organic synthesis. From single-mode to multimode parallel batch reactors. *Org. Process Res. Dev.* **2003,** *7,* 707.
10. Al-Rizzo, H. M.; Ma, F.; Tranquilla, J. M. Incorporation of waveguide feed and cavity wall losses in a Cartesian/cylindrical hybrid finite-difference time domain (FD-TD) analysis of microwave applicator. *J. Microwave Power EE*. **2000,** *35,* 110.
11. Braunstein, J.; Connor, K.; Salon, S.; Libelo, L. Investigation of microwave heating with time varying material properties. *IEEE Trans. Magnetics.* **1999,** *35,* 1813.
12. Clemens, M.; Gjonaj, E.; Pinder, P.; Weiland, T. Numerical simulation of coupled transient thermal and electromagnetic fields with the finite integration method. *IEEE Trans. Magnetics.* **2000,** *36,* 1448.
13. Prosetya, H.; Datta, A. Batch microwave heating of liquids: an experimental study. *J. Microwave Power EE*. **1991,** *26,* 215.
14. Kappe C.O. Microwave dielectric heating in synthetic organic chemistry. *Chem. Soc. Rev.* **2008,** 37, 1127.
15. Hoogenboom, R.; Wilms, T. F. A.; Erdmenger, T.; Schubert, U. S. Microwave-assisted chemistry: a closer look at heating efficiency. *Aust. J. Chem.* **2009,** *62,* 236.
16. So, H. W.; Taube, A. Modelling and experimental investigation of microwave heating of adhesively bonded polypropylene joint. *Int. J. Adhesion Adhesives*. **2004,** *24,* 307.
17. Ma, J.; Diehl, J. F.; Johnson, E. J.; Martin, K. R.; Miskovsky, N. M.; Smith, C. T.; Weisel, G. J.; Weiss, B. L. Zimmerman, D. T. Systematic study of microwave absorption, heating, and microstructure evolution of porous copper powder metal compacts. *J. Appl. Phys.* **2007,** *101,* 074906-1.
18. Cao, Z.; Yoshikawa, N.; Taniguchi, S. Directional selectivity of microwave H field heating of Au thin films and non-doped Si plates. *Materials Chem. Phys.* **2009,** *117,* 14.
19. Housova, J.; Hoke, K. Microwave heating – the influence of oven and load parameters on the power absorbed in the heated load. *Czech. J. Food Sci.* **2002,** *20,* 117.
20. Murphy, E. K.; Yakovlev, V. V. CAD of microwave chemistry reactors with energy efficiency optimized for multiple reactants. *26th Annual review of progress in Applied Computational Electromagnetics.* **2010,** 431.
21. Schon, U.; Messinger, J.; Eichner, S.; Kirschning, A. Comparison of monomode and multimode microwave equipment in Suzuki–Miyaura reactions– *en route* to high-throughput parallel synthesis under microwave conditions. *Tet. Lett*. **2008,** *49,* 3204.
22. Nour, H. A.; Sothilakshmi, R.; Nour, A. Microwave heating and separation of water-in-oil emulsions: an experimental study. *Int. J. Chem. Tech.* **2010,** *2,* 1.
23. Hao, C.; Juming, T.; Fang, L. Coupled simulation of an electromagnetic heating process using the finite difference time domain method. *J. Microwave Power EE.* **2007,** *41,* 50.

24. Robinson, J.; Kingman, S.; Irvine, D.; Licence, P.; Smith, A.; Dimitrakis, G.; Obermayer, D.; Kappe, C. O. Understanding microwave heating effects in single mode type cavities — theory and experiment. *Phys. Chem. Chem. Phys.* **2010,** *12,* 4750.
25. Welty, J. R.; Wicks, C. E.; Wilson, R. E. Fundamentals of Momuntum, Heat, and Mass Transfer. John Wiley & Sons, New York. 1984.
26. Lide, D. R. CRC Handbook of Chemistry and Physics. Taylor & Francis group, Boca Raton. 2000.
27. Metaxas A. C.; Meredith R. J. Industrial microwave heating. Peter Peregrines Ltd, London. 1983.
28. Gabriel, C.; Gabriel, S.; Grant, E. H.; Ben S. J.; Halstead, B. S. J. Mingos, D. M. P. Dielectric parameters relevant to microwave dielectric heating. *Chem. Soc. Rev.* **1998,** *27,* 213.

4

Energy efficient and controlled flow processing under microwave heating by using a milli reactor–heat exchanger

This chapter is published as:
Patil, N. G.; Hermans, A. I. G.; Benaskar, F.; Rebrov, E. V.; Meuldijk, J.; Hulshof, L. A.; Hessel, V.; Schouten, J. C.; Energy efficient and controlled flow processing under microwave heating by using a milli reactor-heat exchanger. *AIChE J.* **2011**, *Accepted*, DOI 10.1002/aic.13713.

Abstract

In this chapter, a continuously operating microwave heated milli reactor setup has been developed for performing reactions of highly microwave absorbing media in a controlled and energy efficient manner. The setup consists of a tubular reactor integrated with a heat exchanger. A microwave transparent liquid was used as coolant to extract the excess heat from the reaction mixture, thus controlling the temperature of the reaction mixture by avoiding overshoots and subsequent boiling. A reactor-heat exchanger shell and tube unit with a diameter of the inner tube of $3 \cdot 10^{-3}$m and a shell of $7 \cdot 10^{-3}$ m inner diameter has been manufactured in quartz. The unit size was defined based on simulation with a heat-transfer model for the microwave cavity part. Microwave heating was incorporated as a volumetric heating source term using the temperature-dependent dielectric properties of the liquid. Model predictions were validated with measurements for a range of $0.167 \cdot 10^{-6}$ to $1.67 \cdot 10^{-6}$ m^3/s flow rates of coolant. The outlet temperature of both the reaction mixture and the coolant, were predicted accurately (tolerance of 3 K) and the process window was determined. The model for the reactor part provided the required length of the reactor for a solid (ion exchange) catalyzed esterification reaction. The predicted conversions, based on the obtained temperature profile in the reactor packed with the catalyst bed, known residence times and kinetics of the esterification reaction, were found to be in good agreement with the experimental results. Efficient utilization of microwave energy with heat recovery up to 20% of the total absorbed microwave power and heating efficiencies up to 96% were achieved.

4.1 Introduction

Over the last few decades, there has been a growing interest in the use of microwave heating as an enabling technology to perform high speed organic synthesis with better process selectivity and product yield. Many chemists showed a spectacular increase of the reaction rates in several batch processes in domestic microwave ovens.[1] However, one of the major obstacles for future applications of the microwave technology at industrial scale is scaling up due to the limited penetration depth of microwaves (few millimeters) resulting in heating by convection in the center of large batch reactors instead of direct 'in core' heating by microwaves.[2] For continuously operated milli reactors, the penetration depth problem does not exist and scale up is done by parallelization.[2-5]

Several authors presented their continuously operating microwave integrated reactor setup for performing a diversity of chemical reactions. Although they reported an increase in yield,[4] the presence of hot spots[6-8] and an increase of the reaction rate,[9] there was a lack of insight into the actual amount of transferred energy which is important for efficient scale up. Esveld *et al.*[10,11] calculated the efficiency of microwave heating to be 37%, while the remaining energy was mostly lost as a result of indirect heating of the support and the surrounding air. In this case, use of a multimode microwave cavity, due to its uneven electromagnetic field distribution, resulted in a low reproducibility and efficiency.[12,13] Patil *et al.*[14] showed that monomode microwave applicators providing a well defined electric field pattern can be a suitable option for transforming fine chemical batch processes into a continuous operation with higher efficiency and reproducibility.

Accurate temperature measurements are crucial for a proper interpretation of microwave heating effects. However, several articles described indirect methods of temperature measurements such as infrared detectors.[3,15-17] Such indirect methods resulted in measuring the temperatures of the reactor wall instead of the reaction medium, subsequently leading either to alleged microwave effects or to poor understanding of the temperature distribution. However, temperature measurements can be done more accurately by using a fiber-optic sensor.[8-10] These sensors

inserted in the reaction mixture, measure the temperature directly and are microwave transparent and do not disturb the microwave field.[18]

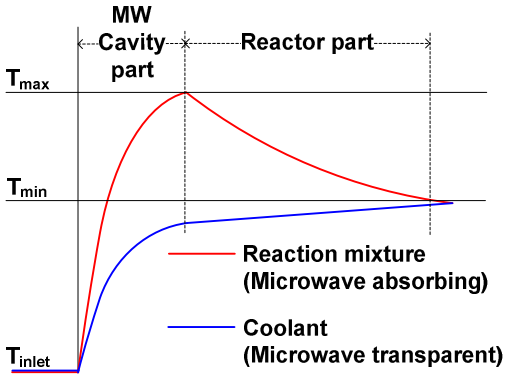

Figure 4.1: Schematic representation of temperature profiles in an integrated reactor-heat exchanger for flow processing with microwave heating.

A completely thermally insulated continuous flow recycle monomode microwave reactor is reported by Chemat *et al.*[4] This configuration allows high microwave absorption due to improved interaction between the microwave field and the reaction mixture.[13,16] The high energy intensity of the focused microwaves, however, makes an efficient and controlled operation impossible especially when a strong microwave absorbing solvent is used. Some of the proposed continuous flow reactor systems suggest use of a dead load to extract the excess of microwave energy for avoiding runaway.[3,15] A tubular reactor integrated with a heat exchanger can provide a solution in such cases where a co-currently flowing microwave transparent (non-polar) solvent is used as coolant to avoid overheating of the reaction mixture (Figure 4.1). Additionally, because of co-current operation rather than counter current, the excess of heat can also be used to maintain the reaction temperature over longer lengths of a continuously operated tubular reactor outside the microwave cavity.

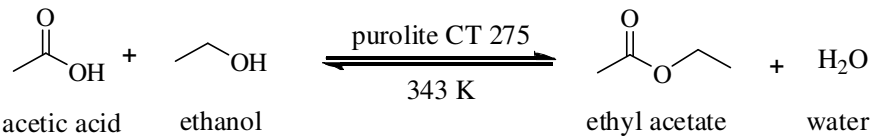

Scheme 4.1: Esterification of acetic acid and ethanol over a solid ion-exchange catalyst to produce ethyl acetate.

In this chapter, we present an integrated heat exchanger reactor system for efficient and controlled flow processing of highly microwave absorbing reaction media. Esterification of ethanol and acetic acid at around 343 K was chosen as a model reaction (Scheme 4.1). Toluene, being a microwave transparent solvent, was used as coolant. To achieve insight into the temperature profiles the reactor-heat exchanger system was divided in two parts *i.e.* the microwave cavity and the reactor downstream the cavity (Figure 4.2). Heat transfer models were developed to describe the temperature profiles for the reaction mixture and the coolant in both parts. Both models were validated experimentally while depicting the controllability and efficiency of operation.

4.2 Theoretical modeling

In the microwave cavity part of the proposed integrated reactor-heat exchanger, microwave energy absorbed by the reaction mixture gets distributed between the reaction mixture, coolant and heat losses to the surroundings. Note that the reaction mixture being the only microwave absorbing component takes up all the microwave energy present in the cavity which subsequently gets transferred to the non absorbing coolant by conduction and convection. Part of the energy absorbed by the coolant gets lost to the surroundings by natural convection. In the reactor part the heat lost by the reaction mixture is equal to the energy gained by the coolant. The overall energy balances for both parts are schematically depicted in Figure 4.2.

Although the reactor part is thermally insulated, the reaction mixture cools down over the reactor length. However, the warm coolant here acts like an extra insulation medium, allowing the reaction mixture to cool gradually. This axial temperature profile was determined by modeling the heat transfer in the fixed bed reactor part. Conversion as a function of the axial position can be calculated by including temperature dependent kinetics of the reaction and by solving standard fixed bed equations.[19]

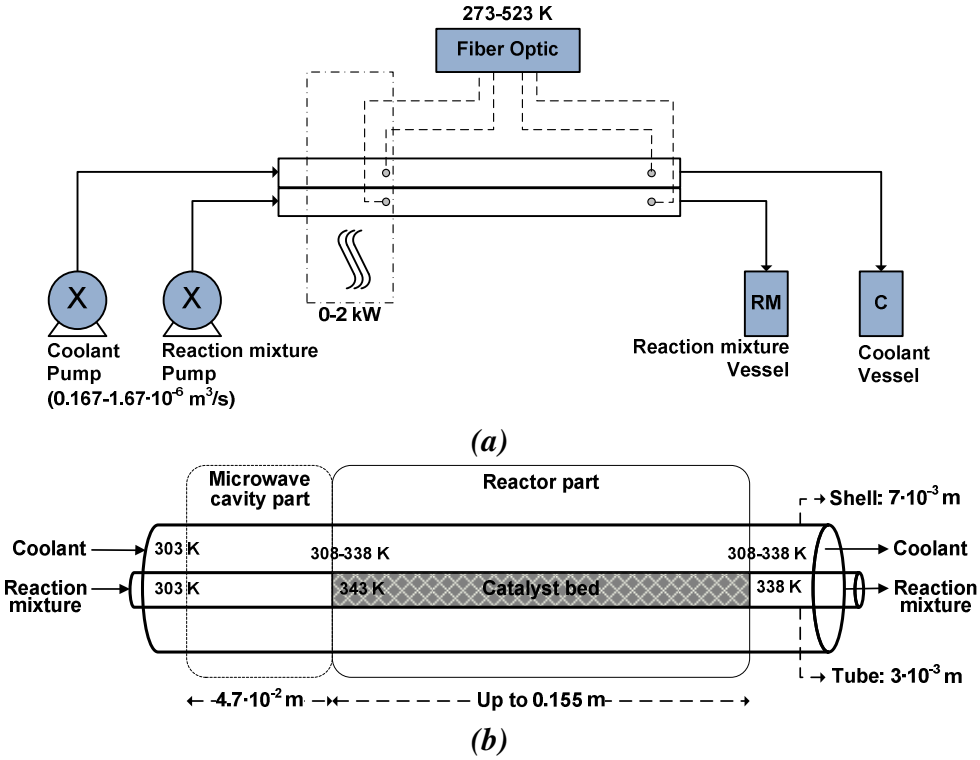

Figure 4.2: (a) Process flow diagram (b) Schematic of the integrated reactor-heat exchanger system with process details, divided into the microwave cavity part and the reactor part, including overall energy balances.

4.2.1 2D heat transfer model for the microwave cavity part

A pseudo 2D model was developed in COMSOL Multiphysics for the microwave cavity part to estimate the dimensions of the reactor and the range of operating conditions (Figure 4.6). Microwave heating was incorporated as a volumetric heating term in the micro heat balance. It was based on the temperature-dependent dielectric properties of the reaction mixture, see the sub-section on volumetric heating. The physical properties of strongly microwave absorbing ethanol, being in excess, were used as reaction mixture properties (microwave absorbing liquid) and those of microwave transparent toluene were used as coolant properties (Table 4.1).[20]

Table 4.1: Physical properties of reaction mixture (ethanol), coolant (toluene) and walls (quartz)

Property	Ethanol	Toluene
Thermal conductivity [k, W/(m.K)]	0.167	0.14
Density [ρ, kg/m^3]	842.76	866.9
Heat capacity [C_p, J/(kg.K)]	2359.34	1698.5
Viscosity [μ, Pa.s]	$1.201 \cdot 10^{-3}$	$0.548 \cdot 10^{-3}$

The tube and shell walls of the heat exchanger were modeled with the physical properties of quartz (k = 1.38 W/m.K). The hydrodynamics of laminar flow was described by the incompressible Navier-Stokes equations (Eq. 4.1). A standard micro heat balance (Eq. 4.2) was used to determine the temperature profiles in the liquids, while heat transfer to the solid wall was used as a boundary condition in solving the micro heat balance in the microwave cavity. The quadrangle element was used as the basic element type for the mesh (mapped mesh parameters), consisting of 4560 elements. The direct linear system solver (UMFPACK) was used to determine the temperature profiles of the reaction mixture and the coolant in the microwave cavity part.

$$\rho\frac{\partial u}{\partial t}+\rho(u\cdot\nabla)u=\nabla\cdot\left[-pI+\mu\left(\nabla u+(\nabla u)^{T}\right)\right]+F \tag{4.1}$$

$$\rho C_{P}\left(\frac{\partial T}{\partial t}+u.\nabla T\right)=\nabla.(k\nabla T)+Q \tag{4.2}$$

4.2.1.1 Assumptions and constraints

Heat transport was computed with the following assumptions:

- The reactor material (quartz) and the coolant (toluene) are microwave transparent.
- The volumetric heating source is uniform in the radial and axial directions of the load.
- Considering laminar flow, the heat transfer coefficients are averaged over the length of the microwave cavity.

The dimensions of the microwave cavity part had the following restrictions:

- The length of the microwave cavity is $4.7\cdot10^{-2}$ m; within this length the temperature of the reaction mixture has to increase from room temperature *i.e.* 303 K to 343 K.
- Outer diameter of the shell cannot be larger than 9 mm due to physical limitations of the setup.

- Minimum required space between the shell and tube and the minimum diameter of the inner (reactor) tube is 1.1 mm to facilitate insertion of fiber optic sensors for validation experiments.

4.2.1.2 Heat transfer coefficients

With fully developed flow of an incompressible fluid through a circular duct and constant heat flux to the wall, the Nusselt number can be assumed to be 4.36.[19] By using this Nusselt value and the thermal conductivity of ethanol (k = 0.167 W/m.K), the heat transfer coefficient of the reaction mixture (h_{RM}) was calculated to be 243 W/m^2.K. The Nusselt value is dependent on the ratio of the inner and the outer diameter for laminar flow through the annular region of the coaxial circular duct[21] and was found to be 8.1, assuming constant heat flux to the wall. By using this Nusselt value and the thermal conductivity of toluene (k = 0.14 W/m.K), the heat transfer coefficient of the coolant (h_C) was calculated to be 378 W/m^2.K. The heat transfer coefficient for the heat losses to the surroundings by natural convection (h_{surr}) was assumed to be 10 W/m^{2}K. Heat transfer in the microwave cavity was assumed to be in series, where heat was transferred from the reaction mixture to the coolant and from the coolant to the surroundings. Thus, the overall heat transfer coefficients at the reaction mixture boundary (U_{RM}) and coolant boundary (U_C) were calculated to be 154.0 W/m^2.K and 11.7 W/m^2.K, respectively.

4.2.1.3 Volumetric heating

Microwave heating was incorporated as a volumetric heating term using the equation of Metaxes and Meredith[22], see Eq. 4.3.

$$Q_{MW} = 2\pi f \varepsilon_0 \varepsilon'' E^2 V_R \tag{4.3}$$

The dielectric loss (ε'') in Eq. 4.3 depends on the temperature. This dependency was determined by using a dielectric probe kit and network analyzer,[14] resulting in Eq. 4.4 based on experimental data in Figure 4.3.

$$\varepsilon'' = -1.9328 \cdot 10^{-3} T^2 + 1.2005 T - 1.7846 \cdot 10^2 \tag{4.4}$$

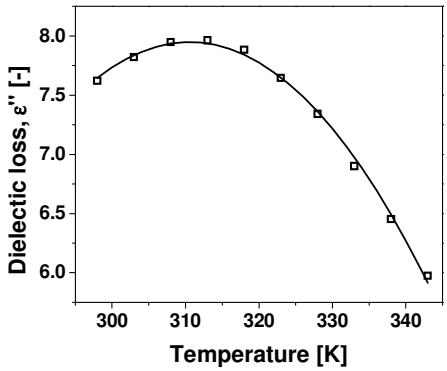

Figure 4.3: Dielectric loss (ε") of ethanol as a function of the temperature. Symbols: experimental values; Line: polynomial fit.

The electric field intensity (E) at the reactor opening (Figure 4.4) was empirically determined as a function of the applied power (Q_{cav}, Eq. 4.5) for small temperature gradients (≤ 5 K), *i.e.* no heat loss to the surroundings (Q_{loss} = 0) and constant dielectric properties (ε' and ε'') of the used solvent. This resulted in the empirical equation 4.5 based on the data in Figure 4.4.

$$E = 1.150 \cdot 10^{-3} Q_{cav}{}^{3} - 4.673 \cdot 10^{-1} Q_{cav}{}^{2} + 1.043 \cdot 10^{2} Q_{cav} + 2.334 \cdot 10^{3} \quad (4.5)$$

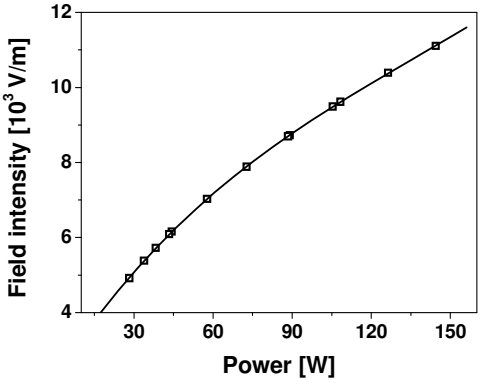

Figure 4.4: Electric field intensity as a function of microwave power. Symbols: experimental values; Line: polynomial fit.

The equations 4.4 and 4.5 were inserted as scalar expressions in the respective sub-domains for instantaneous quantification of the volumetric heating term in the micro heat balance.

4.2.2 1D Heat transfer model for the reactor part

The design of the reactor, was aimed at keeping the temperature of the reaction mixture as long as possible constant and at least between 343 and 338 K (T_{max} and T_{min} respectively, see Figure 4.1). Although the esterification reaction was slightly exothermic (-2400 J/mol, Appendix A), it was necessary to insulate the heat exchanger to avoid heat losses to the surroundings. To predict the axial temperature profiles in the reaction part after the microwave cavity, Polymath (Version: 6.10) was used. The temperatures were described by two coupled one dimensional differential equations described in following sub section on energy balances.

4.2.2.1 Assumptions and constraints

- Heat is transferred through the wall of the reactor.
- Perfect radial mixing *i.e.* no radial temperature gradient in the packed bed reactor.
- Heat of reaction is negligible.
- No heat loss to the surroundings.

4.2.2.2 Energy balances

The energy balances for a plug flow reactor in terms of molar flow rates are presented in Eq. 4.6 and Eq. 4.7.[19]

$$\frac{dT_{RM}}{dL} = A_{RM} \frac{U^*_{RM}\left(T_C - T_{RM}\right)}{\dot{m}_{RM}\, C_{P-RM}} \tag{4.6}$$

Similarly, the coolant temperature varied over the length of the reactor part.

$$\frac{dT_C}{dL} = A_C \frac{U^*_C\left(T_{RM} - T_C\right)}{\dot{m}_C\, C_{P-C}} \tag{4.7}$$

The coupled differential equations were simultaneously solved using Polymath for a range of coolant flow rates. The overall heat transfer coefficient terms (U^*_{RM} and U^*_C) were used as fitting parameters.

4.2.3 Modeling of the chemical reaction

The length of the reactor part, giving temperatures between 343 and 338 K (T_{max} and T_{min}) was determined from the temperature profiles of the liquids given by the heat transfer model of the reactor part. Subsequently the conversion is determined by the amount of solid catalyst, varying with the length of the reactor part, and can be described by the standard design equations for a isothermal packed bed reactor with a pseudo first order irreversible reaction (Eq. 4.8).[19] Thus, the heat transfer model of the reactor part as described in earlier section was further extended by incorporating Eq. 4.9 for chemical reaction modeling to predict conversions.

$$F_v^A dC_A = r_A^{'} = k_{(T)}^v C_A dW \tag{4.8}$$

$$X = \left(1 - \left(\exp\left(\frac{k^v}{F_v} W \right) \right)^{-1} \right) 100\% \tag{4.9}$$

Constant pressure was assumed as Ergun equation predicted a pressure drop of $1.8 \cdot 10^4$ Pa for the longest packed bed of 0.155 m (Appendix B).[19] From batch experiments, the volumetric reaction rate constant was found to be $3.3 \cdot 10^{-3}$ s^{-1} at 343 K (Appendix C). Based on the Arrhenius equation, the activation energy and the pre-exponential factor were calculated to be 53.5 kJ/mol and $2.6 \cdot 10^6$ s^{-1} respectively. The heat produced by the reaction for 10% conversion was found to be negligible at $4.9 \cdot 10^{-2}$ W (Appendix A). Therefore, the reaction rate coefficient was assumed to be constant with respect to temperature (343 K) by ignoring the heat of reaction.

4.3 Experimental set-up and procedures

Figure 4.2 schematically illustrates the process details of the integrated reactor-heat exchanger system. Both the liquids, reaction mixture and coolant, while flowing through the integrated reactor-heat exchanger, first enter the microwave cavity part where the reaction mixture is heated directly by the microwaves and excess of the microwave energy gets transferred to the coolant by heat transfer. At the outlet of the microwave cavity part, the reaction mixture at the reaction temperature *i.e.* 343 K and the coolant with similar elevated temperature enter the reactor packed with catalyst over the predetermined reactor length.

4.3.1 Equipment and chemicals

The microwave setup was designed and developed in collaboration with Fricke und Mallah GmbH (Figure 4.5). The system consisted of a single mode microwave cavity operating at a frequency of 2.45 GHz with adjustable power settings up to 2 kW.[14] Process control and data acquisition over the entire setup was performed via the LABVIEW program. The reflected power was recorded by using a detector diode on an isolator. The power available in the cavity could be calculated with an accuracy of approximately 10%.

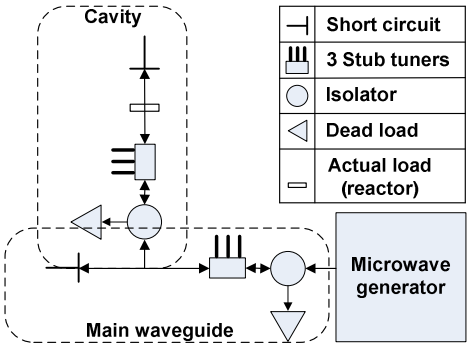

Figure 4.5: Schematic view of microwave setup with microwave energy flow in the setup. Arrows showing directions of wave propagation.

The reactor-heat exchanger consisted of two quartz tubes (Figure 4.2), connected with T-junctions for liquid supply and temperature measurement ports. Heat transfer modeling (see previous section) results revealed that the most suitable diameter for the inner (reactor) tube was $3 \cdot 10^{-3}$ m with a wall thickness of $5 \cdot 10^{-4}$ m,

whilst the shell diameter is $7 \cdot 10^{-3}$ m with a wall thickness of $1 \cdot 10^{-3}$ m. Teflon spacers were used to support the reactor-heat exchanger in axially centric position and also to prevent heat losses to the metal supports. Standard insulation foam was used for insulating the reactor part outside the microwave cavity. Gilson HPLC pumps (flow range: $8.33 \cdot 10^{-9}$ to $2.5 \cdot 10^{-6}$ m^3/s) were used to supply the reaction mixture and the coolant to the inner (reactor) tube and the shell, respectively. Fiber optic sensors, type OTG-A, supplied by OpSense® were used to record the temperature inside the reactor tube and the surrounding shell.

4.3.2 Experimental procedures

Two types of experiments were performed; *i.e.* physical experiments for the determination of temperature profiles inside the microwave cavity and reactor, and chemical experiments for determining the conversion.

4.3.2.1 Physical experiments: determining the temperature profiles of the reaction mixture and coolant

The temperature profiles in the microwave cavity and in the reactor part are necessary to validate both heat transfer models (see previous section). Before starting the physical experiments, the quartz reactor-heat exchanger was placed at a fixed position in the reactor opening of the microwave cavity. After focusing the microwaves on the reaction mixture and placing the fiber optic sensors in the required position, the temperature measurements were ran for few minutes after reaching the steady state. The temperature was recorded against time by using the LABVIEW program. The reaction mixture had a steady state within a few seconds, but a few minutes (around 300 s) of run time was needed to reach the steady state temperature of the coolant because conduction and convection were not as fast as heating by the microwaves. Four fiber optic sensors were simultaneously used for experimental determination of temperature profiles in the reactor tube and shell over the whole length (every $1 \cdot 10^{-2}$ m) of the microwave cavity and reactor parts.

4.3.2.2 Chemical experiments: determining the conversion

In this study, the heterogeneously catalyzed esterification of acetic acid (99.8%, Sigma Aldrich) and ethanol (99.8%, Sigma Aldrich) was chosen as a model reaction (Scheme 4.1).[23] In order to increase the conversion for this equilibrium-limited reaction, a 5-fold excess of ethanol was chosen because of its polarity and enhanced microwave absorption. The reaction was performed between 338 and 343 K (Figure 4.1). The maximum temperature was set at 343 K to avoid boiling of ethanol.[4] The catalyst, an acidic ion exchange resin (CT 275, Purolite®) with average particle diameter of $750 \cdot 10^{-6}$ m, was dried before use for 2 days at room temperature. The experiments were performed by packing the pre-determined length of the reactor part with catalyst. The reaction mixture flowing through the microwave cavity got heated to the reaction temperature and entered the catalyst bed for actual reaction before leaving the system towards the collection vessel. Samples were taken over time and analyzed by gas chromatography (GC) to determine the conversion. The samples for GC analysis were diluted with methyl isobutyl ketone (99.8%, Sigma Aldrich) with a dilution of 10 wt% to lower the concentrations of ethanol and acetic acid to precisely determine the concentrations of the reaction components. From the GC-results, the conversion of acetic acid, the limiting reactant, was calculated over time. After a single pass through the catalyst bed, the conversion was below 0.5%, resulting in large errors by GC-analysis and therefore, the reaction mixture was recycled. During these recycles, the collection vessel of the reaction mixture was stirred firmly at 500 rpm.

4.4 Results & discussion

The heat transfer models, developed for the microwave cavity and reactor sections and the model of the chemical reaction were validated by experiments. The experimental results as well as the results of the model predictions are discussed in detail in the following sections.

4.4.1 Validation of the temperature profile in the microwave cavity part

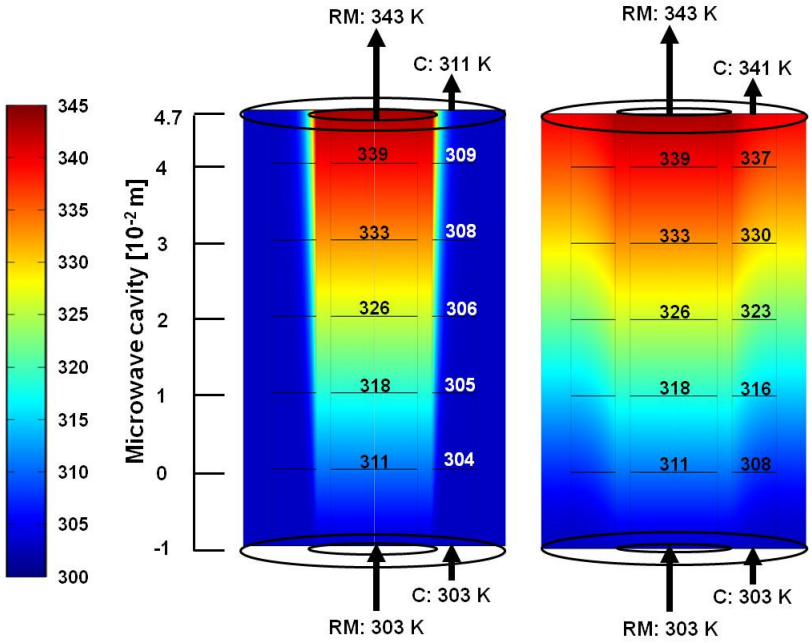

Figure 4.6: Modeling results for two different flow rates of coolant, $8.33 \cdot 10^{-7}$ m^3/s (a) and $8.33 \cdot 10^{-9}$ m^3/s (b), at constant flow rate of the reaction mixture: $6.66 \cdot 10^{-7}$ m^3/s, available power: 163 W. Numbers on several internal boundaries show temperature at the respective boundary. RM: reaction mixture, C: coolant.

The obtained model predictions by the 2D heat transfer model for the microwave cavity part are shown in Figure 4.6. The modeling results demonstrated that the flow rate of the coolant has a negligible influence on the outlet temperature of the reaction mixture even at 100 times increase in the coolant flow rate (Figure 4.6). Thus controlling the outlet temperature of a highly microwave absorbing reaction mixture by varying the flow rate of the coolant was not possible in the chosen reactor-heat exchanger geometry. There can be two reasons for this, *i.e.* firstly, the limited heat transfer area due to the design restrictions of the reactor-heat exchanger and, secondly, the time constant for microwave heating is much lower than the time constant for convective heat transfer to the coolant. However, the results of the model predictions demonstrate that the outlet temperature of the reaction mixture could be well controlled by adapting the flow rate of the reaction mixture and the applied microwave power. The experimental results demonstrated that at a distance of $1 \cdot 10^{-2}$ m before the microwave cavity, the reaction mixture and the coolant were already heated to a temperature considerably above room temperature (Figure 4.7,

data point at 0 m), due to the propagation of microwaves outside the cavity in the direction of the liquids inlet. Therefore, the volumetric heating source in the heat transfer model was also added for this $1 \cdot 10^{-2}$ m making the microwave cavity $1 \cdot 10^{-2}$ m longer than its actual size of $4.7 \cdot 10^{-2}$ m mm (Figures 6 and 7).

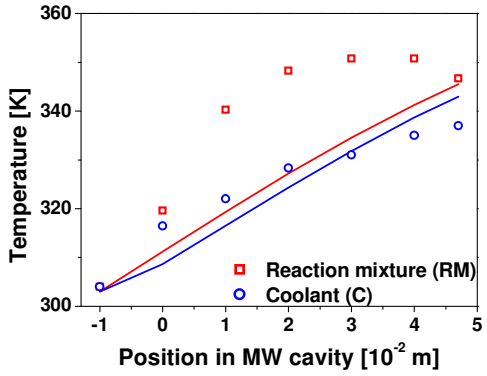

Figure 4.7: Model versus experimental data, showing temperature profiles of the reaction mixture (RM) and the coolant (C) inside the microwave cavity. Symbols: experimental results; Lines: model predictions. Flow rates RM: $6.66 \cdot 10^{-7}$ m^3/s, C: $8.33 \cdot 10^{-9}$ m^3/s, available power: 163 W.

Inside the cavity, a linear increase of temperature for both the reaction mixture and the coolant was predicted by the model while an exponential rise was observed experimentally (Figure 4.7). The model predicted a linear temperature increase in both the liquids because microwave heating was incorporated as a volumetric heating source with a constant and uniform field distribution over the entire load rather than taking into account instantaneous interaction of the microwaves with varying applied load (*i.e.* changing dielectric constant, ε'). Note that this simplified modeling of the microwave heating process has previously proven to be useful in predicting temperature profiles of the reaction mixture.[3] A hot spot was observed for the reaction mixture around $2 \cdot 10^{-2}$ m inside the microwave cavity (Figure 4.8). The temperature of this hot spot was higher when no coolant was present in the shell of the reactor-heat exchanger (Figure 4.8). Thus, the coolant plays the role of avoiding overheating of the reaction mixture by taking up excessive microwave energy. Further studies to understand the hot spot formation inside the microwave cavity especially with a focus on the field distribution are discussed in chapter 5.

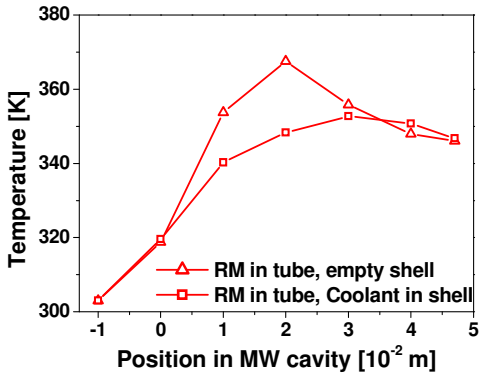

Figure 4.8: Experimentally observed temperature profile of the reaction mixture (RM) with (open square) and without (filled square) coolant flow in the shell. Flow rate RM: $6.66 \cdot 10^{-7}$ m^3/s, C: $8.33 \cdot 10^{-9}$ m^3/s, available power: 150-160 W.

Although the axial temperature profile of the reaction mixture in the cavity is not completely understood, the model predicted the outlet temperatures with an accuracy of ± 3 K; therefore the model was further used to determine the process window (Figure 4.9). The graph represents the power needed in the cavity to achieve an outlet temperature of 343 K at the end of the microwave cavity part for different flow rates of the reaction mixture. The flow rate of the coolant was kept constant at $8.33 \cdot 10^{-9}$ m^3/s for all these simulations. In the most favorable situation for the esterification reaction, the flow rate of the reaction mixture should be as low as possible to achieve a long residence time for conducting the reaction in the reactor part. However, in this case a very low microwave power had to be applied (Figure 4.9). Stability of operation restricted the continuous flow setup to a minimum microwave power of 155 W. As a consequence the flow rate of the reaction mixture had to be adapted to $6.66 \cdot 10^{-7}$ m^3/s to achieve an outlet temperature of 343 K (Figure 4.9). Accurate knowledge of the microwave power level in the setup was necessary for further calculation of the microwave heating efficiency.

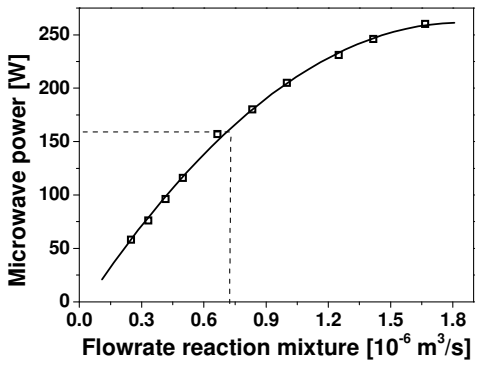

Figure 4.9: Process window for the applied microwave power and reaction mixture flow rate to achieve 343 K at the outlet of the microwave cavity part. Flow rate of the coolant: $8.33 \cdot 10^{-9}$ m^3/s; Symbols: modeling points, Line: a guide to the eye.

4.4.2 Validation of the temperature profile in the reactor part

During the experiments, the inlet temperature of the reactor part was not always exactly 343 K (± 2 K) due to differences in the reflective microwave power. So, for validation of the 1D heat transfer model of the reactor part, the inlet temperatures in the model were adapted to the experimental results. The flow rate of the reaction mixture was kept constant at $6.66 \cdot 10^{-7}$ m^3/s in these experiments (see previous section). The flow rate of the coolant was varied between 8.33 and $250 \cdot 10^{-8}$ m^3/s. A higher coolant flow rate, having a lower coolant temperature at the end of the microwave cavity part, resulted in a larger driving force for heat exchange in the reactor part. This influenced the axial temperature profiles of both reaction mixture and coolant in the reactor part. Heat exchange started at the outlet of the microwave cavity part. So x=0 in Figure 4.10 is the inlet of the reactor part, and the outlet of the microwave cavity part.

The heat transfer model predicted the temperature profile of the reaction mixture quite accurately (Figure 4.10). Deviations in the model predictions from the experiments could be due to errors in the experimental measurements and the different reflective powers during the experiment. The predictions were less accurate for higher flow rates of the coolant, probably because the heat transfer coefficient can be a function of the flow rate in this case, while it was assumed to be constant in the model.

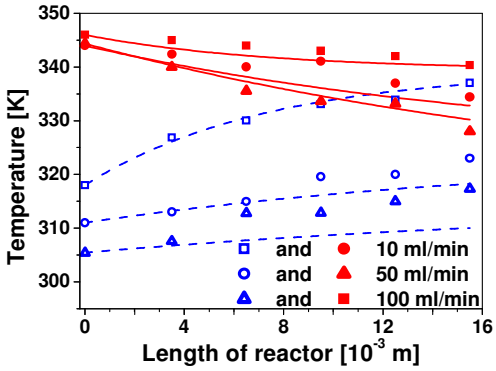

Figure 4.10: Axial temperature profile in the reactor part. Experimental results versus model predictions for different flow rates of the coolant (1.66, 8.33, $16.66 \cdot 10^{-7}$ m^3/s). Flow rate of the reaction mixture: $6.66 \cdot 10^{-7}$ m^3/s, available power: 163 W symbols: experimental data, filled: reaction mixture (RM), open: coolant (C), Lines: modeling results, red lines: reaction mixture (RM), blue lines: coolant (C).

For the esterification reaction, a near isothermal operation with the temperature of the reaction mixture between 338 and 343 K was required. Note that the flow rate of the coolant determined the length of the reactor part for reaction since its temperature at the end of the microwave cavity part influenced the driving force for heat transfer in the reactor part (Figure 4.10). The lengths of the reactor part predicted by the heat transfer model were found to be in good agreement with the experimental results (Figure 4.11). When the coolant flow rate was less than $1.66 \cdot 10^{-7}$ m^3/s, the complete reactor length of 0.155 m could be used for reaction whereas it was about 0.043 m for a coolant flow rate above $1.25 \cdot 10^{-6}$ m^3/s. Thus the optimized integration of heat has clearly lead to good prediction of the length of the reactor part which can essentially be used to conduct a reaction.

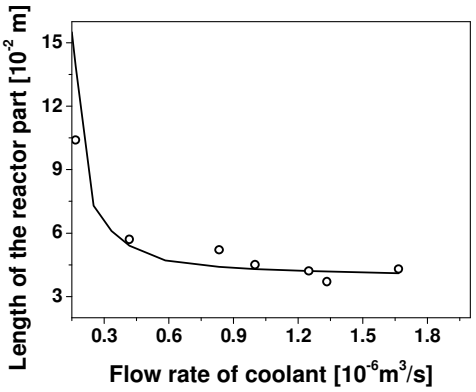

Figure 4.11: Validation of the length of the reactor part. Symbols: experimental data, Line: modeling results.

4.4.3 Validation of chemical reaction

The last step in this study was performing the esterification reaction in the catalyst bed downstream the microwave cavity part. As discussed in the previous section, the length of the reactor and thus the length of the catalyst bed were determined by the flow rate of the coolant. The expected conversion was calculated by incorporating Eq. 4.6 in the heat transfer model of the reactor part and compared with the experimental values. A maximum deviation of 2.5% has been found between the observed and the calculated conversions (Figure 4.12). This presumably was due to an inaccurate determination of the length of the reactor part or inaccurate GC analysis. In conclusion, these validation results demonstrate that microwave heating can be incorporated in milli reactor flow processing in a controllable manner, giving predictable temperatures and conversions.

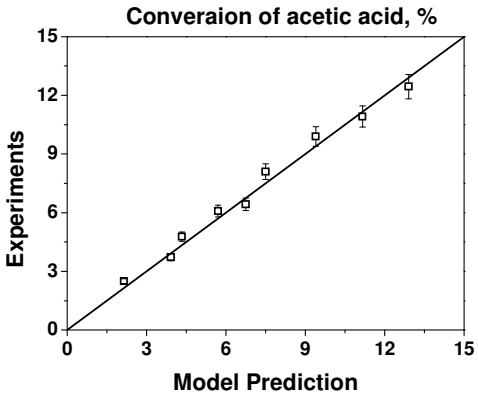

Figure 4.12: Parity plot of experimentally obtained versus model predicted conversion of acetic acid.

4.4.4 Microwave heating efficiency

To make microwave heating a justified heating technology, the energy efficiency has been calculated to check its viability when compared with conventional heating technologies. While heating the reaction mixture with microwaves, some of the power was reflected. The rest of the power was absorbed by the reaction mixture, and the coolant took up some of this energy by heat transfer. A part of this transferred heat got lost to the surroundings. However, considering usability the energy utilized only for heating the reaction mixture and the coolant (Q_{abs}, Eq.

4.10) was used to determine the efficiency of microwave heating by comparing it with the maximum amount of absorbed microwave energy that could be converted into heat (Q_{MW}, Eq. 4.3). The average heating efficiency (Eq. 4.11) of 96% with heat recovery (heat extracted by coolant, Q_c) up to 20% was calculated from the available data of several experiments.

$$Q_{abs} = \left(\dot{m} C_P \Delta T \right)_{RM} + \left(\dot{m} C_P \Delta T \right)_C \tag{4.10}$$

$$Efficiency = \frac{Q_{abs}}{Q_{MW}} 100\% \tag{4.11}$$

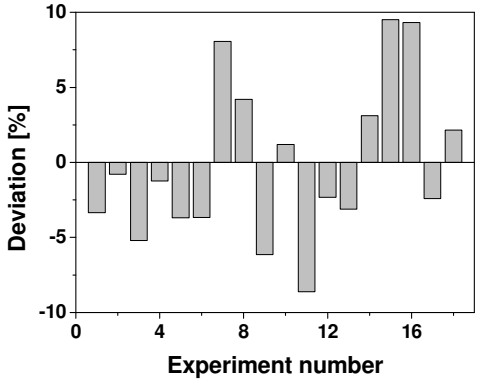

Figure 4.13: Deviation in heating efficiency from its average value of 96% calculated over several experiments. Flow rate reaction mixture: 5-8.33·10^{-7} m^3/s, coolant: 8.33-2500·10^{-9} m^3/s, available power: 150-175 W.

The deviation from the average value of the heating efficiency was found to be within 10% (Figure 4.13). This deviation was probably due to inaccurate temperature and reflective power measurements. Especially for the cases of high flow rates of the coolant, 1 K error in the temperature measurement lead to an error of 8% in heating efficiency.

Nevertheless having a heating efficiency of more than 90% is very important to prove microwave heating as a viable technology for industrial applications, at least for fine chemical synthesis. Usually, the electrical efficiency (conversion of electrical energy taken from the grid) of the standard marketed magnetrons like many other technologies such as resistive heating is in the range of 50-65%.[24] This brings the overall energy efficiency of such heating systems down to half (90 x 0.5 = 45%). Therefore, it is very important to carefully design a reactor system, which

shall facilitate complete utilization of the produced (microwave) energy and provide heating efficiency above 90%. With our integrated reactor – heat exchanger approach, we prove that such a possibility exists to make microwave heating an attractive option for fine-chemical production scales of 1 kg/day (24 hr period).

4.5 Conclusions

Microwave heating can be beneficial over conventional heating (*i.e.* oil bath) especially with its clean and fast heating of polar reaction media at molecular level (volumetric heating). The major challenge of microwave heating being recognized as an alternative to conventional heating technology, however, lies in the possibility of taking microwave batch processes to continuous operation. Therefore a novel concept for continuous reactor operation under microwave heating is proposed where the temperature is maintained between a predefined low and high limit of operation by a co-current heat-exchanger by implementing a microwave transparent solvent, toluene, as a coolant. The heat transfer models for predicting the temperature profiles inside the microwave cavity as well as in the reactor part were developed and employed. The 2D heat transfer model of the microwave cavity predicted temperatures at the outlet of the microwave cavity with an accuracy of ± 3 K. However, future investigations are needed to understand the observed hot spot formation inside the microwave cavity. The 1D heat transfer model for the reactor provided the lengths of the reactor packed with the catalyst bed for conducting the reaction between T_{max} (343 K) and T_{min} (338 K). Optimized integration of heat has clearly lead to good prediction of the length of the reactor part which was principally used to conduct a reaction. The observed conversions were found to be in good agreement with the predictions. Converting microwave energy into heat had an average efficiency of 96%. Thus it can be concluded that application of microwave heating technology not only provides clean and fast heating at the molecular level but also helps in performing a controlled and energy efficient continuous operation in a milli reactor setup where temperatures and yields can be predicted accurately.

Nomenclature

Symbol	Description
A	surface area perpendicular to flow, m^2
C_p	heat capacity, J/kg.K
C_A	concentration of component A, mol/m^3
d	diameter, m
D_p	particle diameter, m
E	electric field intensity, V/m
E_a	activation energy, J/mol
f	microwave frequency, 2.45 x 10^9 Hz
F_v	volumetric flow rate, m^3/s
F	body force vector, N/m^3
$\Delta_r H_T^0$	heat of reaction at reaction temperature (T = 70°C), J/mol
$\Delta_r H_{Ts=298K}^0$	heat of reaction at room temperature, J/mol
k_{obs}	observed reaction rate constant, $m^3_{cat}/m^3_R.s$
k^v	volumetric reaction rate constant, 1/s
K_0	frequency factor in Arrhenius equation
L	length of reactor, m
$\dot{m}$	mass flow rate, kg/s
P	pressure, Pa
Q	microwave power, W
r'_A	rate of reaction, $mol/m^3_{cat}.s$
R	gas constant, 8.314 J/mol.K
T	temperature, K
t	time, s
U^*	overall heat transfer coefficient, W/m^3K
u	velocity, m/s
V	volume, m^3
W	volume of catalyst, m^3
X	conversion
z	direction
Greek symbols	
ε	Voidage
ε'	dielectric constant
ε''	dielectric loss
ε_0	permittivity of free space, $8.85 \cdot 10^{-12}$ F/m
v	moles
μ	Viscosity, Pa.s
ρ	Density, kg/m^3
λ	thermal conductivity of solids, W/m.K
k	thermal conductivity of liquids, W/m.K
Subscripts	
C	coolant

RM	reaction mixture
R	reactor
cav	Cavity
abs	absorbed heat
MW	microwave
loss	loss to the surroundings
f	Formation
cat	catalyst
r	reaction
T	Temperature
s	Surroundings
i	component number

Appendix 4.A

Heat of reaction

The heat of reaction at 343 K was calculated solving following equations.

$$\Delta_r H_T^0 = \Delta_r H_{T_s=298K}^0 + \int_{T_s}^{T} \Delta_r Cp^0 dT \tag{4A.1}$$

$$\Delta_r H_{T_s=298K}^0 = \sum \upsilon_i * \Delta_f H_{i,T_s=298K}^0 \tag{4A.2}$$

$$\Delta_r Cp^0 = \sum \upsilon_i * Cp_i^0 \tag{4A.3}$$

$$Cp_i^0 = a_0 + a_1 * T + a_2 * T^2 + a_3 * T^3 + a_4 * T^4 \tag{4A.4}$$

Solving Eq. 4A.1 to 4A.4 with the data of the Table 4A.1 gave the heat of reaction of -2438 J/mol. Thus the reaction is slightly exothermic.

Table 4A.1: Thermodynamic data of reaction components for heat of reaction calculations.

Component	υ_i	$\Delta_f H_{i,T_s=298K}^0$	Cp_i				
		kJ/mol	a_0	a_1 x 10^{-4}	a_2 x 10^{-5}	a_3 x 10^{-8}	a_4 x 10^{-11}
Acetic acid	-1	-484.3	4.38	-24.0	6.76	-8.76	2.69
Ethanol	-1	-277.6	4.40	6.28	5.55	-7.02	3.48
Ethyl acetate	1	-479.3	10.23	-149	13.0	-15.7	6.00
Water	1	-285.8	4.40	-41.9	1.41	-1.56	0.663

Appendix 4.B

Pressure drop calculations

The pressure drop over a packed bed can be computed by using the Ergun equation (Eq. 4B.1). The pressure drop was calculated for the longest possible catalyst bed length of 0.155 m.

$$\frac{dP}{dz} = -\frac{150 * u * \mu}{D_P^2} * \frac{(1-\varepsilon)^2}{\varepsilon^3} + 1.75 \frac{\rho * u^2}{D_p} * \frac{(1-\varepsilon)}{\varepsilon^3} \quad (4B.1)$$

The pressure drop was calculated by using physical properties of the system (Table 4B.1) to be $0.18 \cdot 10^5$ Pa.

Table 4B.1: Physical properties of system and components for pressure drop calculations by Ergun equation.

Variable	Value	Description
ε	0.2	Porosity, [m^3_{cat}/m^3_R]
D_p	$7.50 \cdot 10^{-4}$	diameter of particle, [m]
μ	$4.87 \cdot 10^{-4}$	Viscosity, [Pa.s]
z	$1.55 \cdot 10^{-1}$	length of the bed, [m]
u	$9.4 \cdot 10^{-2}$	superficial velocity, [m/s]
rho	770	Density, [Kg/m^3]

Appendix 4.C

Reaction rate constant

In this work the solid acid catalyzed esterification reaction[6,9,11,15] of ethyl acetate formation from acetic acid and ethanol was chosen as a model reaction.[22] This is a simple reaction with well-understood kinetics.[26,27] The reaction equation is presented in scheme 4.1. In order to increase the conversion for this equilibrium limited reaction a 5-fold excess of ethanol was chosen because of its dielectric properties. This excess made the reaction to obey a pseudo first order rate law. The effect of temperature on the reaction rate constant and the effect of catalyst loading on the conversion were determined. The effect of temperature was determined to establish the activation energy. The effect of catalyst loading was needed to calculate the volumetric reaction rate constant (independent of the catalyst loading), which was used later for reaction modeling.

Experimental set-up and procedure

The used set-up for the kinetic experiments is schematically depicted in Figure 4C.1. The experiments were performed in a batch reactor. An oil bath was used to achieve the reaction temperature and to keep it constant.

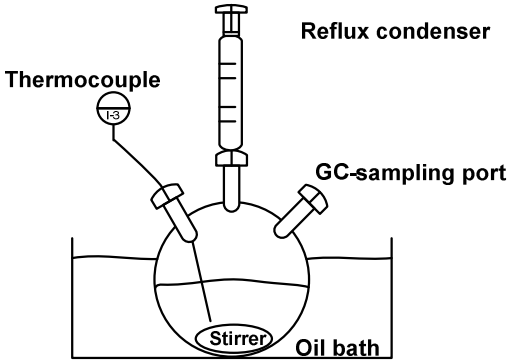

Figure 4C.1: Schematic of the set up used for kinetic experiments

The batch reactor (three-neck round bottom flask) had a capacity of $50 \cdot 10^{-6}$ m^3 and was equipped with a reflux condenser to prevent any losses of the reactants by evaporation. Samples were taken via one of the necks. The reaction mixture was magnetically stirred at 750 rpm. The reaction vessel was kept at a constant temperature in a stirred constant temperature oil bath, where the temperature could be monitored and adapted manually with a thermocouple. Chemicals and catalysts used for this study were as explained in the experimental section. Experiments were carried out at a molar ratio of ethanol to acetic acid of 5:1 at different temperatures (323 to 343 K, at 20 wt% dry catalyst loading) and different catalyst loadings (5 to 20 wt% at 343 K). The volume of the reaction mixture was $25 \cdot 10^{-6}$ m^3 for all experiments. The reaction mixture was charged to the reactor, and the catalyst was added when the reaction mixture has reached the desired reaction temperature. The liquid samples were analyzed by gas chromatography by following the procedure described in the experimental section.

Results

Figure 4C.2 shows a typical concentration time history for the reactants and products during the reaction.

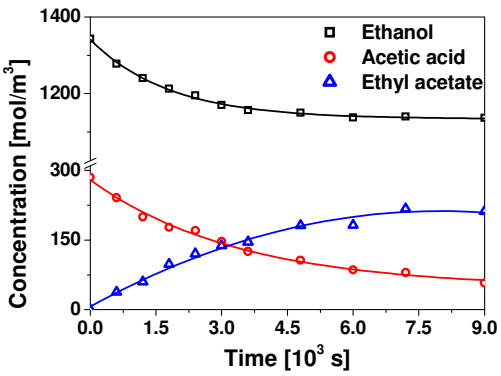

Figure 4C.2: Typical concentration-time profile of the esterification reaction. Catalyst loading: 5%, Temperature: 343 K, Agitation speed: 750 rpm.

Effect of temperature

The effect of temperature on the conversion of the limiting reactant *i.e.* acetic acid, was checked by calculating $-\ln(C_A/C_{A0})$ over time, this gave a linear line, as expected for a (pseudo) first order reaction with slope being the observed reaction rate constant (k_{obs}). The ln k_{obs} showed a linear dependence over the reciprocal of the temperature, see Figure 4C.3.

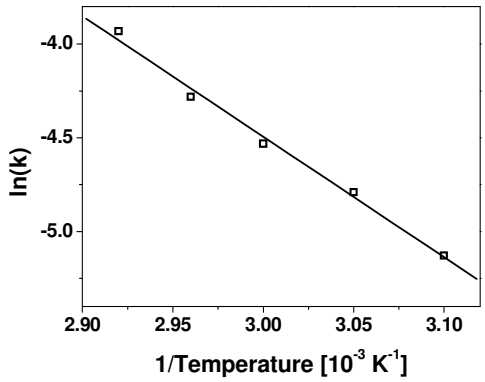

Figure 4C.3: Effect of temperature on the reaction rate coefficient of the esterification reaction. Catalyst loading: 20%, Reaction volume: $2.5 \cdot 10^{-5}$ m^3, Agitation speed: 750 rpm.

The activation energy (E_a) and frequency factor (K_0) were calculated to be 53500 J/mol and $2.65 \cdot 10^6$ s^{-1} respectively by applying the Arrhenius equation (Eq. 4C.1).

$$k_{obs}(T) = K_0 e^{-\frac{E_a}{RT}} \tag{4C.1}$$

Effect of catalyst loading

The effect of the catalyst loading on k_{obs} at 343 K was determined. A linear dependence was found as shown in Figure 4C.4.

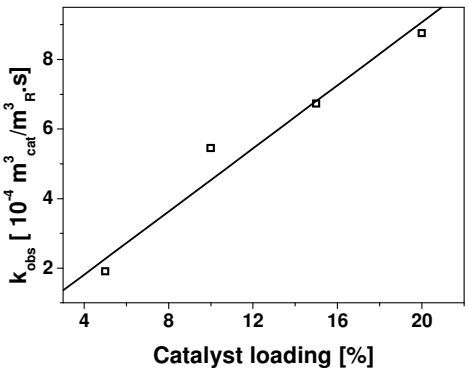

Figure 4C.4: Effect of Catalyst loading on the reaction rate coefficient (k_{obs}) of the esterification reaction. Temperature: 343 K, Reactor volume: $2.5 \cdot 10^{-5}$ m^3, Agitation speed: 750 rpm.

The observed reaction rate constant was corrected for the catalyst loading by equating Eq. 4C.2 and 4C.3. The first order rate coefficient based on the reaction rate per unit volume of catalyst (k^V) of $3.28 \cdot 10^{-3}$ s^{-1} was calculated from k_{obs} using Eq. 4C.5.

$$V_R \frac{dC_A}{dt} = k_{obs} C_A V_R \tag{4C.2}$$

$$V_R \frac{dC_A}{dt} = k^V C_A V_{cat} \tag{4C.3}$$

Therefore,

$$k^V V_{cat} = k_{obs} V_R \tag{4C.4}$$

$$k^V = \frac{k_{obs} V_R}{V_{cat}} \left[\frac{1}{s} \right] \tag{4C.5}$$

References

1. Gedye, R.; Smith, F. The use of microwave ovens for rapid organic synthesis. *Tetrahedron lett.* **1986,** *27,* 279.
2. Damm, M.; Glasnov, N. T.; Kappe, O. C. Translating high-temperature microwave chemistry to scalable continuous flow processes. *Org. Process Res. Dev.* **2010**, *14,* 215.
3. Plazl, I.; Pipus, G.; Koloini, T. Microwave heating of the continuous flow catalytic reactor in a nonuniform electric field. *AIChE J.* **1997,** *43,* 754.
4. Chemat, F.; Poux, M.; Di Martino, J. L.; Berlan, J. A new continuous-flow recycle microwave reactor for homogeneous and heterogeneous chemical reactions. *Chem. Eng. Technol.* **1996,** *19,* 420.
5. Glasnov, N. T.; Kappe, O. C. Microwave-assisted synthesis under continuous-flow conditions. Macromol. *Rap. Com.* **2007,** *28,* 395.
6. Chemat, F.; Esveld, E.; Poux, M.; Di-Martino, L. J. The role of selective heating in the microwave activation of heterogeneous catalysis reactions using a continuous microwave reactor. *J. of microwave power EE.* **1998,** *33,* 88.
7. Baxendale, I. R.; Griffiths-Jones, M. C.; Ley, V. S.; Tranmer, K. G. Microwave-assisted Suzuki coupling reactions with an encapsulated palladium catalyst for batch and continuous-flow transformations. *Chem. Eur. J.* **2006,** *12,* 4407.
8. Cecilia, R.; Kunz, U.; Turek, T. Possibilities of process intensification using microwaves applied to catalytic microreactors. *Chem. Eng. Process.* **2007,** *46,* 870.
9. Roberts, A. B.; Strauss, R. C. Towards rapid, 'green' predictable microwave-assisted synthesis. *Acc. Chem. Res.* **2005,** *38,* 653.
10. Esveld, E.; Chemat, F.; van Haveren, J. Pilot scale continuous microwave dry-media reactor - Part 1: design and modeling. *Chem. Eng. Technol.* **2000,** *23,* 279.
11. Esveld, E.; Chemat, F.; van Haveren, J. Pilot Scale Continuous Microwave Dry-Media Reactor - Part II: Application to waxy ester production. *Chem. Eng. Technol.* **2000,** *23,* 429.

12. Kabza, G. K.; Chapados, R. B.; Estwicki, E. J.; McGrath, L. J. Microwave-induced esterification using heterogeneous acid catalyst in a low dielectric constant medium. *J. Org. Chem.* **2000,** *65,* 1210.
13. Strauss, R. C. Microwave-assisted reactions in organic synthesis – are there any nonthermal microwave effects? Response to the Highlight by N. Nuhnert. *Angew. Chem. Int. Ed.* **2002,** *41,* 3589.
14. Patil, N. G.; Rebrov, E. V.; Esveld, E.; Eränen, K.; Benaskar, F.; Meuldijk, J.; Mikkola, J. -P.; Hessel, V.; Hulshof, L. A.; Murzin, D.Y.; Schouten, J. C. Effect of the load size on the efficiency of microwave heating under stop flow and continuous flow conditions. *J. of Microwave Power and Electromagnetic Energy*. **2012**. *submitted / in press*.
15. Pipus, G.; Plazl, I.; Koloini, T. Esterification of benzoic acid in microwave tubular flow reactor. *Chem. Eng. J.* **2000,** *76,* 239.
16. Wilson, S. N.; Sarko, R. C.; Roth, P. G. Development and applications of a practical continuous flow microwave cell. *Org. Proc. Res. Dev.* **2004,** *8,* 535.
17. Hoogenboom, R.; Wilms, A. F. T.; Schubert, S. U. Microwave irradiation – a closer look at heating efficiencies. *Aust. J. Chem.* **2009,** *62*, 236.
18. Herrero, M. A.; Kremsner, J. M.; Kappe, C. O. Nonthermal Microwave Effects Revisited: On the Importance of Internal Temperature Monitoring and Agitation in Microwave Chemistry. *J. Org. Chem.* **2008,** *73,* 36.
19. Fogler, H. S. Elements of chemical reaction engineering (*4th edition*), Pearson Education International, United States, 2006.
20. Lide, D. R. CRC Handbook of Chemistry and Physics. Taylor & Francis group, Boca Raton, 2000.
21. Shah, K. R.; London, L. A. Laminar flow forced convection in ducts: A source book for compact heat exchanger analytical data. Academic Press, New York, 1978.
22. Metaxas, C. A.; Meredith, J. R. Industrial microwave heating. Peter Peregrinus ltd., London, 1983.
23. Kirbaslar, I. S.; Baykal, B. Z.; Dramur, U. Esterification of acetic acid with ethanol catalysed by an acidic ion-exchange resin. *Turk. J. Eng. Environ. Sci.* **2001,** *25,* 569.
24. Moseley, J. D.; Kappe, C. O. A critical assessment of the greenness and energy efficiency of microwave-assisted organic synthesis. *Green Chem.* **2011,** *13,* 794.
25. Benaskar, F.; Engels, V.; Patil, N. G.; Rebrov, E. V.; Meuldijk, J.; Hessel, V.; Hulshof, L. A.; Jefferson, D. A.; Schouten, J. C.; Wheatley, A. E. H. Copper(0) in the Ullmann heterocycle-aryl ether synthesis of 4-phenoxypyridine using multimode microwave heating, *Tetrahedron Lett.* **2010,** *51,* 248.
26. Toukoniitty, B.; Mikkola, J. P.; Eranen, K.; Salmi, T.; Murzin, D. Y. Esterification of propionic acid under microwave irradiation over an ion-exchange resin. *Cat. Today.* **2005,** *100,* 431.
27. Teo, H. T. R.; Saha, B. Heterogeneous catalysed esterification of acetic acid with isoamyl alcohol: kinetic studies. *J. Cat.* **2004,** *228,* 174.

5

Microwave assisted flow synthesis: coupling of electromagnetic and hydrodynamic phenomena

This chapter will be submitted as:
Patil, N.G.; Esveld, D.C.; Benaskar, F.; Rebrov, E.V.; Meuldijk, J.; Hulshof, L.A.; Hessel, V.; Schouten, J.C Microwave assisted flow synthesis: coupling of electromagnetic and hydrodynamic phenomena. *AIChE J.* 2012, *In preparation*.

Abstract

This chapter describes the results of a modeling study performed to understand the microwave heating process in continuous-flow reactors. It demonstrates the influence of liquid velocity profiles on temperature and microwave energy dissipation in a microwave integrated milli reactor-heat exchanger. Horizontal co-current flow of a strong microwave absorbing reaction mixture (ethanol + acetic acid, molar ratio 5:1) and a microwave transparent coolant (toluene) was established in a Teflon supported quartz tube (i.d.: $3 \cdot 10^{-3}$ m, o.d.: $4 \cdot 10^{-3}$ m) and shell (i.d.: $7 \cdot 10^{-3}$ m, o.d.: $9 \cdot 10^{-3}$ m), respectively. Modeling showed that the temperature rise of the highly microwave absorbing reaction mixture was up to 4 times higher in the almost stagnant liquid at the reactor walls than in the bulk liquid. The coolant flow was ineffective in controlling the outlet reaction mixture temperature. However, at high flow rates it limits the overheating of the stagnant liquid film of the reaction mixture at the reactor walls. It was also found that the stagnant layer around a fiber optic temperature probe, when inserted from the direction of the flow, resulted in much higher temperatures than the bulk liquid. This was not the case when the probe was inserted from the opposite direction. The experimental validations of these modeling results proved that the temperature profiles depend more on the reaction mixture velocity profiles than on the microwave energy dissipation/electric field intensity. Thus, in flow synthesis, particularly where a focused microwave field is applied over a small tubular flow reactor, it is very important to understand the large (direct/indirect) influence of reactor internals on the microwave heating process.

5.1 Introduction

Fast and volumetric heating by microwaves is attracting attention for application in continuous flow synthesis of specialty chemicals.[1,2] Major efforts in developing continuous flow reactors for microwave assisted organic synthesis[3-11] demonstrate an increase of the reaction rate and product yield as compared to conventional heating.[6,11] In addition, the presence of hot spots,[3-5] efficiency of microwave heating,[6,7,10] and design of flow reactors[8-10] has been discussed. Most of these articles reveal the enhancement of the reaction rate or yields due to volumetric or selective nature of microwave heating. The high energy intensity of the focused microwaves, however, hampers the efficiency and controllability of operation especially when a strong microwave absorbing component is present.[12,13] In such scenarios, use of a microwave transparent coolant avoids overheating of the reaction mixture and at the same time permits extension of usable reactor lengths.[12,13] However, the use of a focused microwave field even in small well defined reactor geometries does not always provide the expected temperature profiles.[13] This is majorly due to a lack of position specific information with respect to the velocity profile of the liquid, *i.e.* the reaction mixture. Additionally, the reliability of these predictions in microwave heating is limited when the spatial distribution of the volumetric heating source is not considered.[12]

Although experimentally demonstrated, the selective nature of microwave heating and the interaction of system components with the oscillating electric field of the microwaves is not explicitly understood in most of the cases.[14-18] Most reaction mixtures contain polar and non-polar components, some interact with microwaves very strongly while others are completely microwave transparent. Additionally, many chemical reactors require some internals, *e.g.* mixers, distributors, measurement ports (*i.e.* temperature sensors), for various functions during operation. These internals in general influence the mixing/velocity profiles in the (batch/continuous) reactors and, consequently, can interfere in the microwave heating process. Therefore, at the early stage of process design, understanding of the system interactions (in a geometrical as well as in a fluid-dynamic sense) with microwaves and their influence on the microwave heating process are necessary to

allow a robust process control and operation. Particularly in the case of flow reactors, the velocity profiles can strongly influence both processes, *i.e.* heat transport and microwave absorption/interaction. Additionally, changes in the velocity profiles by reactor internals might add complexity to the microwave heating process. Especially, stagnant zones may have a considerable influence on heat transport and by that on the temperature profile. Therefore, it is of utmost importance to understand the spatial distribution of the intensity of microwave absorption and the corresponding local heating rate in the microwave heating process by detailed physical modeling.

The modeling efforts to understand the detailed mechanism of microwave assisted operation in combination with convective heat transport are largely applied in the food and drying industry.[19,20] In contrast, qualitative insight into the mechanisms behind microwave heating in reactive systems is rather limited.[21-24] Most of these efforts are used either to show the existence of a hot spot or to provide design guidelines for microwave applicators. Datta *et al.* have nicely demonstrated the possibility of combining the heat transfer and interactions of the oscillating electric field with the applied load, which they broadly referred as microwave combination heating.[25,26] These authors proposed an iterative procedure to reach the steady state solution. In this iterative procedure, the temperature-change simulated by heat transfer, which consequently changed the dielectric properties of the load, was used to quantify interactions with the applied microwave field. In this study, similar approach is used to model the coupled phenomena in a continuous (milli) reactor-heat exchanger to see the influence of the liquid velocity profiles on the temperature and microwave energy absorption profiles (Figure 5.1).

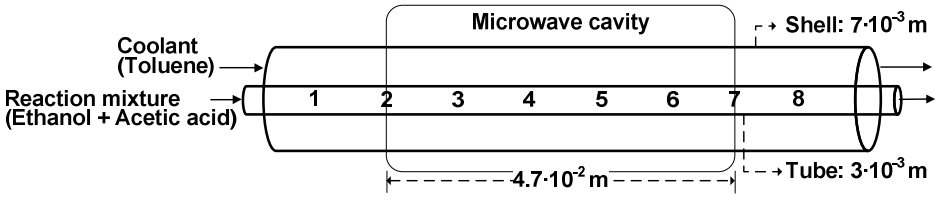

Figure 5.1: Schematic view and process details of the microwave integrated reactor-heat exchanger assembly used for experimental validation. Numbers show the temperature measurement positions in the tube as well as in the shell.

5.2 Experimental methods

5.2.1 Reactor assembly and flow regime

The continuous reactor-heat exchanger consists of a horizontal quartz tube (i.d.: $3 \cdot 10^{-3}$ m, o.d.: $4 \cdot 10^{-3}$ m) for the reaction mixture and a quartz shell (i.d.: $7 \cdot 10^{-3}$ m, o.d.: $9 \cdot 10^{-3}$ m), for the coolant (Figure 5.1). The reaction mixture is strongly microwave absorbing (ethanol + acetic acid, molar ratio 5:1), while the coolant (toluene) is microwave transparent. The purpose of the co-current coolant flow was to avoid overheating of the reaction mixture by the microwaves. Two Gilson HPLC pumps (flow range: $8.33 \cdot 10^{-9}$ to $1.66 \cdot 10^{-6}$ m^3/s) are used to supply the reaction mixture and the coolant to the inner (reactor) tube and to the shell of the reactor-heat exchanger assembly, respectively. Measurements are performed, either with a low or with a high coolant velocity (Table 5.1), to study the influence of the cooling.

Table 5.1: Operating conditions for modeling and experimental studies

Condition	Reaction mixture		Coolant		Microwave power
	Φ_R (10^{-7} m^3/s)	u_R (10^{-2} m/s)	Φ_C (10^{-9} m^3/s)	u_C (10^{-2} m/s)	P_{set} (W)
Slow coolant	16.67	26.5	8.33	0.03	~150
Fast coolant	6.66	10.6	1667	6.4	~60

5.2.2 Microwave setup

The tubular milli-reactor heat exchanger assembly is perpendicularly fed through a vertical WR340 waveguide (Cavity, Figure 5.2). It is supported on each side by PTFE cylinders in metal tubes (length $3 \cdot 10^{-2}$ m, diameter $1.4 \cdot 10^{-2}$ m). Thus, only the central part is exposed to the microwaves over a length of $4.7 \cdot 10^{-2}$ m (Figure 5.1). Note that for the two reaction mixture flow rates studied (Table 5.1), the average heating time of the reaction mixture is only 0.18 and 0.44 seconds, respectively. The top of the cavity is shorted by an adjustable slider (short circuit, Figure 5.2) and the bottom of the cavity is coupled via a three stub tuner and an isolator with an antenna to a horizontal main waveguide. The main waveguide was connected to an adjustable generator which can provide up to 2 kW at the frequency of 2.45 GHz (Figure 5.2). Process control and data acquisition over the entire setup is performed

via a custom made LABVIEW program. The dissipated power in the cavity could be determined from the recorded foreward and reflected powers with an accuracy of approximately ±10 %.

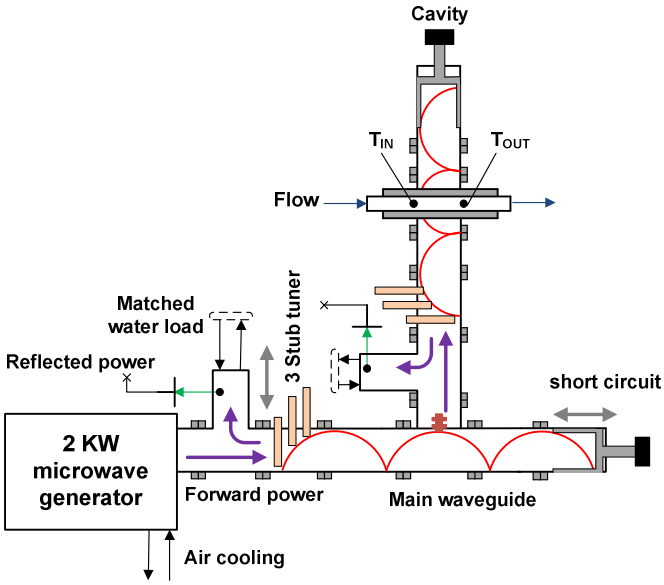

Figure 5.2: Schematic view of the microwave setup with an electric field pattern (red lines) in the setup. Arrows signify flow of energy (purple), signals (green), liquids (blue), movement of stub tuner, and short circuit (grey). Actual load (reactor) opening diameter: $1.4 \cdot 10^{-2}$ m. Design: TU Eindhoven. Manufacturer: Fricke und Mallah GmbH, Germany.

5.2.3 Temperature measurements

The temperature inside the reactor tube and the surrounding shell is recorded at fixed positions (*i.e.* numbered positions in Figure 5.1) by microwave transparent fiber optic sensors (OpSense®, type OTG-A). The $1 \cdot 10^{-3}$ m diameter of these probes was significant with respect to the only $3 \cdot 10^{-3}$ m inner diameter of the reactor tube. Two probes were initially inserted from either side of the assembly which stayed at least $3 \cdot 10^{-2}$ m apart to maintain the empty volume in the microwave irradiation zone. Thus temperatures were measured at positions 1 to 4 with a probe from the left (*i.e.* inlet) and at positions 5 to 7 with the probe from the right (*i.e.* outlet), see Figure 5.1. This, however, led to a serious misinterpretation of the temperature distribution inside the reactor tube. For more details please see the discussion on the hot spot formation in chapter 4. The probe direction has a strong influence on the probe tip temperature. This effect will be discussed in detail in the results and discussion section.

5.2.4 Dielectric properties measurement

A high temperature dielectric probe kit (85070D, Agilent) and a network analyzer (NWA E5062A, Agilent) are used for the measurements of the dielectric constant (ε') and the dielectric loss (ε") of the reaction mixture (ethanol + acetic acid, molar ratio 5:1) at a frequency of 2.45 GHz. The measurements of the batch sample at different temperatures are repeated and averaged over three runs (Figure 5.3). An oil bath was used to maintain the temperature at the desired value.

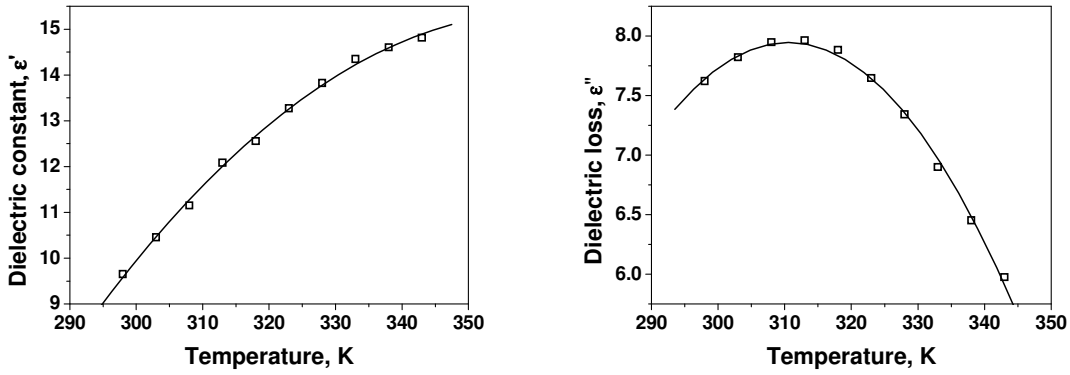

(a) *(b)*

Figure 5.3: Dielectric constant, ε' *(a)* and dielectric loss, ε'' *(b)* of the reaction mixture as a function of temperature.

5.3 Modeling methods

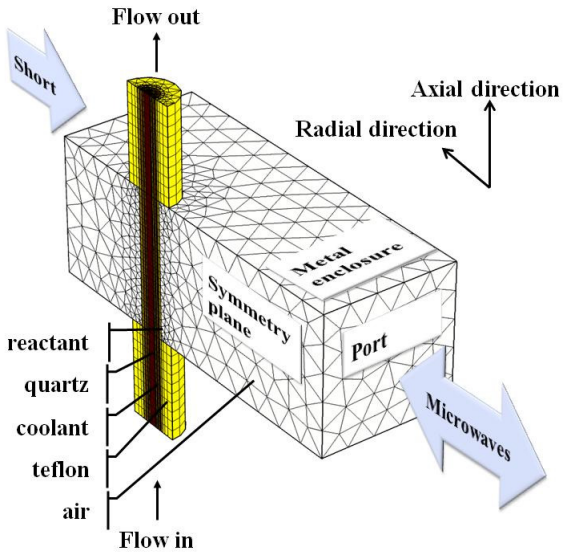

Figure 5.4: 3D computational domain of the microwave cavity, showing individual components of the reactor assembly. See Figure 5.1 for dimensions of the reactor assembly.

The harmonic electromagnetic field, steady state liquid flow and temperature in the setup are calculated with the finite element method in Comsol Multiphysics 4.2a

(Figure 5.4). The laminar flowing fluid is heated by the microwaves and the heat is transported via convection to the outlet and via conduction to the coolant. The model is fully coupled since both the electromagnetic field pattern and the flow profile are determined by the temperature dependent permittivity, fluid density and the viscosity. Temperature dependent material parameters are used as defined in the Comsol material library, where the reaction mixture (ethanol + acetic acid, molar ratio 5:1) is assumed to behave like pure ethanol. Only the complex permittivity of the reaction mixture was interpolated from the dielectric property measurements (Figure 5.3). The dielectric constant (ε') of toluene, quartz glass and PFTE are 2.4, 4.2 and 2.0 respectively and these materials have a negligible loss factor (ε'').

5.3.1 Electromagnetic field model

The modeled 3D geometry with the mesh is shown in Figure 5.3. Symmetry permitted modeling half of the complete geometry. The shape of the 2.45 GHz electromagnetic field depends on the metal enclosed geometry and the permittivity of the internal materials. The electric field should obey the Helmholtz equation which follows from the Maxwell equations in a source free domain (Eq. 5.1).

$$\nabla^2 E = \gamma^2 E \tag{5.1}$$

where E is the electric field intensity and the complex propagation constant γ in a medium is defined as

$$\gamma^2 = -\omega^2 \mu_0 \varepsilon_0 \left(\varepsilon' - j\varepsilon''\right) \tag{5.2}$$

where ω ($=2\pi f$) is the angular velocity, μ_0 is the magnetic susceptibility, ε_0 is the absolute permittivity of free space and ε' and ε'' are the real (*i.e.* dielectric constant) and imaginary (*i.e.* dielectric loss) parts of the relative permittivity. The boundary condition at the perfect conducting metallic boundary is given by Eq. 5.3 and at the symmetry plane we have a perfect magnetic conductor (Eq. 5.4).

$$n \times E = 0 \tag{5.3}$$

$$n \times H = 0. \tag{5.4}$$

The field is excited at the port boundary by a TE_{10} mode (Eq. 5.5).

$$E_z = E_0 \sin\left(\pi x / a\right) \tag{5.5}$$

where a is the waveguide width (*i.e.* $8.33 \cdot 10^{-2}$ m). A 2D axial symmetric version of the same geometry is also modeled. The physics was the same except that in the latter case the waveguide represents a cylindrical cavity, which is driven by a uniform circular magnetic field at the outer wall.

5.3.2 Thermal model

The temperature is determined by a micro heat balance where convection and diffusion were augmented with the microwave source term (Eq. 5.6).

$$\rho C_p (u \cdot \nabla) T = -\nabla \cdot \left(-\hat{\lambda} \nabla T\right) + Q_{mw} \tag{5.6}$$

where u is the fluid velocity vector (which is zero in the solid) and $\hat{\lambda}$ is the effective thermal conductivity. The next section discusses the reasons behind using the effective thermal conductivity. The inlet and metallic boundaries are assumed to be at a fixed temperature (303 K) and the air is assumed to be perfectly isolating. Heating by viscous dissipation (*i.e.* friction) is ignored. The microwave energy density (Q_{mw}) is proportional to the square of the electric field (E_{rms}) and the imaginary part of the permittivity (ε''), see Eq. 5.7.

$$Q_{mw} = \omega \varepsilon_0 \varepsilon'' E_{rms}^2 \tag{5.7}$$

Instead of tuning the driving boundary conditions to match the experimental conditions, the power density term Q_{mw} is internally scaled to equate the total dissipated power with the requested power (Eq. 5.8).

$$\int Q_{mw} dV_R = P_{set} \tag{5.8}$$

5.3.3 Flow model

The flow in the reaction mixture tube and coolant shell is determined by the Navier-Stokes momentum balance at the steady state.

$$\rho (u \cdot \nabla) u = \nabla \cdot \left(-pI + \hat{\mu}\left(\nabla u + (\nabla u)^T\right) - \tfrac{2}{3}\hat{\mu}(\nabla \cdot u) I\right) + F \tag{5.9}$$

with the conservation of mass (constant density fluid)

$$\nabla \cdot (\rho u) = 0 \tag{5.10}$$

The fluid velocity (Table 5.1) and the pressure (ambient) are fixed at the two inlets, and no viscous stress is assumed at the outlets. The tubular walls have a no-slip condition. With the straight cylindrical geometry, this would result in simple parabolic Poiseuille profiles (except for a small deviation caused by the temperature dependent fluid properties). In the 3D simulation, we included a vertical buoyancy force term (Eq. 5.11) related to the thermal expansion (density difference), since a mixed convection pattern could result from the horizontal flow.

$$F_y = -g\left(\rho - \rho_{ref}\right) \tag{5.11}$$

In the 2D simulation, this term was ignored. In the computationally lighter 2D case, we have instead studied the effect of different fiber optic probe insertions. A disturbance to the flow profile, in the form of small recycles, is noted directly behind the probe tip. These cause an enhanced local dissipation of momentum and heat. This cannot be resolved by a refinement of the grid and led to numerical instabilities. Therefore we used the so called low Reynolds κ/ε turbulence model in the 2D case.[27] It is especially suited to preserve validity near the important stagnant boundary and does not need special wall functions. The intricate details of this turbulence model are outside the scope of this chapter.[28,29] In short, it allows to estimate the extra momentum transport by the additional turbulent viscosity term in the effective viscosity (Eq. 5.12) which also enhances the effective thermal conductivity (Eq. 5.13, where the turbulent Prandtl number according to the Kays-Crawford model is about 1).

$$\hat{\mu} = \mu + \mu_T \tag{5.12}$$

$$\hat{\lambda} = \lambda + C_p \frac{\mu_T}{\mathrm{Pr}_T} \tag{5.13}$$

The result is that the apparent diffusion of momentum and heat was 60 to 80% larger in the wake of the probe tip than in the pure laminar region.

5.4 Results and Discussion

The calculated electric field intensity profile in the microwave cavity is shown in Figure 5.5. Since the dielectric properties of the reaction mixture changed by a

factor of 2 with temperature (Figure 5.3), it was intuitively expected that this would influence the electric field intensity along the reactor tube. However, this effect turned out to be of minor importance. Figure 5.5 shows that the position of the shorting plane in the waveguide can be chosen such that the electric field intensity of the standing wave is maximal at the reactor assembly. Furthermore, it can force the electric field to be almost cylindrically symmetric around the reactor axis.

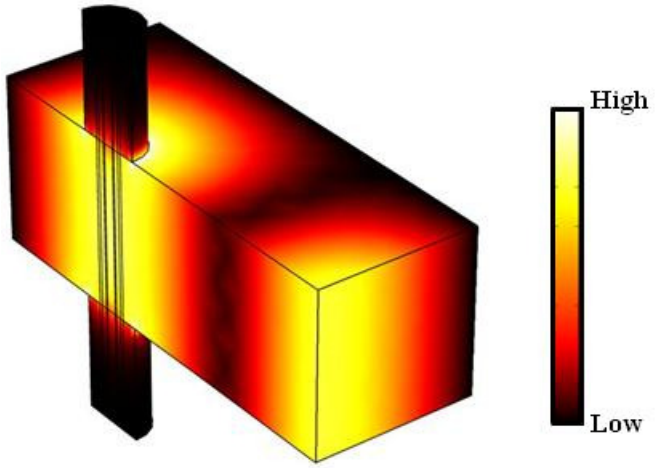

Figure 5.5: Electric field intensity (arbitrary unit) in and around the microwave integrated reactor-heat exchanger assembly. See Figure 5.1 for dimensions of the reactor assembly. $\Phi_R = 6.66 \cdot 10^{-7}$ m^3/s, $\Phi_C = 1.66 \cdot 10^{-6}$ m^3/s, $P_{set} = 60$ W.

Despite the fact that there was no difference in the electric field intensity between the feeding port and the shorting plane (see Figures 5.4 and 5.5), there was a non-symmetric effect of the gravity due to the horizontal arrangement of the reactor-heat exchanger assembly. The buoyancy effect was very significant in the coolant section, particularly at the slow coolant flow condition in comparison to the fast coolant flow condition (Figure 5.6). In the slow coolant flow case, the temperature in the coolant section was up to 40 K higher at the top than at the bottom part of the assembly (Figure 5.6b). The upward force on the hot and thus less dense coolant fluid near the reactor tube induced a dominating fluid circulation pattern, as demonstrated in Figures 5.6a and 5.6b. Note that the circulating forward and backward coolant velocities are orders of magnitude larger than the net forward transport velocity of $0.3 \cdot 10^{-3}$ m/s. Experimental validation of these modeling results was not possible due to a limited flexibility of the experimental setup. Nevertheless, it is important to note here that the horizontal arrangement of the reactor assembly,

even at millimeter sized tubes, could show a significant gravitational influence on temperature and flow.

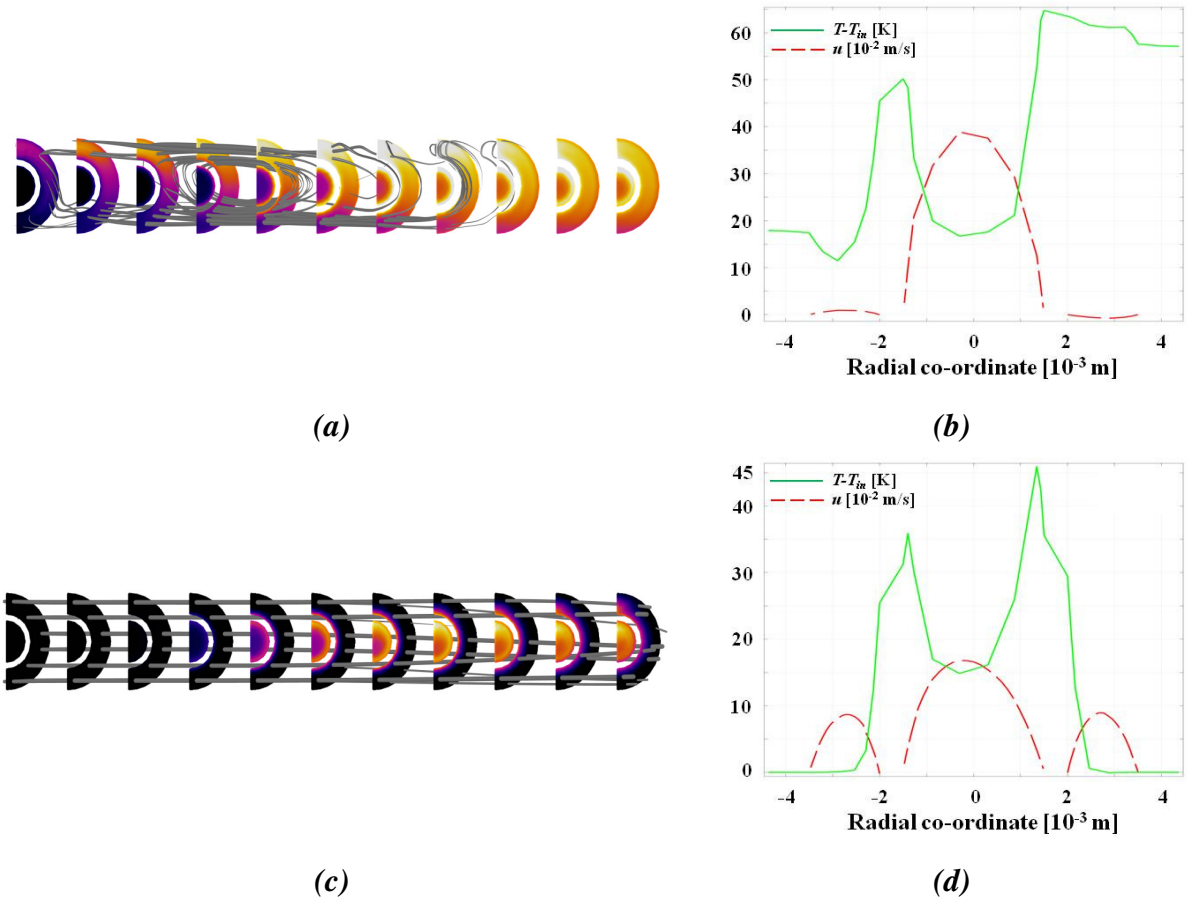

Figure 5.6: Effect of buoyancy in a horizontal arrangement of the microwave integrated reactor-heat exchanger assembly for slow coolant flow *(a, b)* and fast coolant flow *(c, d)* conditions. *(a, c)*: contour plots. *(b, d)*: radial velocity and temperature profiles at axial co-ordinate of zero. Gray lines (with thickness indicating the strength) show the velocity profiles of the coolant in contour plots. The axially sectioned colored pattern shows the temperature of the reaction mixture and the coolant. *(a)*: slow coolant flow condition, $\Phi_R = 1.66 \cdot 10^{-6}$ m^3/s, $\Phi_C = 8.33 \cdot 10^{-9}$ m^3/s, $P_{set} = 150$ W, *(b)*: fast coolant flow condition, $\Phi_R = 6.66 \cdot 10^{-7}$ m^3/s, $\Phi_C = 1.66 \cdot 10^{-6}$ m^3/s, $P_{set} = 60$ W.

Figure 5.6 also shows that the temperature of the reaction mixture near the tubular wall was much higher than in the middle of the tube for both conditions. The radial distribution was studied in more detail with the 2D model, which ignored the buoyancy effect. Figure 5.7 shows the distribution of the microwave energy density (Q_{mw}, Figure 5.7a), velocity (u, Figure 5.7b) and temperature (T, Figure 5.7c) with a reaction mixture flow rate of $6.66 \cdot 10^{-7}$ m^3/s and a coolant flow rate of $1.66 \cdot 10^{-6}$ m^3/s at an applied microwave power of 60 W. The dissipated microwave energy

density was about $2.2 \cdot 10^8$ W/m^3 in the reaction mixture section (Figure 5.7a). The obtained velocity profile in the reaction mixture section was typical for laminar flow (Figure 5.7b). It was highest at the cylindrical symmetry (*i.e.* $18 \cdot 10^{-2}$ m/s) and zero (*i.e.* a stagnant liquid film) at the reactor walls due to the no-slip boundary condition. The temperature of the reaction mixture increased linearly in the axial direction of the flow as a result of microwave absorption. It climbed from the inlet temperature of 303 K to 328 K at the cylindrical symmetry (Figure 5.7c). However at the inner reactor wall, the reaction mixture became much hotter (*i.e.* 353 K), thus reaching almost to the boiling point of ethanol. The coolant was microwave transparent and, therefore, the microwave energy density was zero in the coolant section (Figure 5.7a). Some convectively transferred heat from the reaction mixture was gained by the coolant, but the temperature in the bulk remained at the inlet temperature (303 K) due to the high coolant velocity (Figure 5.7c).

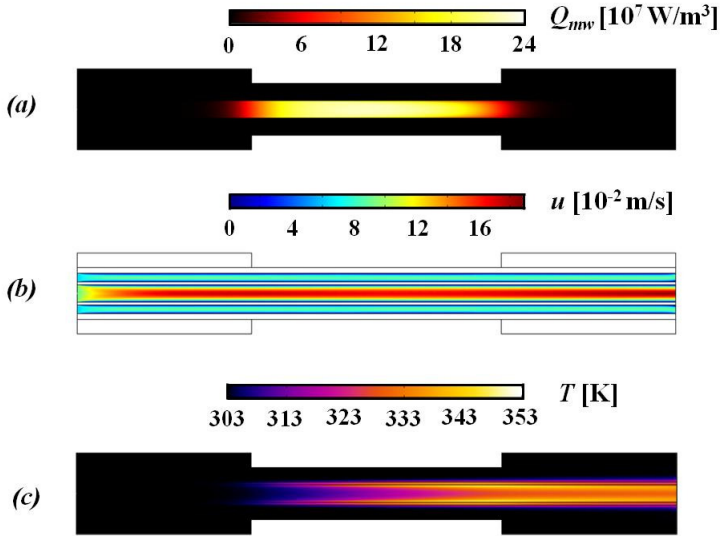

Figure 5.7: Profiles of microwave energy density *(a)*, velocity *(b)*, and temperature *(c)* obtained with the 2D model. See Figure 5.1 for dimensions of the reactor assembly. Fast coolant flow condition; $\Phi_R = 6.66 \cdot 10^{-7}$ m^3/s, $\Phi_C = 1.66 \cdot 10^{-6}$ m^3/s, $P_{set} = 60$ W.

The coolant flow rate had a minor effect on the axial temperature profiles of the reaction mixture (Figures 5.8a and 5.8c), as almost identical axial temperature profiles of the reaction mixture were obtained for coolant flow rates of $8.33 \cdot 10^{-9}$ and $1.66 \cdot 10^{-6}$ m^3/s, respectively. Figures 5.8b and 5.8d show the radial profiles of velocity (u, red lines), temperature rise ($T - T_{in}$, green lines) and microwave energy density (Q_{mw}, blue lines) at the cylindrical symmetry for slow and fast coolant flow

conditions. As mentioned earlier, in both cases, velocities of the reaction mixture and coolant had a near parabolic flow profile (Figures 5.8b and 5.8d), except the coolant velocity was almost zero (Figure 5.8b) at the slow coolant flow condition. The temperature rise of the reaction mixture and the coolant ($T - T_{in} \approx 50$ K) was in this case highest near the reactor wall (Figure 5.8b). This is due to fact that the microwave heated stagnant reaction mixture film near the tube wall is not renewed. The stagnant volume fraction near the wall keeps receiving microwave energy and can only loose it by radial heat conduction. These observations suggest that the temperature depends more on the liquid velocity profile than on the electric field intensity, especially in systems where the focused microwave field is applied over tubular reactors with small diameters (*i.e.* in the millimeter range).

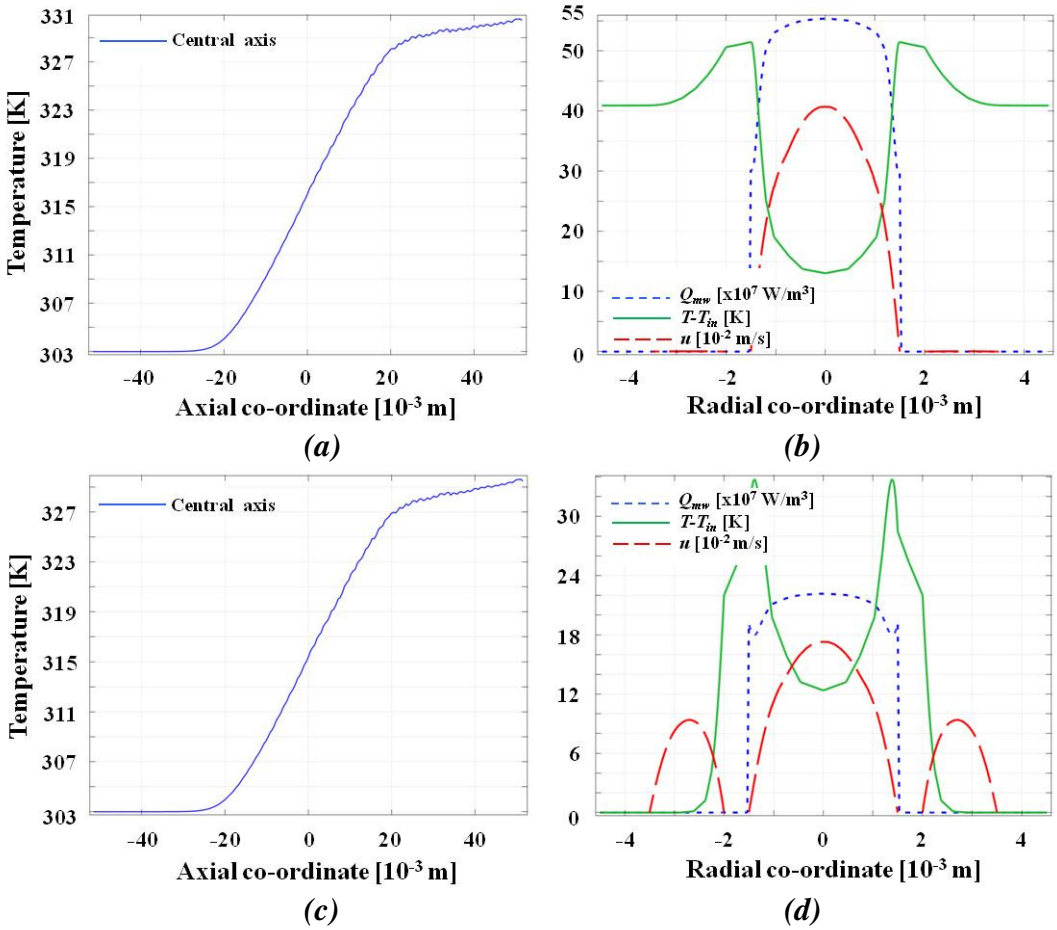

Figure 5.8: Axial temperature profiles *(a, c)* at cylindrical symmetry, and microwave energy density (Q_{mw}, W/m^3), temperature rise (T-T_{in}, K) and velocity (u, m/s) profiles *(b, d)* as a function of radial co-ordinate. *(a, b):* slow coolant flow condition, $\Phi_R = 1.66 \cdot 10^{-6}$ m^3/s, $\Phi_C = 8.33 \cdot 10^{-9}$ m^3/s, $P_{set} = 150$ W, *(c, d):* fast coolant flow condition, $\Phi_R = 6.66 \cdot 10^{-7}$ m^3/s, $\Phi_C = 1.66 \cdot 10^{-6}$ m^3/s, $P_{set} = 60$ W. The origin of the co-ordinate system in this chapter is placed at a different position compared to that in the previous chapters.

The temperature rise near the reactor wall resulted in a drop of the microwave energy density from $5.5 \cdot 10^8$ W/m^3 at the center of the reactor to $3 \cdot 10^8$ W/m^3 at the inner reactor wall (Figure 5.8b). This was due to the drop in the dielectric loss factor (ε'') at higher temperature (see Figure 5.3 and Eq. 5.7). However, with a high coolant flow rate, and a more effective convective cooling of the inner reactor wall, it shows a much smaller drop of the microwave energy density near the wall, and even a slight increase (Figure 5.8d). As a consequence, the coolant having only a minor influence on the reaction mixture outlet temperature (Figures 5.8a and 5.8c), allowed control over the microwave energy dissipation at the inner reactor wall (Figures 5.8b and 5.8d). This additional control provided by the coolant is definitely an interesting feature, for wall coated reactors where the reaction occurs at the catalyst film on the inner wall of the reactor.

The interpretation of the model results imply that any static internals in a microwave flow reactor, such as baffles or packed particles, will disturb the temperature distribution by disturbing the flow pattern. This was verified by inserting a microwave transparent fiber optic probe (commonly used for temperature measurement) in the geometry. Two separate cases were studied with the 2D model, *i.e.* insertion of the probe from the outlet (Figure 5.9a) and insertion of the probe from the inlet (Figure 5.9b).

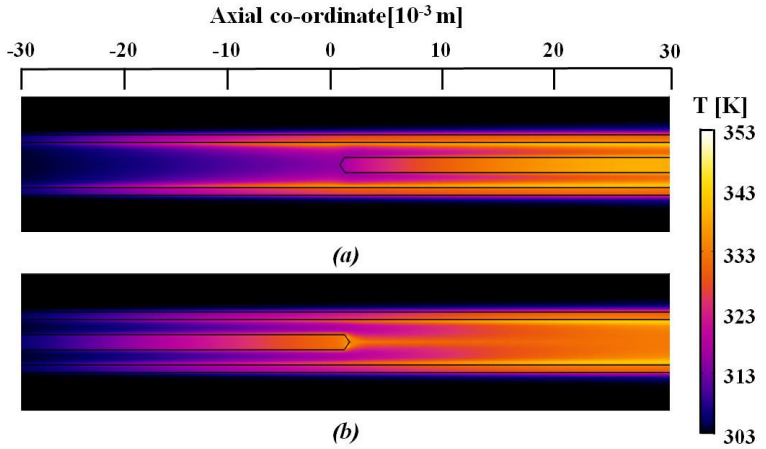

Figure 5.9: Influence of the direction of the probe insertion on the temperature profiles obtained by modeling, *(a)* probe inserted from the outlet, *(b)* probe inserted from the inlet. See Figure 5.1 for dimensions of the reactor assembly. Fast coolant flow condition, $\Phi_R = 6.66 \cdot 10^{-7}$ m^3/s, $\Phi_C = 1.66 \cdot 10^{-6}$ m^3/s, $P_{set} = 60$ W.

The laminar flow of the reaction mixture rearranged itself around the probe which has a stagnant liquid film (no-slip condition). Just as observed earlier near the reactor wall, the liquid in the stagnant film surrounding the inserted probe also reached a higher temperature than the bulk liquid. Thus, the temperature measured by the probe is directly ruled by the temperature of the stagnant liquid film (Figure 5.9). This effect is seen to be building up from the cool inlet side to the hot outlet side. Now for the probe inserted from the outlet (Figure 5.9a), the stagnant film is just starting at the probe tip and it, therefore, shows the bulk temperature. Further downstream, the probe gets hotter, but that is not measured by the tip. On the other hand, for the probe inserted from the inlet, the overheating of the stagnant liquid film is building up towards the probe tip and thus it shows a higher steady state temperature (Figure 5.9b). In this case, it can be noticed that the hot zone continues for about $2 \cdot 10^{-2}$ m directly after the probe tip (Figure 5.9b), because it takes some distance before the liquid at the center is accelerated to the bulk velocity and the excess heat is diffused away. These model observations for both cases, *i.e.* insertion of the probe from the outlet and the inlet, were then validated by experiments (Figure 5.10).

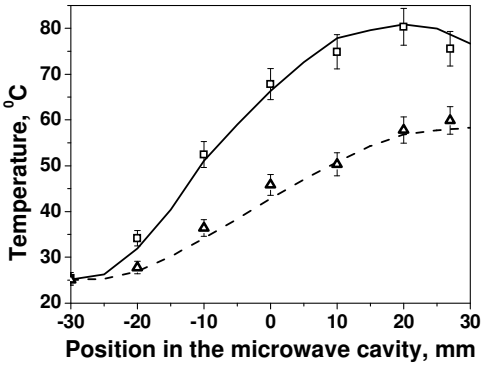

Figure 5.10: Influence of the direction of the probe insertion on the temperature profiles obtained by modeling (lines) and experiments (data points). Solid line and squares: probe inserted from inlet, dotted line and triangles: probe inserted from outlet. Experimental as well as modeling condition: fast coolant flow, $\Phi_R = 6.66 \cdot 10^{-7}$ m^3/s, $\Phi_C = 1.66 \cdot 10^{-6}$ m^3/s, $P_{set} = 60$ W.

Figure 5.10 shows the experimentally observed and calculated axial temperatures at different probe positions. The results in Figure 5.10 demonstrate that the model calculations were in excellent agreement with the experimental observations. The

agreement of the theoretically calculated results with the observed experimental results confirms that the disturbances to the flow profile caused by the inserted probe (or reactor internals) have a considerable influence on the temperature distribution. Therefore, it is important to understand the direct (*e.g.* microwave absorption) or the indirect (*e.g.* disturbance to the velocity profile) influence of the reactor internals on the microwave heating process, in the case of processes where the selectivity is temperature dependent. Additionally, this approach of modeling can also be used in finding the reasons for reported hot spots in many of the microwave assisted flow synthesis studies. Although this modeling study is focused on volumetric liquid heating by the microwaves, for a better understanding it can also be expanded to processes where microwaves are employed for selective heating of catalytically active metal films on the reactor walls.

5.5 Conclusions

A modeling study was conducted for milli-sized flow reactors to understand the influence of the velocity profiles on the microwave heating process. Almost stagnant zones in the microwave absorbing fluid influenced the temperature distribution in a microwave integrated flow reactor-heat exchanger. The temperature increase of the highly microwave absorbing reaction mixture was 2-4 times higher in the almost stagnant regions in the vicinity of the reactor walls compared to the bulk liquid. A buoyancy influence (as a result of gravitational forces) was clearly visible for a horizontal arrangement of a reactor-heat exchanger assembly at millimeter sizes, *i.e.* a fluid circulation was observed due to density difference. The coolant flow was found to be ineffective in controlling the outlet reaction mixture temperature. However, the coolant at high flow rates limited the overheating and, consequently, improved the microwave energy dissipation at the inner reactor wall. Additionally, the disturbances to the velocity profile by reactor internals and their influence on the microwave heating process were investigated. The stagnant layer formation caused by insertion of a fiber optic probe from the inlet (*i.e.* from the direction of the flow) resulted in higher temperatures. The model predictions were experimentally validated and, therefore, demonstrated that the

temperature profile depends more on the reaction mixture velocity profile than the electric field intensity, especially in systems where the focused microwave field is applied over a small tubular reactor. This study also shows that fully coupled simulation of microwave field and non-isothermal flow is feasible and required to understand the thermal performance of microwave heated flow reactors.

Nomenclature

Symbol	Description
a	Waveguide width, $8.33 \cdot 10^{-2}$m
C_P	Heat capacity, J/kg·K
E	Electric field, V/m
E_0	Driving electric field amplitude, V/m
E_z	Electric field at port parallel to tube, V/m
F	Volume Force, N/m^3
F_y	Buoyancy force in vertical direction, N/m^3
f	Microwave frequency, $2.45 \cdot 10^9$ Hz
g	Acceleration due to gravity, 9.80 m/s^2
H	Magnetic field, A/m
I	Identity matrix
n	Normal direction
P_{set}	Set microwave power, W
Pr_T	Turbulent Prandtl number
p	Pressure, Pa
Q_{mw}	Microwave energy density, W/m^3
T	Temperature, K
u	Velocity, m/s
V_R	Reactor volume, m^3
Greek symbols	
ε_0	Permittivity of free space, $8.854 \cdot 10^{-12}$ F/m
ε'	Dielectric constant
ε"	Dielectric loss
γ	Complex propagation constant, 1/m
$\hat{\lambda}$	Effective thermal conductivity, W/m·K
μ_0	Permeability of free space, $4\pi \cdot 10^{-7}$ H/m
$\hat{\mu}$	Effective dynamic viscosity, Pa·s

μ_T	Turbulent dynamic viscosity, Pa·s
Φ_R	Reaction mixture flow rate, m^3/s
Φ_C	Coolant flow rate, m^3/s
ρ	Instantaneous Density, kg/m^3
ρ_{ref}	Density at reference temperature, kg/m^3
ω	Angular velocity ($2\pi f$), rad/s

References

1. Roberts, A. B.; Strauss, R. C. Towards rapid, 'green' predictable microwave-assisted synthesis. *Acc. Chem. Res.* **2005,** *38*, 653.
2. Shore, G.; Morin, S.; Organ, M. G. Catalysis in Capillaries by Pd Thin Films Using Microwave-Assisted Continuous-Flow Organic Synthesis (MACOS). *Angew. Chem.* **2006**,*118*, 2827.
3. Chemat, F.; Esveld, E.; Poux, M.; Di-Martino, L. J. The role of selective heating in the microwave activation of heterogeneous catalysis reactions using a continuous microwave reactor. *J. microwave power EE.* **1998,** *33,* 88.
4. Baxendale, I. R.; Griffiths-Jones, M. C.; Ley, V. S.; Tranmer, K. G. Microwave-assisted Suzuki coupling reactions with an encapsulated palladium catalyst for batch and continuous-flow transformations. *Chem. Eur. J.* **2006,** *12*, 4407.
5. Cecilia, R.; Kunz, U.; Turek, T. Possibilities of process intensification using microwaves applied to catalytic microreactors. *Chem. Eng. Process.* **2007,** *46*, 870.
6. Esveld, E.; Chemat, F.; van Haveren, J. Pilot scale continuous microwave dry-media reactor - Part 1: design and modeling. *Chem. Eng. Technol.* **2000,** *23*, 279.
7. Esveld, E.; Chemat, F.; van Haveren, J. Pilot Scale Continuous Microwave Dry-Media Reactor - Part II: Application to waxy ester production. *Chem. Eng. Technol.* **2000,** *23*, 429.
8. Plazl, I.; Pipus, G.; Koloini, T. Microwave heating of the continuous flow catalytic reactor in a nonuniform electric field. *AIChE J.* **1997,** *43,* 754.
9. Pipus, G.; Plazl, I.; Koloini, T. Esterification of benzoic acid in microwave tubular flow reactor. *Chem. Eng. J.* **2000,** *76,* 239.
10. Hoogenboom, R.; Wilms, A. F. T.; Schubert, S. U. Microwave irradiation – a closer look at heating efficiencies. *Aust. J. Chem.* **2009,** *62*, 236.
11. Chemat, F.; Poux, M.; Di Martino, J. L.; Berlan, J. A new continuous-flow recycle microwave reactor for homogeneous and heterogeneous chemical reactions. *Chem. Eng. Technol.* **1996,** *19*, 420.
12. Patil, N. G.; Hermans, A. I. G.; Benaskar, F.; Rebrov, E. V.; Meuldijk, J.; Hulshof, L. A.; Hessel, V.; Schouten, J. C.; Energy efficient and controlled flow processing under microwave heating by using a milli reactor-heat exchanger. *AIChE J.* **2011**, *Accepted*, DOI 10.1002/aic.13713.
13. Patil, N. G.; Benaskar, F.; Rebrov, E. V.; Meuldijk, J.; Hulshof, L. A.; Hessel, V.; Schouten, J. C. Continuous multi-tubular milli-reactor with a Cu thin film for microwave assisted fine-chemical synthesis. *Ind. Eng. Chem. Res.* **2012**, *submitted / in press.*

14. Comer, E.; Organ, M. G.; A microreactor for microwave-assisted capillary (continuous flow) organic synthesis. *J. Am. Chem. Soc.* **2005**, *127*, 8160.
15. Comer, E.; Organ, M. G. A Microcapillary System for Simultaneous, Parallel Microwave-Assisted Synthesis, *Chem. Eur. J.* **2005**, *11*, 7223.
16. Shore, G.; Yoo, W.; Li, C.; Organ, M. G. Propargyl Amine Synthesis Catalysed by Gold and Copper Thin Films by Using Microwave-Assisted Continuous-Flow Organic Synthesis (MACOS). *Chem. Eur. J.* **2010,** *16*, 126.
17. He, P.; Haswell, S. J.; Fletcher, P. D. I. Microwave heating of heterogeneously catalysed Suzuki reactions in a micro reactor. *Lab Chip.* **2004**, *4*, 38.
18. He, P.; Haswell, S. J.; Fletcher, P. D. I. Efficiency, monitoring and control of microwave heating within a continuous flow capillary reactor. *Sensors and Actuators B.* **2005,** *105*, 516.
19. Datta AK, Geedipalli SSR, Almeida MF. Microwave combination heating. *Food Technol.* **2005,** *59,* 36.
20. McMinn WAM, McLoughlin CM, Magee TRA. Thin-layer modeling of microwave, microwave-convective, and microwave-vacuum drying of pharmaceutical powders. *Drying Technol.* **2005,** *23,* 513.
21. Bonnet, C.; Estel, L.; Ledoux, A.; Mazari, B.; Louis, A. Study of the thermal repartition in a microwave reactor: application to the nitrobenzene hydrogenation. *Chem. Eng. & Process.* **2004,** *43,* 1435.
22. Saillard, R.; Poux, M.; Berlan, J.; Audhuy-Peaudecerf, M.; Microwave Heating of Organic Solvents : Thermal Effects and Field Modelling. *Tetrahedron.* **1995,** *51,* 4033.
23. Robinson, J.; Kingman, S.; Irvine, D.; Licence, P.; Smith, A.; Dimitrakis, G.; Obermayer, D.; Kappe, C. O. Understanding microwave heating effects in single mode type cavities — theory and experiment. *Phys. Chem. Chem. Phys.* **2010,** *12,* 4750.
24. Sturm, G. S. J.; Stefanidis, G. D.; Van Gerven, T.; Verweij, M. D.; Stankiewicz, A. I. Design principles of microwave applicators for small scale process equipment. *Chem. Eng. & Process.* **2010,** *49,* 912.
25. Rakesh, V.; Seo, Y.; Datta, A. K.; McCarthy, K. L.; McCarthy, M. J. Heat transfer during microwave combination heating: computational modeling and MRI experiments. *AIChE J.* **2010,** *56,* 2468.
26. Rakesh, V.; Datta, A. K.; Walton, J. H.; McCarthy, K. L.; McCarthy, M. J. Microwave Combination Heating: Coupled Electromagnetics- Multiphase Porous Media Modeling and MRI Experimentation. *AIChE J.* **2012,** *58,* 1262.
27. CFD module user guide, Comsol, Stockholm, Sweden, 2011.
28. Abe, K.; Kondoh, T.; Nagano, Y. A New Turbulence Model for Predicting Fluid Flow and Heat Transfer in Separating and Reattaching Flows-I. Flow field calculations. *Int. J. Heat and Mass Transfer*, **1994,** *37,* 139.
29. Ignat, L.; Pelletier, D.; Ilinca, F. A Universal Formulation of Two-equation Models for Adaptive Computation of Turbulent Flows. *Computer Methods in Applied Mechanics and Engineering,* **2000,** *189,* 1119.

6

Continuous multi-tubular milli-reactor with a Cu thin film for microwave assisted fine chemical synthesis

This chapter is submitted as:
Patil, N. G.; Benaskar, F.; Rebrov, E. V.; Meuldijk, J.; Hulshof, L. A.; Hessel, V.; Schouten, J. C. Continuous multi-tubular milli-reactor with a Cu thin film for microwave assisted fine chemicals synthesis. *Ind. Eng. Chem. Res.* **2012,** *Submitted*.

Abstract

This chapter demonstrates the parallelization of multiple milli-tubular reactors for scale-up. The productivity of microwave assisted continuous fine chemical synthesis was brought to a commercially interesting scale of 1 kg/day. To that end, a counter-current multi-tubular milli-reactor/heat exchanger (MTMR) assembly was developed with the reactant flow through milli-tubular reactors while the coolant flows in the shell side. The efficiency of microwave absorption under continuous operation in a single mode microwave cavity has been improved with the deposition of a thin (350 ± 40 nm) Cu film on the inner walls of the reactor tubes. The Cu film improved the uniformity of microwave energy absorption in the reactor tubes along the radial direction. A near-isothermal operation was achieved by cooling with a counter-current flow of a microwave transparent coolant in the outer shell of the MTMR. A production rate of 213 ± 11 $kg_{prod}/(kg_{cat}\cdot hr)$ was achieved in a single microwave cavity at 373 ± 5 K and at a total reactant flow rate of $1.66\cdot10^{-9}$ m^3/s. The average production rate of 1,3-diphenyl-2-propynyl piperidine in the MTMR assembly (6 parallel tubes in a shell and tube reactor/heat exchanger) was 93 % of the production rate in a single tube due to a slightly uneven flow and temperature distribution. Kinetically determined mean Cu film temperature was 477 ± 10 K. Although the reactor tubes were placed at an equal distance from axial symmetry (6 parallel tubes in a hexagonal arrangement), a maximum temperature deviation of 8.0 ± 0.5 K was observed over the reactor tubes. The parallelization approach was demonstrated to be successful for scale-up of continuously operated microwave reactors.

6.1 Introduction

Microwave heating, being a fast and selective heating technology, has brought the focus of the specialty chemical industry to microwave assisted continuous organic synthesis (MACOS).[1-4] Some of the prominent researchers in this field have claimed microwave heating as a green technology considering the aspect of energy efficiency although they retrospect it to be case specific.[5] Since 1986, the major efforts in this research field are focused around proving the specific benefits associated with the use of microwave heating, such as selective and/or rapid heating, resulting in a substantial reduction of reaction times.[6] Realization of MACOS at commercial scale, however, requires a proper design of microwave integrated tubular reactors. This type of reactors needs to provide sufficient microwave penetration depth as well as proper temperature control which are important to achieve high selectivity and energy efficiency.[7-8]

The scaling up of microwave assisted organic synthesis can be categorized based on the mode of operation, *i.e.* (semi-) batch or continuous.[9-25] The choice in most of the cases is based on the benefits and limitations associated with the respective mode of operation. Batch scale-up literature mostly comprises scaling small reaction volumes of 5 ml conducted in single mode type of microwave cavities to 1 dm^3 multimode microwave ovens.[9-20] Most of these papers evaluate the limitations related to the volumetric scale-up while using standard microwave reactors available in the market.[19] However, few of the papers look in to the possibility of designing a microwave setup which satisfies the requirements of large batch processes assuring homogeneous heating.[11-12, 20]

Similarly, studies on continuous operation revealed evaluation of the design of commercial continuous flow microwave reactors,[21-23] of micro-reactors[24] and of a process specific microwave integrated reactor setups[25]. Organ *et al.*[26] in their work on MACOS have discussed the possibility of parallelization of milli-reactor tubes. Although this work does not focus on scale-up, it addresses the possibility of library (organic) synthesis in multiple parallel tubes. Most of the scale-up (batch as well as continuous) related studies assume a proper performance of state-of-the-art microwave setups and standard reactors therein. Our previous findings however

suggest that, being case specific, design efforts are necessary for both, the microwave system and the reactor.[7-8] One of the suitable approaches for scaling up MACOS is numbering up. The numbering-up approach is based, at the one hand, on numbering up of mono mode microwave cavities connected to a single waveguide and, at the other hand, on parallelization of tubular structured reactors with a channel diameter in the millimeter range. The former provides high energy efficiency by avoiding conversion losses at multiple grids to applicator points. The latter ensures high throughput while taking care of the penetration depth limitation.

The use of microwave technology in green chemical synthesis has been explored extendedly for liquid-phase reactions. However, the dielectric microwave absorption by solvents or reagents, resulting in rotational heat losses, is limited to polar or ionic derivates.[27] The use of highly active catalysts increases the reaction rate and simultaneously supplies the required heat as a result of extremely fast response of metallic surfaces to microwave irradiation. This response leads, under certain conditions, to a very fast and controlled temperature rise when the catalyst possesses a magnetic character. Buchelnikov *et al.*[28] reported the heating of metallic powders in a multimode (2.45 GHz) microwave applicator, where direct experimental evidence and theoretical explanation on the microwave penetration in powdered metals were provided. The authors described the process of metal heating by magnetic reversal losses and eddy current losses, being complementary processes of dielectric losses in liquid microwave absorption.

This interaction of metals with the microwave field allows performing metal-catalyzed organic synthesis in non-polar solvents and maintaining the bulk temperature of the reaction mixture below the actual reaction temperature on the metal surface, *i.e.* the locus of the reaction.[26] This way of conducting organic synthesis increases the product selectivity due to the much lower bulk solvent temperature. The metal-catalyzed three-component coupling of aldehyde, alkyne, and amines via C–H activation has previously been done using various metal-coated reactors in a microwave field (Scheme 6.1).[29] The two step mechanism of this type of coupling reactions has been elucidated by Climent *et al.*[30]. In the first non-catalytic step an iminium intermediate is produced from the aldehyde and the

amine which subsequently reacts in the second catalytic step with the catalytically activated C–H bond of the alkyne (metal acetylide) leading to the final product. However, the substitution of gold by copper as catalyst using efficient microwave energy, by means of single mode microwaves, brings a tremendous cost advantage with respect to the overall process productivity and feasibility.[31-32] Benaskar *et al.*[33] have recently shown that the catalyst cost substantially governs the economic feasibility of medium-scale continuously operated processes using both milli-reactor based processes and microwave heating.

This chapter reports the scale-up of a microwave assisted continuous fine chemical synthesis by using a multi-tubular milli-reactor/heat exchanger (MTMR) to the commercially interesting capacity of 1 kg/day (Figure 6.1). This is achieved, among others, by providing a uniform temperature distribution in all parallel tubes of the MTMR assembly. Thin Cu metal films were deposited on the inner walls of the tubular milli-reactors following the approach of Shore *et al.*[29]. This allowed investigating the dual effect of the Cu film as a microwave absorbing material and as an active catalyst in a Cu-catalyzed multi-component reaction (Scheme 6.1). The performance of each individual reactor tube was evaluated and compared with the overall performance of the MTMR assembly in rapid and efficient synthesis of 1,3-diphenyl-2-propynyl-piperidine.

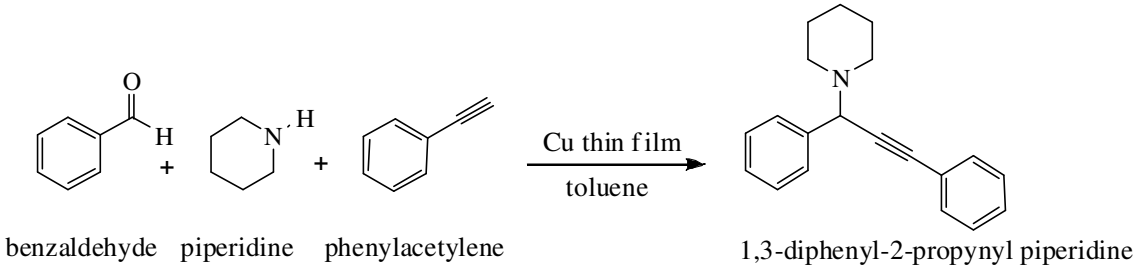

Scheme 6.1: Multi component reaction of benzaldehyde, piperidine and phenylacetylene to produce 1,3-diphenyl-2-propynyl piperidine

6.2 Experimental

The synthesis of 1,3-diphenyl-2-propynyl-piperidine was studied as a test reaction (Scheme 6.1). The reactants (benzaldehyde, piperidine, and phenylacetylene, all 99.9wt.%, Aldrich) were preheated to 50 °C and premixed with toluene (anhydrous,

99.8 wt %, Sigma-Aldrich) to obtain concentrations of $1.5 \cdot 10^{-3}$, $1.8 \cdot 10^{-3}$, $2.25 \cdot 10^{-3}$ mol/m^3, respectively.

6.2.1 MTMR experiments

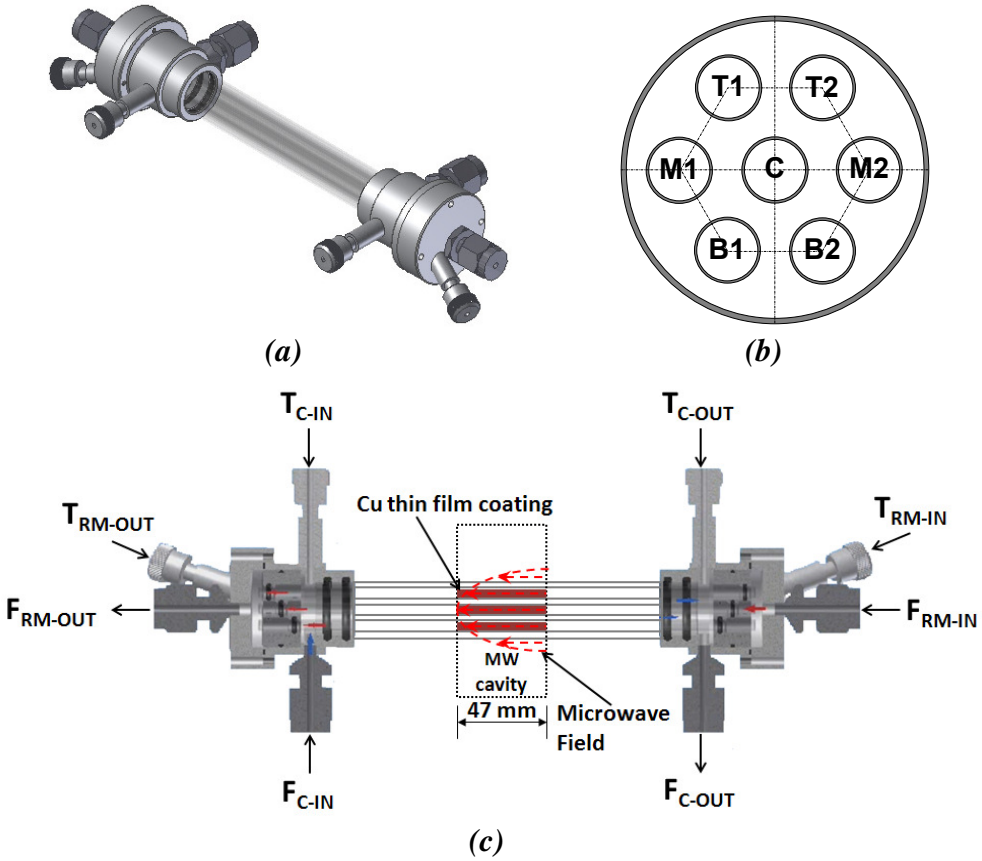

Figure 6.1: Schematic of a multi-tubular milli-reactor/heat exchanger (MTMR) setup. a) Complete assembly. b) Tube distribution with section wise designation of each tube position. Tube size; $2 \cdot 10^{-3}$ m (id) x $3 \cdot 10^{-3}$ m (od) x $1.66 \cdot 10^{-1}$ m (length). Shell size: $1.2 \cdot 10^{-2}$ m (id) x $1.4 \cdot 10^{-2}$ m (od) x $1.37 \cdot 10^{-1}$ m (length). c) Schematic of the MTMR assembly with coated milli-reactor tubes (brown) in the microwave cavity. Red dotted lines show the focused microwave field (red) on the MTMR assembly. Metal fittings showing the temperature (T) and flow (F) ports for the reactant flow through tubes and coolant flow through shell. RM: reaction mixture, and C: coolant.

The MTMR assembly (Figure 6.1a) consisted of seven quartz tubes (one in the center and six in a hexagonal arrangement at a distance of $3.5 \cdot 10^{-3}$ m from the central axis) with an inner diameter of $2.0 \cdot 10^{-3}$ m and a length of 0.166 m, inserted in a shell with an inner diameter of $1.2 \cdot 10^{-2}$ m and a length of 0.137 m. All reactor tubes in the MTMR assembly were designated based on their location (Figure 6.1b): top section (position: T1, T2), middle section (position: M1, M2), bottom

section (position: B1, B2), and central tube (position: C). The reactants and coolant were fed counter-currently by Gilson HPLC pumps (range of flow rate: $8.33 \cdot 10^{-9}$ to $2.5 \cdot 10^{-6}$ m^3/s) to the reactor tube and the shell, respectively (Figure 6.1c). Metal fittings provided a supply/collection chamber for the reactant flow through all reactor tubes and an inlet/outlet port for the shell side coolant flow (Figure 6.1c). Four fiber optic sensors with the diameter of 1.1 mm (OTG-A, OpSense®), were used to record the temperature inside the reactor tube and the surrounding shell (Figure 6.1c).

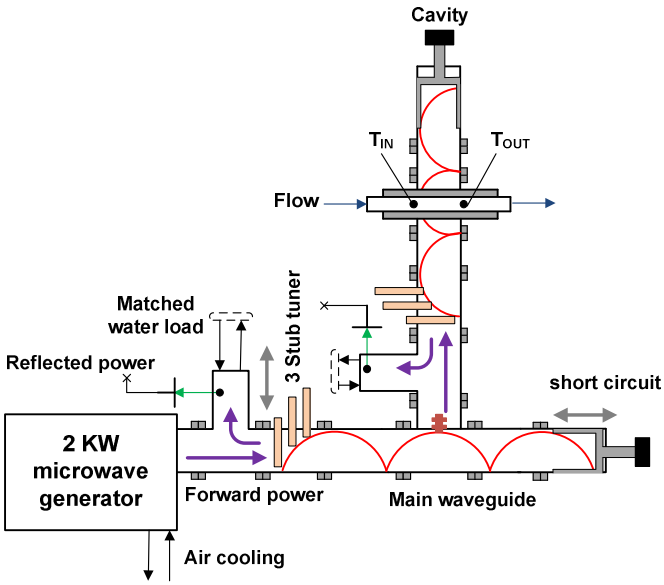

Figure 6.2: Schematic view of the microwave setup with an electric field pattern (red lines) in the setup. Arrows signify flow of energy (purple), signals (green), liquids (blue), movement of stub tuner, and short circuit (grey). Actual load (reactor) opening diameter: $1.4 \cdot 10^{-2}$ m. Design: TU Eindhoven, The Netherlands. Manufacturer: Fricke und Mallah GmbH, Germany.

The microwave setup consisted of a single mode microwave cavity operating at a frequency of 2.45 GHz with adjustable power settings up to 2 kW (Figure 6.2).[7] Focusing of the resonating microwaves in the cavity was possible over the inserted reactor (MTMR assembly in this case) by tuning the cavity with the help of short circuit and 3 stub tuners (Figure 6.2). Focusing of the microwaves allowed getting the microwave field maxima on the reactor assembly (as shown schematically in Figure 6.1c). This assured maximum absorption by the reactor assembly and minimum losses to the dead load at the isolator of the cavity. The reflected power was recorded by using a detector diode on an isolator. This allowed calculation of

the microwave power available in the cavity with in accuracy of 90%. Process control and data acquisition were performed via the LABVIEW program.

The reaction mixture was fed to a single reactor tube (tubes at the other six positions were sealed) at a flow rate of $(0.83 – 1.66)\cdot10^{-9}$ m^3/s. In the numbering-up experiment, the reaction mixture was fed at a reactant flow rate of $1\cdot10^{-8}$ m^3/s simultaneously to the six peripheral tubes (Position: T1, T2, M1, M2, B1, B2, Figure 6.1b). The coolant (toluene) was fed counter-currently through the shell side of the MTMR at various flow rates between $4.16\cdot10^{-7}$ and $1.66\cdot10^{-6}$ m^3/s. Microwave power was varied in the range of 10-50 W.

6.2.2 Cu coatings

Coatings of Cu thin films on the inner wall of reactor tubes were obtained by a modified procedure originally reported by Shore *et al.*[29]. The tubes were filled with a solution of Copper (II) acetate (99 %, Merck) in hydrazine (100 %, Merck) (500 mol/m^3). Then, the tubes were sealed at both ends and heated in an oven at 333 K for 1500 s. A film of CuO was deposited on the inner walls. The tubes were then cleaned by ethanol and dried in an air flow. The oxide film was reduced in a flow of 10 vol% H_2 in helium at a flow rate of $8.33\cdot10^{-7}$ m^3/s at 773 K for 1800 s with a heating rate of 0.166 K/s at atmospheric pressure. The hydrogen flow was switched off during the cooling step (-0.166 K/s).

6.2.3 Analysis

Cu thin films were qualitatively and quantitatively analyzed by scanning electron microscopy, X-ray photoelectron spectroscopy, inductively coupled plasma spectrometry and chemisorption analysis. The reaction components and products in the multi component reaction were analyzed by gas chromatography and ^1H nuclear magnetic resonance spectroscopy.

Scanning electron microscopy (SEM): Thin film and support surface morphology were analyzed by SEM. Images were recorded on a FEI Quanta series FEG 3D G2 SEM using an acceleration voltage of 5 kV and magnifications between 5,000x-100,000x, providing a maximum lateral resolution of 50 nm. In conjunction with

SEM, catalyst elemental compositions were elucidated by qualitative EDX analysis at a spot size of 50 nm and an interaction-volume of 100 µm. The samples were prepared by adhesion of different cross sections of the coated tubes on a carbon grid. The average thickness of the Cu thin film was calculated over ten different samples analyzed by SEM.

X-ray photoelectron spectroscopy (XPS): XPS-measurements were carried out using a Kratos AXIS Ultra spectrometer equipped with a monochromatic Al Kα X-ray source and a delay-line detector (DLD). Spectra were obtained using an aluminium anode (Al Kα = 1486.6 eV) operating at 150 W. For survey and region scans, constant pass energies of 160 eV and 40 eV were used, respectively. The background pressure was 2 x 10^{-12} bar. Samples were prepared on a carbon holey-film in a glove box (< 10 ppm O_2) and transported in a closed sample holder for oxygen-free XPS analysis.

Inductively coupled plasma measurements and optical emission spectroscopy (ICP-OES): The metal loading was determined by ICP-OES. Measurements were performed using a SPECTRO CIROS^{CCD} spectrometer. The sample introduction was performed by a cross-flow nebulizer with a double pass spray chamber and a sample uptake rate of $3.33 \cdot 10^{-8}$ m^3/s. Samples were prepared by collecting equal volumetric amounts of sample at the outlet of the reactor. The solvent was evaporated then the residue was dissolved in H_2SO_4 (5 M) and stirred for 24 hr to ensure a complete solution.

Chemisorption analysis: The copper surface area per unit volume (a_{film}) was determined by a pulse chemisorption using a mixture of 10 vol. % hydrogen in argon at a flow rate of $8.33 \cdot 10^{-7}$ m^3/s at 323 K and atmospheric pressure (AutoChem II, 2920 V4.02 chemisorption analyzer, Micrometrics®). A single Cu coated reactor tube was used directly without further modifications. Prior to chemisorptions, the Cu film was reduced at 473 K for 2 hr.

Gas Chromatography: The reaction samples containing reactants (piperidine, benzaldehyde, phenylacetylene) and the product (1,3-diphenyl-2-propynyl-piperidine) were collected for GC analysis and diluted by 100 times with toluene

prior to analysis. The samples were analyzed by an offline GC (Varian 430, column: CP-Sil 5 CB) equipped with an FID detector.

Nuclear magnetic resonance: ^{1}H NMR data were collected on a Varian 400 NMR spectrometer (400 MHz) as a means to cross-check the conversions obtained from GC and to determine the selectivity of the reaction. Spectra were obtained at 300 K and calculated relative to TMS. Chemical shifts are expressed in δ ppm. The ^{1}H NMR assignments (400 MHz, $CDCl_3$) for the product are: δ 7.70-7.65 (m, 2H), 7.59-7.55 (m, 2H), 7.49-7.30 (m, 6H), 4.89 (s, 1H), 2.66-2.59 (m, 4H), 1.69-1.60 (m, 4H), 1.46 (m, 2H).

This work focuses mainly on evaluating the reactor performance therefore further analysis by product isolation was not performed. The selectivity of the multi component reaction is very high.[29] Shore *et al.* has reported almost equal isolated yields for the same reaction. Therefore, all the reaction results are discussed in the form of conversion of the limiting reactant *i.e.* phenylacetylene.

6.3 Results and Discussion

In this section the effect of the Cu film on uniform microwave energy absorption, the effect of forced cooling on the Cu film stability, the effect of the tube position on the steady state performance of the coated milli-reactor tube in the MTMR assembly, the kinetically estimated catalytic film temperature, and the throughput of the MTMR assembly are discussed in detailed in the following sub-sections.

6.3.1 Energy uniformity

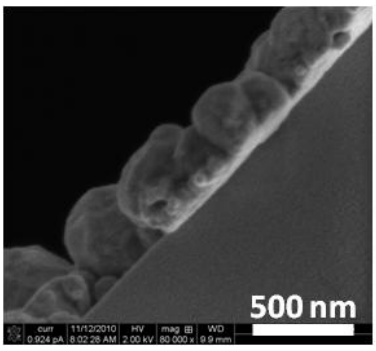

Figure 6.3: SEM image of a Cu thin film on the inner wall of quartz reactor tube (Cross-sectional view). Average film thickness (δ) of 350 ± 40 nm was calculated from 10 different SEM images.

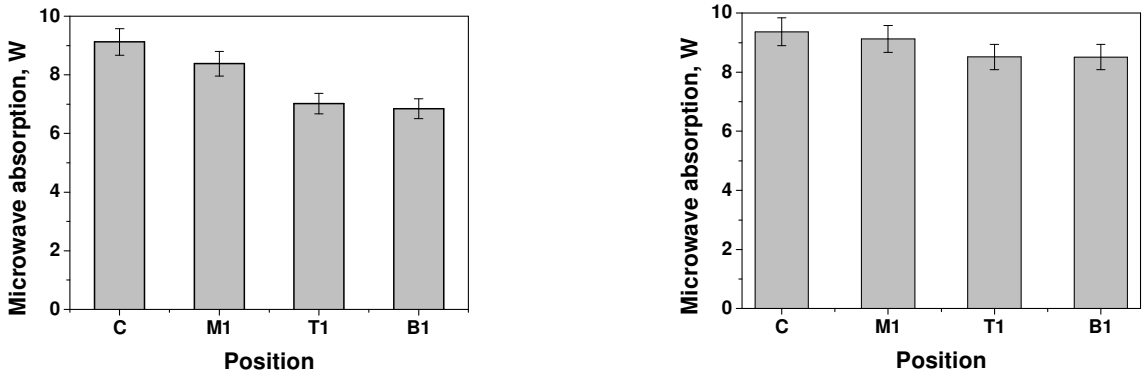

(a) *(b)*

Figure 6.4: a) Microwave absorption in a non-coated reactor tubes at different tube positions in the MTMR assembly. Solvent: water, flow rate: $1.66 \cdot 10^{-7}$ m^3/s, applied power: 50 W. b) Microwave absorption in a Cu coated reactor tubes at different tube positions in the MTMR assembly. Solvent: toluene, flow rate: $1.66 \cdot 10^{-7}$ m^3/s, applied power: 50 W. The individual positions in the x-axis are designated in Figure 6.1b.

Cu film with an average thickness (δ) of 350 ± 40 nm (Figure 6.3) was obtained by the procedure described in the experimental section. Cu thin films diminished the temperature non-uniformity resulting in similar if not equal heat generation in the central and outside tubes in the MTMR (Figure 6.4). Thus the effect of a non-uniform field intensity (Figure 6.4a) of the microwave field was considerably reduced by the presence of the metal films (Figure 6.4b). A microwave transparent liquid (toluene) was used in the coated tubes experiment. Being microwave transparent toluene barely absorbs microwaves therefore most of the convective heat in the bulk liquid came from the hot Cu film surface. This confirmed the selective heating of the Cu coatings and thus presented an opportunity of obtaining enhanced reaction rates on the hot catalytic film.

6.3.2 Cu film stability

Unstable absorption of microwaves was observed in the absence of the coolant (Figure 6.5a). The average steady state phenylacetylene conversion of 18 ± 2 % (verified by ^1H NMR) at a total flow rate of $8.33 \cdot 10^{-10}$ m^3/s and at the outlet temperature of 403 ± 10 K was obtained at 30 ± 10 W of microwave power (Figure 6.5).

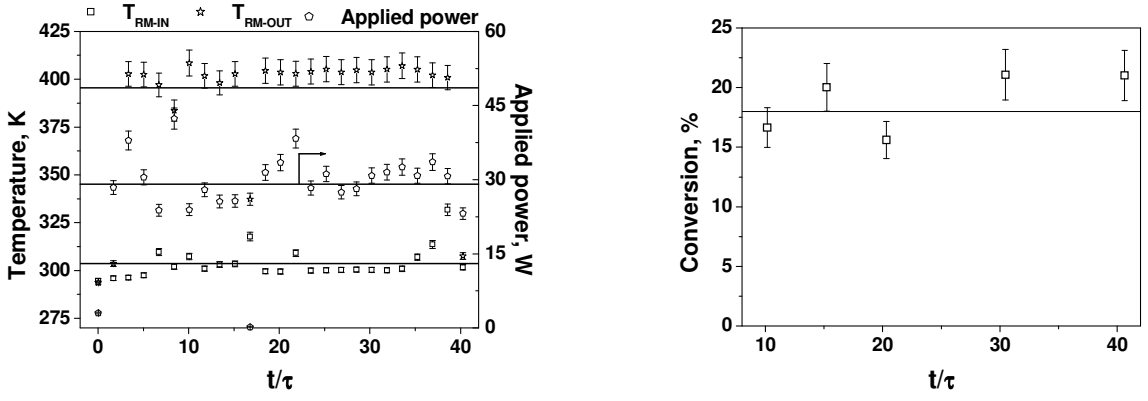

(a) *(b)*

Figure 6.5: a) Temperature-time (normalized with residence time, τ = 180 s) history of a single Cu thin film coated reactor tube without surrounding coolant flow (□: reactant inlet temperature, ☆: reactant outlet temperature, ⬠: applied microwave power). b) Conversion of phenylacetylene over time (normalized with residence time). Reactor tube (quartz, id: $2 \cdot 10^{-3}$ m & od: $3 \cdot 10^{-3}$ m) is positioned in the center (Position: C in Figure 6.1b). Reaction mixture flow rate: $8.33 \cdot 10^{-10}$ m^3/s; RM: reaction mixture.

Similar required microwave power has been reported by Shore *et al.*[29] for seven times lower flow rates using a different microwave setup. The lower energy demand in our work was due to minimized losses as a result of tuning the microwave cavity and focusing most of the microwave energy present in the cavity on the Cu film. Our microwave setup, as explained earlier in the experimental section, permitted the tuning of the microwave cavity by using the short circuit and the stub tuners. Tuning of the cavity results in the focused microwaves on the reactor ultimately leading to enhanced heating efficiencies (≈ 95 %) as reported earlier.[7] Important to note here that the same work by Shore *et al.*[29] had reported poor performance of the same reaction (drop in conversion) with the conventional oil bath heating.

However, in the absence of the coolant flow, the reactor tube could only be used for a period of up to 2 hours. Beyond this time interval the microwave absorption dropped resulting in a decrease in the temperature and consequently in the conversion. According to the XPS and ICP analysis this effect is related to oxidative leaching of the metal film (Figures 6 and 7).

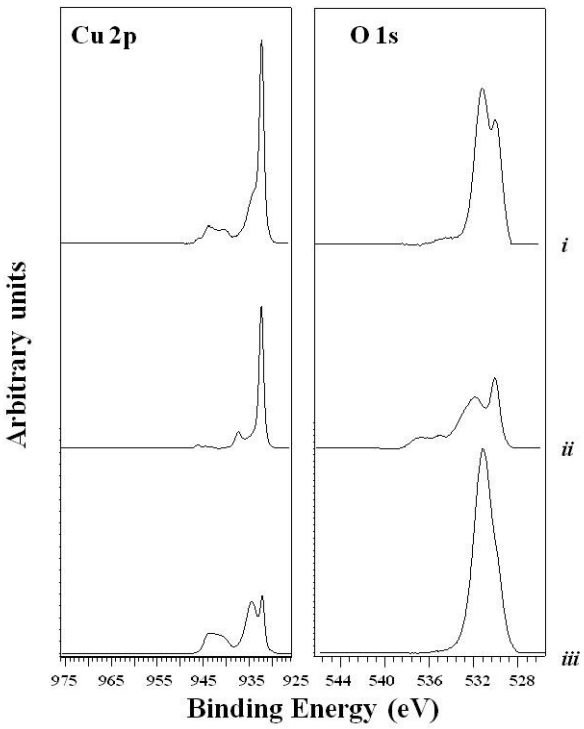

Figure 6.6: XPS analysis of different samples normalized on the carbon 1s signal. *i*) as synthesized, *ii*) calcined, *iii*) spent (after reaction).

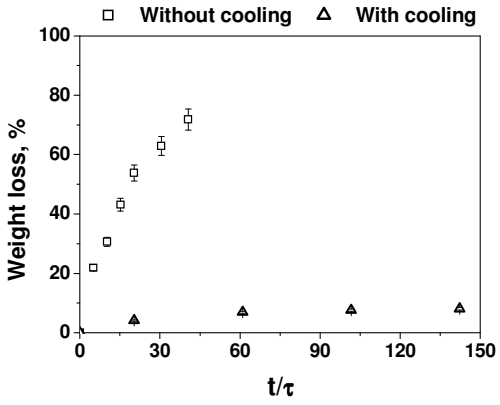

Figure 6.7: Weight loss profile of Cu thin film over time (normalized with residence time, τ) measured by ICP analysis. □: experiment without the flow of surrounding coolant (τ = 180 s), Δ: experiment with the flow of surrounding coolant (τ = 90 s).

Figure 6.6 shows the XPS peaks of Cu2p and O1s, which demonstrate an increase in the oxidation of copper after the microwave experiments. The Cu 2p3/2 peak at 932.9 eV in the calcined film (sample *ii*) signifies the dominant presence of Cu^0. The two small shake-up signals between 938 and 945 eV originate from a negligible Cu 2p3/2 component at 934 eV indicating the presence of copper (II) oxide. Oxidation of cooper is indicative due to the dominant presence of the Cu 2p3/2 component at 934 eV in sample *iii* (spent Cu film).[34] Although less visible

when comparing samples *ii* and *iii* a longer experimental run (2 hours) proved complete leaching of the Cu from the wall of the reactor.

Based on the XPS results, further exploration on the leaching of copper from the film was carried out by monitoring the copper dissolved in the product mixture leaving the reactor by using Inductively Coupled Plasma analysis combined with Optical Emission Spectroscopy (ICP-OES). In line with the XPS data, oxidation of the Cu film subsequently led to leaching of the coating as shown in Figure 6.7. These Cu losses due to leaching were most severe at the beginning (first 900 s) of the microwave irradiation experiment. For the reactor system without counter-current cooling (given as squares in Figure 6.7) the effect was most dramatic, almost 70 wt% of the copper was lost by leaching in 2 hours. The heat capacity of the reaction mixture was not sufficient to extract the heat generated at the film. As a result, a complete breakdown of the reactor tubes was observed in several experiments without using a coolant flow.

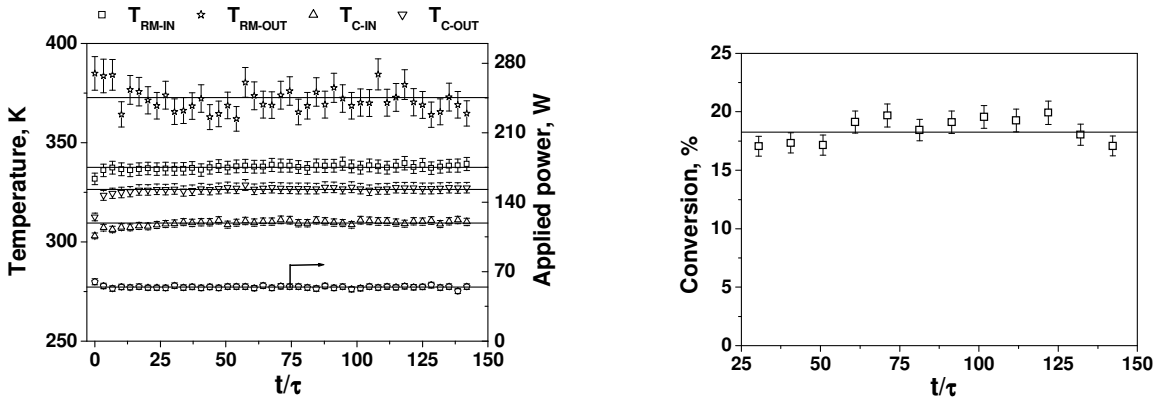

(a) *(b)*

Figure 6.8: a) Temperature-time (normalized with residence time, τ = 90 s) history of a single Cu thin film coated reactor tube with the flow of surrounding coolant (□: reactant inlet temperature, ☆: reactant outlet temperature, △: coolant inlet temperature, ▽: coolant outlet temperature, ⬠: applied microwave power). b) Conversion of phenylacetylene over time (normalized with residence time). Reactor tube (quartz, id: $2 \cdot 10^{-3}$ m & od: $3 \cdot 10^{-3}$ m) was positioned in the middle (Position: M2 in Figure 6.1b). Flow rates of reaction mixture and coolant: $1.66 \cdot 10^{-9}$ and $4.16 \cdot 10^{-7}$ m^3/s, respectively. RM: reaction mixture; C: Coolant.

Therefore, a microwave-transparent coolant flow was necessary to provide stable operation for longer duration, *i.e.* at least 8 hours (tested for 4 hours in Figure 6.8) and to substantially reduce the copper oxidation rate (given as triangles in Figure

6.7). Since the copper losses were significantly reduced in the counter-currently cooled reactor system, overheating of the catalyst film was, therefore, recognized as the major reason for oxidation and subsequent leaching. As the wall-coating procedure was always similar, a weak adhesion of the copper film onto the glass surface could only play a minor role in the leaching. The counter-current flow of the coolant had a two-fold effect. It effectively extracted the heat from the Cu film but also additionally preheated the liquid reaction mixture before it entered the microwave cavity. The thermal heat flux towards the coolant amounted up to 50% of the total energy input to the system.

6.3.3 Tube configuration

An average production rate (for 1,3-diphenyl-2-propynyl piperidine) of 213 ± 11 kg_{prod}/kg_{cat}·hr was achieved in a single tubular reactor at 373 ± 5 K and a total reactant flow rate of $1.66 \cdot 10^{-9}$ m^3/s (Figure 6.8). The steady state performance of the milli-reactor tubes at each of the 7 positions in the MTMR over 4 hours of operation is given in Table 6.1.

Table 6.1: Steady state temperatures and conversion of phenylacetylene at all seven positions in the MTMR assembly

Position[1,2]	**$T_{RM\text{-}IN}$ (K)**	**$T_{RM\text{-}OUT}$ (K)**	**$T_{C\text{-}IN}$ (K)**	**$T_{C\text{-}OUT}$ (K)**	**Conversion (%)**
T1	371.0	380.5	307.7	313.3	15.4
T2	358.8	352.6	303.7	311.9	15.6
M1	339.7	371.6	309.6	326.5	18.3
M2	344.6	369.2	313.0	330.2	18.2
B1	347.6	313.5	304.3	330.0	12.5
B2	353.4	308.2	303.2	332.9	12.7
C	338.6	366.0	310.5	342.0	25.4

[1] Individual positions are designated in Figure 6.1

[2] Flow rates of reaction mixture and coolant: $1.66 \cdot 10^{-9}$ and $4.16 \cdot 10^{-7}$ m^3/s, respectively. RM: reaction mixture; C: Coolant; all experiments conducted for over 4 hours of the run time.

The steady state temperatures of the reactant ($T_{RM\text{-}IN}$ and $T_{RM\text{-}OUT}$), the coolant ($T_{C\text{-}IN}$ and $T_{C\text{-}OUT}$) and the conversion of phenylacetylene obtained for each individual position in the MTMR varied significantly (Table 6.1). These deviations in the performance of the reactor tube at each individual position in the MTMR (Figure

6.1b) can be due to i) flow distribution, ii) varying active catalytic surface or iii) microwave field (energy) distribution. The reactant flow distribution could not influence steady state performance, since every experiment was performed with a single coated tubular reactor at the required position in the MTMR. The remaining tube positions in the MTMR were sealed during these experiments to prevent any flow through them.

Catalyst properties (*i.e.* active surface area) could be one of the reasons for the observed deviations (Table 6.1) since every experiment was performed with a freshly prepared Cu coated milli-reactor tube. However, the same reactor tube showed different performance (steady state temperatures and conversion) at two different positions (Position T2 and B2, see Figure 6.1b) in the MTMR (Figure 6.9).

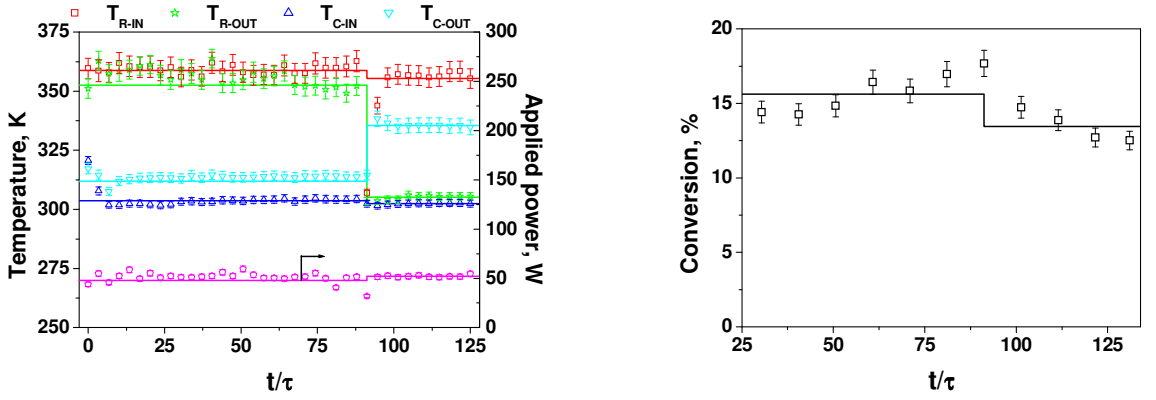

(a) *(b)*

Figure 6.9: a) Temperature-time (normalized with residence time, τ = 90 s) history of a single Cu thin film coated reactor tube with surrounding coolant flow (□: reactant inlet temperature, ☆: reactant outlet temperature, △: coolant inlet temperature, ▽: coolant outlet temperature, ⬠: applied microwave power). b) Conversion of phenylacetylene over time (normalized with residence time). Reaction started when the coated milli-reactor tube was first at position T2 (see Figure 6.1b) until t/τ = 90. The MTMR was then turned clockwise by 120 deg to bring the reactor tube at position B2 (see Figure 6.1b). Flow rates of reaction mixture and coolant: $1.66 \cdot 10^{-9}$ and $4.16 \cdot 10^{-7}$ m^3/s, respectively. RM: reaction mixture; C: Coolant.

The MTMR assembly was turned at t/τ (real time/residence time) of 90 to bring the coated reactor tube from the position T2 to the position B2 of the MTMR. The steady state temperatures of the reaction mixture and coolant as well as the conversion of phenylacetylene changed as soon as the MTMR was turned (Figure 6.9). This immediate change in steady state temperature and conversion pattern

suggested that the deviations in an individual reactor tube performance were resulting from the microwave field (energy) distribution at respective position of the MTMR.

The influence of the microwave field (energy) distribution was also evident, when the steady state conversions of phenylacetylene at each of the MTMR section were compared with each other (Table 6.1). Being in the highest field intensity region, the central tube (position C) gave highest conversion. The middle section (positions M1, M2) being exposed to a stronger microwave field as compared to the top (positions T1, T2) and bottom (positions B1, B2) sections also gave higher conversions than both of these sections (Table 6.1). The deviations in the steady state conversion at the top (positions T1, T2) and the bottom sections (positions B1, B2) could be due to local coolant flow pattern in a horizontal arrangement of the reactor assembly. Rather low coolant temperatures at the top section (positions T1, T2) confirmed the poor cooling of the top section (Table 6.1). The cooling, however, can be improved by using baffles in the shell part of the MTMR assembly.[35] Thus the combined effect of the local coolant flow pattern and microwave energy non-uniformity resulted in a different performance of the reactor tubes in the top, middle and bottom sections (Table 6.1) of the MTMR.

6.3.4 Cu film temperature

In this section the temperature on the Cu film was kinetically estimated to analyze further the deviations in the steady state conversion of phenylacetylene in a milli-reactor tube at various positions of the MTMR. It was assumed that the same surface reaction occurred on the copper particles in the batch reactor as on the copper surface in the tubular microwave heated reactor. Thus a plug flow behavior and uniform microwave absorption by the coating over the entire length of the reactor allows a relation between the temperature of the Cu film and the steady state conversion (as given by Eq. 6.1). Appendix A gives the details of the derivation for catalyst surface temperature as a function of conversion in a wall-coated plug flow reactor.

$$\ln\left(\frac{1}{1-X}\right)=\frac{k_0 e^{-Ea/RT}}{(1-\varepsilon)}\frac{d_P}{6}\frac{a_{film}\pi d_R \delta l}{F_V} \tag{6.1}$$

It was also verified that there are no mass transfer limitations in the wall-coated plug flow reactor by calculating the liquid solid mass transfer coefficient (k_{ls}) and comparing it with the overall reaction rate coefficient (k_{ov}). The details of these calculations can be found in Appendix B. Kinetic batch experiments for the synthesis of 1,3-diphenyl-2-propynyl piperidine (Scheme 6.1) were conducted for the determination of activation energy, E_a and frequency factor, k_0. The detailed results and discussion of these batch experiments can be found in Appendix C. The activation energy (E_a) of (52 ± 2)·10^3 J/mol and the frequency factor (k_0) of (1.14± 0.05)·10^3 s^{-1} was obtained from the temperature dependence batch experiments. The active catalytic surface area (a_{film}) determined by pulse chemisorptions was (8.9 ± 0.5)·10^6 m^2_{cat}/m^3_{cat}. The estimated dependence of the catalyst temperature for the multi component reaction (Scheme 6.1) on the steady state conversion of phenylacetylene is graphically shown in Figure 6.10.

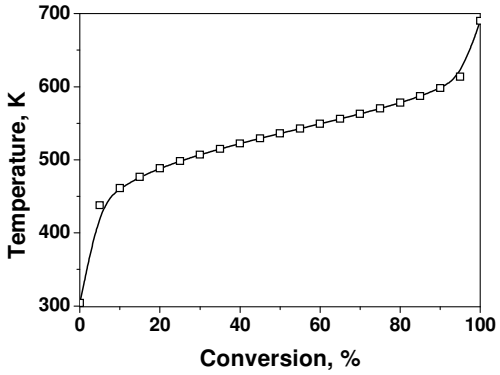

Figure 6.10: Temperature on the copper surface as a function of steady state conversion of phenylacetylene determined based on the surface kinetics (Eq. 6.1).

The mean catalyst temperature over the six peripheral reactor tubes (B1, B2, M1, M2, T1, and T2) was 477 ± 10 K with the maximum deviation of 8.5 ± 0.5 K (Table 6.2). It is important to note here that the estimated mean catalyst temperature was almost 100 K higher than the recorded bulk liquid temperatures. If only 50 % of the determined surface area ($a_{film}/2$) is assumed to be active for the reaction of the bulky reactants, then the calculated mean catalyst temperature

further raised to 504 ± 12 K. The catalyst temperature (hence conversion) in the central tube (position C, Figure 6.1b) was exceptionally high due to highest microwave field intensity. Therefore it was omitted from the calculations of the mean catalyst temperature. These calculations suggest that although there are deviations in reaction temperature at individual positions in the MTMR, parallelization of reactor tubes for scaling out the microwave assisted continuous fine chemical synthesis is a viable option, provided that all the reactor tubes are hexagonally arranged around a central axis.

Table 6.2: Steady state temperatures on the catalyst surface and their deviations from the mean value at all seven positions in the MTMR assembly

Position[1,2,3]	**Conversion (%)**	**Catalyst temperature (K)**	**Deviation (T - $\overline{T}$) (K)**
T1	15.4	477.5	0.2
T2	15.6	478.1	0.7
M1	18.3	484.4	7.1
M2	18.2	484.4	7.1
B1	12.5	469.5	-7.8
B2	12.7	470.1	-7.3
C	25.4	499.0	21.7

[1] Individual positions are designated in Figure 6.1

[2] Average over 6 (peripheral) positions is $\overline{T}$ = 477.3 K

[3] Flow rate of reaction mixture and coolant: $1.66 \cdot 10^{-9}$ and $4.16 \cdot 10^{-7}$ m^3/s, respectively. RM: reaction mixture; C: Coolant; all experiments conducted for over 4 hours of the run time.

6.3.5 Throughput

The numbering-up approach was employed by performing the reaction in six peripheral reactor tubes (B1, B2, M1, M2, T1, and T2, Figure 6.1b). Parallelization of the reactor tubes resulted in a production rate of 1193 kg_{prod}/kg_{cat}·hr of 1,3-diphenyl-2-propynyl piperidine (overall flow rate: $1 \cdot 10^{-8}$ m^3/s, applied power: 300 W, run time: 8 hr) which was a 5.6-fold increase as compared to that in a single tube. This was slightly lower than the expected factor of 6, probably due to uneven distribution of the reactant flow. A supply chamber instead of a well designed distributor was employed for the reactant flow through all the milli-reactor tubes (Figure 6.1c, discussed in the sub-section 2.1). The gravitational effect due to horizontal arrangement of the MTMR assembly can be strong on the fluid entering

the supply chamber. Therefore, it was suspected that the flow of the reaction mixture was higher through the bottom reactor tubes (B1, and B2) which gave the lowest steady state conversions of phenylacetylene. However, the flow distribution can easily be tackled by implementing a properly designed distributor at the inlet of the MTMR assembly.[36]

6.4 Conclusions

A multi-tubular milli-reactor/heat exchanger (MTMR) was developed and tested to bring microwave assisted fine chemical synthesis to a commercially relevant production scale of 1 kg/day. The MTMR system was successfully tested for the Cu catalyzed production of 1,3-diphenyl-2-propynyl piperidine starting from benzaldehyde, piperidine and phenylacetylene. The deposition of Cu thin films (350 ± 40 nm) on the inner wall of the reactor tube resulted in uniform and efficient microwave absorption by all the tubes in the MTMR assembly. However, XPS and ICP analysis clearly indicated that the oxidation and leaching of the Cu coatings led to a decreased activity during the course of operation. The main cause for the copper leaching was attributed to uncontrolled and excessive heat built up from the microwave irradiation. Cooling the outer surface of the tubes by a counter-current flow of a microwave transparent coolant (toluene) reduced this copper leaching. Extraction of excessive heat boosted the steady performance of the reactor tubes. The thermal flux towards the coolant amounted up to 50% of the total microwave energy input to the system. A production rate of 213 ± 11 kg_{prod}/kg_{cat}·hr was achieved in a single reactor tube at a bulk temperature of 373 ± 5 K and a reactant flow rate of $1.66 \cdot 10^{-9}$ m^3/s. Higher field intensity due to a focused microwave field at the central section (position C, Figure 6.1) resulted in a better performance than the surrounding reactor tubes (T1, T2, M1, M2, B1, B2) in the MTMR assembly. Estimation of the temperature of the microwave-heated cooper film was done on the basis of the kinetics of the reaction on the surface of the copper particles dispersed in the reaction mixture. Surface reaction rate coefficients were determined in a conventionally heated batch reactor. The temperature of the copper surface in the reactor tubes was found to be at least 100 K higher than the bulk

temperature of the reaction mixture. The temperature deviation in the multiple reactor tubes in terms of the kinetically determined reaction temperature was not more that 8.0 ± 0.5 K. These minor deviations were due to the local coolant flow and microwave energy non-uniformity. The obtained throughput factor of 5.6 was lower than the expected factor of 6 as a result of the flow distribution. It was successfully demonstrated that the numbering up approach wherein parallelization of multiple milli-reactor tubes can successfully be implemented in scaling up the microwave assisted fine chemical synthesis towards commercially interesting production rates.

Nomencleture

Symbol	Description
a_{cat}	surface area per unit volume of copper power, m^2_{cat}/m^3_{cat}
a_{film}	surface area per unit volume of the copper film, m^2_{cat}/m^3_{cat}
a_{Cu}	surface area per unit reactor length of the copper film, m^2_{cat}/m_R
C_{A0}	initial concentration of component A, mol/m^3_R
C_A	instantaneous concentration of component A, mol/m^3_R
D_{mol}	molecular diffusivity (assumed to be of toluene = $8.97 \cdot 10^{-8}$), m^2/s
d_p	particle diameter of the powdered copper catalyst, m_{cat}
d_R	reactor tube diameter, m_R
E_a	activation energy, J/mol
F_A	molar flow rate of species A, mol/s
F_V	volumetric flow rate, m^3/s
k	global reaction rate constant, s^{-1}
k'	surface reaction rate constant, $m^3_R/m^2_{cat} \cdot s$
k_0	pre-exponential factor in Arrhenius equation, s^{-1}
k_{ov}	overall rate constant, m_R/s
k_r	reaction rate coefficient, m_R/s
$<k_{ls}>$	liquid-solid mass transfer coefficient, m/s
l	reactor length, m_R
M_B	molecular weight of the solvent, g/mol
Mw	molecular weight of the product, g/mol
R	gas constant, 8.314 J/mol.K
Re	Reynolds number
r_A	reaction rate, $mol/m^3_R.s$
Sh	Sherwood number
Gz_l	Graetz number
T	temperature, K
t	real time, s
V_{cat}	catalyst volume, m^3_{cat}

V_{film}	copper film volume per unit reactor length, m^3_{cat}/m_R
V_R	reactor volume, m^3_R
V_A	molar volume of the solute, cm^3/mol
$<v>$	cross-sectional velocity of reaction mixture, m_R/s
x	differential reactor length, m_R
X	conversion of phenylacetylene

Greek symbols

$1-\varepsilon$	catalyst volume fraction
δ	catalyst film thickness, m
τ	residence time, s
μ	viscosity of solvent, cP
Ψ_B	association factor

Subscripts

RM	reaction mixture
C	coolant
IN	inlet
OUT	outlet

Appendix 6.A

Catalyst surface temperature as a function of conversion in a wall-coated plug flow reactor

The reaction is at the copper surface in the batch reactor as well as in the wall-coated tubular reactor. Therefore, the observed reaction rate constant (k) determined from the kinetic batch experiments has to be converted to a surface reaction constant (k').

$$r_A = kC_A \tag{6A.1}$$

with $k = k'a_{cat}\frac{V_{cat}}{V_R}$ (6A.2)

and $V_{cat} = (1-\varepsilon)V_R$ (6A.3)

assuming a spherical catalyst particle; surface per unit volume of the catalyst is

$$a_{cat} = \frac{6}{d_P} \tag{6A.4}$$

Thus, after combining Eq. 6A.2 to Eq. 6A.4 the surface reaction rate constant (k') becomes

$$k' = k\frac{d_P}{6(1-\varepsilon)} \tag{6A.5}$$

with $k = k_0 e^{-Ea/RT}$, the temperature dependence of the surface rate coefficient becomes

$$k' = \frac{k_0 e^{-Ea/RT}}{(1-\varepsilon)} \frac{d_P}{6} \tag{6A.6}$$

Now the plug flow reactor equation linearized for the available surface of copper for a first order reaction is[37]:

$$\frac{dF_A}{dx} = -k' a_{Cu} C_A \tag{6A.7}$$

Rearrangement with $F_A = F_V C_A$ leads to

$$\frac{dC_A}{C_A} = \frac{-k' a_{Cu}}{F_V} dx \tag{6A.8}$$

Integration leads to

$$\ln\left(\frac{C_{A0}}{C_A}\right) = \frac{k' a_{Cu} l}{F_V} \tag{6A.9}$$

The copper surface area (a_{Cu}) per unit reactor length is

$$a_{Cu} = a_{film} V_{film} \tag{6A.10}$$

where the volume of the copper film (with thickness δ) per unit reactor length (d_R) for δ <<< d_R is

$$V_{film} = \pi d_R \delta \tag{6A.11}$$

and a_{film} is the surface area per unit volume of the copper film (m^2_{Cu}/m^3_{Cu}) which was experimentally determined by pulse chemisorption.

After combining Eq. 6A.6 with Eq. 6A.9 to Eq. 6A.11 and replacing concentrations with conversion we get,

$$\ln\left(\frac{1}{1-X}\right) = \frac{k_0 e^{-Ea/RT}}{(1-\varepsilon)} \frac{d_P}{6} \frac{a_{film} \pi d_R \delta l}{F_V} \tag{6A.12}$$

Equation 6A.12 gives a relation between conversion and the temperature of the copper film.

Appendix 6.B

Verification of mass transfer limitations

For a 1st order reaction in a plug flow reactor with a smooth catalyst film deposited on the wall, the overall rate constant (k_{ov}) can be calculated by using the following equation

$$k_{ov} = \frac{F_V}{\pi d_R l} \ln\left(\frac{1}{1-X}\right) \tag{6B.1}$$

The overall rate constant (k_{ov} = 9.18·10^{-8} m_R/s at 373 K) is a sum of the resistances defined in terms of liquid-solid mass transfer coefficient (<k_{ls}>) and reaction rate coefficient (k_r).

$$\frac{1}{k_{ov}} = \frac{1}{k_r} + \frac{1}{\langle k_{ls} \rangle} \tag{6B.2}$$

The liquid-solid mass transfer coefficient for such a reactor systems can be calculated by using the following Sherwood correlation for developed laminar flow (Re = 1.56) in tubes.[38]

$$Sh = \frac{\langle k_{ls} \rangle d_R}{D_{mol}} = 1.62 Gz_l^{-1/3} \tag{6B.3}$$

where Graetz number is

$$Gz_l = \frac{D_{mol} l}{\langle v \rangle d_R^2} \tag{6B.4}$$

$$\text{with, } \langle v \rangle = \frac{4F_V}{\pi d_R^2} \tag{6B.5}$$

and the molecular diffusivity (D_{mol}) by the Wilke-Chang correlation[39] is

$$D_{mol} = \frac{7.4 \times 10^{-8} T(\psi_B M_B)}{\mu V_A^{0.6}} \tag{6B.6}$$

At an association factor (Ψ_B) of 1 for toluene (assumed to be same as for benzene), the molecular diffusivity (D_{mol}) was found to be 2.7·10^{-9} m^2/s and the liquid-solid mass transfer coefficient (<k_{ls}>) of 5.6·10^{-6} m/s.

Mass transfer limitations can said to be nonexistent if the resistance due to liquid-solid mass transfer ($\frac{1}{\langle k_{ls} \rangle}$) is much less than over all resistance ($\frac{1}{k_{ov}}$).

$$\frac{\frac{1}{\langle k_{ls} \rangle}}{\frac{1}{k_{ov}}} \ll 1 \tag{6B.7}$$

In our case the ratio of resistances (Eq. 6B.7) was found to be 1.6·10^{-2}. Therefore, it was assumed that there are no mass transfer limitations in the wall-coated plug flow reactor system. Note that in the actual situation, see Figure 6.3, the area for mass transfer is considerably larger than $\pi d_R l$.

Appendix 6.C

Batch experiments of the multi component reaction for determination of kinetics

A temperature dependence of the kinetic constant for the synthesis of 1,3-diphenyl-2-propynyl-piperidine (Scheme 6.1) was determined to calculate the mean reaction temperatures on the catalyst surface in the different tubes of the MTMR assembly. The concentration of phenylacetylene and benzaldehyde was measured over time in a three-neck round-bottomed flask equipped with a reflux condenser using oil bath heating in the 353-393 K temperature range. A 0.8 wt% (based on the total mass of the reaction mixture) Cu(0) catalyst with an average particle size of 50 μm (> 99.5 wt. %, Aldrich) was added after the temperature had reached the desired set-point. The reaction mixture of $2.5 \cdot 10^{-5}$ m^3 was magnetically stirred at 1000 rpm. The temperature of the reaction mixture was monitored with a thermocouple with an accuracy ±1 K. These experiments were carried out at the same reactant concentration as used in the MTMR experiments and same GC analysis procedure was followed.

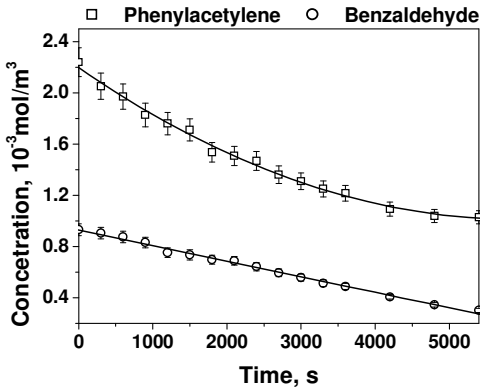

Figure 6C.1: Typical reactant concentration-time profiles in the batch reactor (□: phenylacetylene, ○: benzaldehyde). Initial concentrations of benzaldehyde, piperidine, and phenylacetylene, were $1.5 \cdot 10^{-3}$, $1.8 \cdot 10^{-3}$, $2.25 \cdot 10^{-3}$ mol/m^3, respectively. Reaction volume: $2.5 \cdot 10^{-5}$ m^3; temperature: 393 K; agitation speed: 1000 rpm; Cu catalyst loading: 0.8 wt%; d_p = 50 μm.

Figure 6C.1 shows a typical concentration time profile of the reactants phenylacetylene and benzaldehyde obtained during these batch experiments with a dispersion of Cu particles in the reaction mixture. A fast equilibrium of benzaldehyde and piperidine resulted in an iminium intermediate which reacted with phenylacetylene activated by the copper surface to the final product.[30]

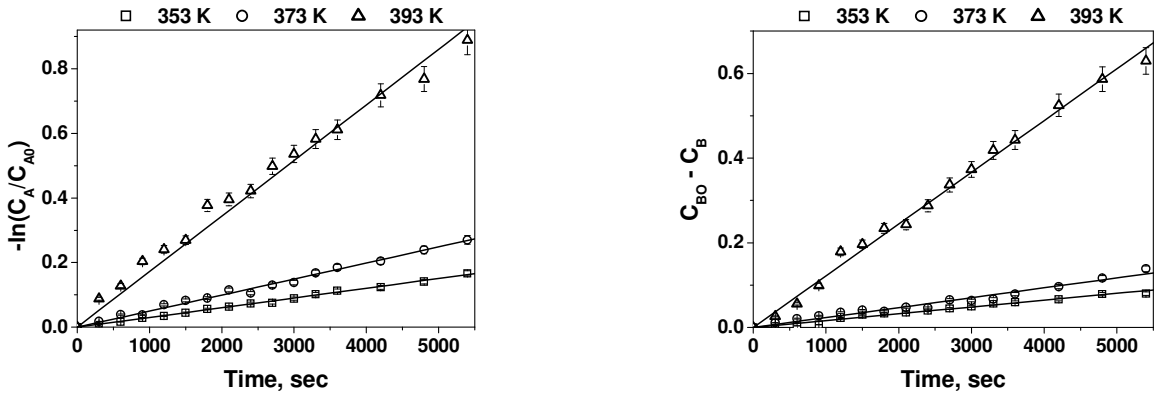

(a) *(b)*

Figure 6C.2: a) 1st order dependency of the multi component reaction on phenylacetylene concentration (C_A) at different reaction temperatures (□: 353 K, ○: 373 K, △: 393 K). b) 0th order dependency of the multi component reaction on benzaldehyde concentration (C_B) at different reaction temperatures (□:353 K, ○: 373 K, △: 393 K). Initial concentrations of benzaldehyde, piperidine, and phenylacetylene, were $1.5 \cdot 10^{-3}$, $1.8 \cdot 10^{-3}$, $2.25 \cdot 10^{-3}$ mol/m^3, respectively. Reaction volume: $2.5 \cdot 10^{-5}$ m^3; agitation speed: 1000 rpm; Cu catalyst loading: 0.8 wt%; d_p = 50 μm.

Accordingly, the global rate law showed a first-order dependence on the phenylacetylene concentration (C_A) and a zeroth order dependence on the benzaldehyde concentration (C_B) (Figure 6C.2).

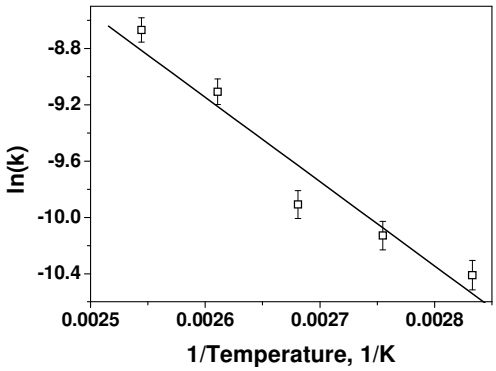

Figure 6C.3: Effect of temperature on the reaction rate coefficient based on the reaction rate per unit volume reaction mixture of the multi-component reaction. Initial concentrations of benzaldehyde, piperidine, and phenylacetylene, were $1.5 \cdot 10^{-3}$, $1.8 \cdot 10^{-3}$, $2.25 \cdot 10^{-3}$ mol/m^3, respectively. Reaction volume: $2.5 \cdot 10^{-5}$ m^3; agitation speed: 1000 rpm; Cu catalyst loading: 0.8 wt%; d_p = 50 μm.

This allowed determination of the reaction rate constant ($k \approx 5.0 \times 10^{-5}$ s^{-1} at 373 K) based on phenylacetylene concentration-time profiles and its dependence on the temperature (Figure 6C.3). The activation energy (E_a) and frequency factor (k_0) were calculated to be $(52 \pm 2) \cdot 10^3$ J/mol and $(1.14 \pm 0.05) \cdot 10^3$ s^{-1}, respectively, by using the Arrhenius equation.

At several places in this manuscript, results are discussed in the form of production rate which was calculated based on conversion by using equation 6C.1. Additionally the claimed production scale of 1 kg/day is an extrapolation of the production rate which can be achieved by using required catalyst amount, *i.e.* number of coated reactor tubes. With average catalyst weight of $2 \cdot 10^{-6}$ kg in each reactor, around 18 tubes are necessary for achieving the claimed production scale of 1 kg/day. This can easily be achieved by having three parallel MTMR systems running simultaneously on three microwave cavities for the whole day.

$$P = \frac{XC_A F_V Mw}{W} 3600 \qquad (6C.1)$$

References

1. Gerven T. Van.; Stankiewicz, A. Structure, energy, synergy, time - The fundamentals of process intensification. *Ind. Eng. Chem. Res.* **2009**, *48*, 2465.
2. Shore, G.; Morin, S.; Organ, M. G. Catalysis in Capillaries by Pd Thin Films Using Microwave-Assisted Continuous-Flow Organic Synthesis (MACOS). *Angew. Chem.* **2006**,*118*, 2827.
3. He, P.; Haswell, S. J.; Fletcher, P. D. I. Efficiency, monitoring and control of microwave heating within a continuous flow capillary reactor. *Sens. Actuators B.* **2005**, *105*, 516.
4. Benaskar, F.; Hessel, V.; Krtschil, U.; Lo□b, P.; Stark, A. Intensification of the Capillary-Based Kolbe−Schmitt Synthesis from Resorcinol by Reactive Ionic Liquids, Microwave Heating, or a Combination Thereof. *Org. Process Res. Dev.* **2009**, *13*, 970.
5. Moseley, J. D.; Kappe, C. O. A critical assessment of the greenness and energy efficiency of microwave-assisted organic synthesis. *Green Chem.* **2011**, *13*, 794.
6. Kappe, C. O. Microwave dielectric heating in synthetic organic chemistry. *Chem. Soc. Rev.* **2008**, *37*, 1127.
7. Patil, N. G.; Hermans, A. I. G.; Benaskar, F.; Rebrov, E. V.; Meuldijk, J.; Hulshof, L. A.; Hessel, V.; Schouten, J. C.; Energy efficient and controlled flow processing under microwave heating by using a milli reactor-heat exchanger. *AIChE J.* **2012**, Accepted, DOI 10.1002/aic.13713.
8. Patil, N. G.; Rebrov, E. V.; Esveld, E.; Eränen, K.; Benaskar, F.; Meuldijk, J.; Mikkola, J. -P.; Hessel, V.; Hulshof, L. A.; Murzin, D.Y.; Schouten, J. C. Effect of the load size on the efficiency of microwave heating under stop flow and continuous flow conditions. *J. Microwave Power EE.* **2012,** submitted / in press.
9. Amore, K. M.; Leadbeater, N. E. Microwave-Promoted Esterification Reactions: Optimization and Scale-Up. *Macromol. Rapid Commun.* **2007**, *28*, 473.
10. Kremsner, J. M.; Stadler, A.; Kappe, C. O. The Scale-Up of microwave-Assisted Organic Synthesis. *Top. Curr. Chem.* **2006**, *266*, 233.
11. Takeuchi, K.; Nagahata, R. Microwave-assisted Polymer Synthesis: First commercial plant for mass production of lactic acid polymer using a microwave heating. National institute of advanced industrial science and technology, Tsukuba, Japan, 2009. http://www.aist.go.jp/aist_e/latest_research/2009/20091216/20091216.

12. Feher, L. E.; Thumm, M. K. Microwave Innovation for Industrial Composite Fabrication—The HEPHAISTOS Technology. *IEEE Trans. Plasma Sci.* **2004**, *32*, 73.
13. Lehmann, H.; LaVecchia, L. Scale-Up of Organic Reactions in a Pharmaceutical Kilo-Lab Using a Commercial Microwave Reactor. *Org. Process Res. Dev*. **2010**, *14,* 650.
14. Nakamura, T.; Nagahata, R.; Kunii, K.; Soga, H.; Sugimoto, S.; Takeuchi, K. Large-Scale Polycondensation of Lactic Acid Using Microwave Batch Reactors. *Org. Process Res. Dev.* **2010**, *14,* 781.
15. Moseley, J. D.; Woodman, E. K. Scaling-Out Pharmaceutical Reactions in an Automated Stop-Flow Microwave Reactor. *Org. Process Res. Dev.* **2008**, *12,* 967.
16. Bowman, M. D.; Schmink, J. R.; McGowan, C. M.; Kormos, C. M.; Leadbeater, N. E. Scale-Up of Microwave-Promoted Reactions to the Multigram Level Using a Sealed-Vessel Microwave Apparatus. *Org. Process Res. Dev*. **2008**, *12,* 1078.
17. Marafie, J. A.; Moseley, J. D.; The application of stop-flow microwave technology to scaling-out SNAr reactions using a soluble organic base. *Org. Biomol. Chem.*, **2010**, *8*, 2219.
18. Bowman, M. D.; Holcomb, J. L.; Kormos, C. M.; Leadbeater, N. E.; Williams, V. A. Approaches for Scale-Up of Microwave-Promoted Reactions. *Org. Process Res. Dev*. **2008**, *12,* 41.
19. Moseley, J. D.; Lenden, P.; Lockwood, M.; Ruda, K.; Sherlock, J. -P.; Thomson, A. D.; Gilday, J. P. A Comparison of Commercial Microwave Reactors for Scale-Up within Process Chemistry. *Org. Process Res. Dev.* **2008**, *12,* 30.
20. Schmink, J. R.; Kormos, C. M.; Devine, W. G.; Leadbeater, N. E. Exploring the Scope for Scale-Up of Organic Chemistry Using a Large Batch Microwave Reactor. *Org. Process Res. Dev*. **2010**, *14,* 205.
21. Moseley, J. D.; Lawton, S. J. Initial results from a commercial continuous flow microwave reactor for scale-up. *Chem. Today*. **2007**, *25*, 16.
22. Bergamelli, F.; Iannelli, M.; Marafie, J. A.; Moseley, J. D. A Commercial Continuous Flow Microwave Reactor Evaluated for Scale-Up. *Org. Process Res. Dev*. **2010**, *14*, 926.
23. Bagley, M. C.; Fusillo, V.; Jenkins, R. L.; Lubinu, M. C.; Mason, C. Continuous flow processing from microreactors to mesoscale: the Bohlmann–Rahtz cyclodehydration reaction. *Org. Biomol. Chem.* **2010**, *8*, 2245.
24. Bierbaum, R.; Nuchter, M.; Ondruschka, B. Microwave–assisted reaction engineering: Microwave apparatus at mini plant scale with online analysis. *Chem. Eng. Technol.* **2005**, *28*, 427.
25. Matsuzawa, M.; Togashi, S.; Hasebe, S.; Basic Examination of a Pilot Plant for Continuous Flow Microwave-Assisted Chemical Reaction Combined with Microreactors. *J. Thermal Sci. Tech*. **2011**, *6*, 69.
26. Comer E.; Organ, M. G. A Microcapillary System for Simultaneous, Parallel Microwave-Assisted Synthesis, *Chem. Eur. J.* **2005**, *11*, 7223.
27. Kappe, C. O. Aqueous microwave-assisted chemistry. *ChemSusChem.* 2010, *3*, 1085.
28. Buchelnikov, V. D.; Louzguine-Luzgin, D. V.; Xie, G.; Li, S.; Yoshikawa, N.; Sato, M.; Anzulevich, A. P.; Bychkov, I. V.; Inoue, A. *J. App. Phys.* **2008**, *104*, 113505.
29. Shore, G.; Yoo, W.; Li, C.; Organ, M. G. Propargyl Amine Synthesis Catalysed by Gold and Copper Thin Films by Using Microwave-Assisted Continuous-Flow Organic Synthesis (MACOS). *Chem. Eur. J.* **2010,** *16*, 126.

30. Climent, M. J.; Corma, A.; Iborra, S. Homogeneous and heterogeneous catalysts for multi component reactions. *RSC Adv.* **2012**, *2*, 16.
31. Wetzel, C.; Kunz, P. C.; Thiel, I.; Spingler, B. Gold(I) Catalysts with Bifunctional P, N Ligands, *Inorg. Chem.* **2011**, *50*, 7863.
32. Lakshmi Kantam, M.; Laha, S.; Yadav, J.; Bhargava, S. An efficient synthesis of propargylamines via three-component coupling of aldehydes, amines and alkynes catalyzed by nanocrystalline copper(II) oxide, *Tet. Lett.* **2008**, *49,* 3083.
33. Benaskar, F.; Ben-Abdelmoumen, A.; Patil, N. G.; Rebrov, E. V.; Meuldijk, J.; Hulshof, L. A.; Hessel, V.; Krtschil, U.; Schouten, J. C. *J. Flow Chem.* **2011**, *1*, 74
34. Benaskar, F.; Engels, V.; Rebrov, E.; Patil, N. G.; Meuldijk, J.; Thüne, P. C.; Magusin, P. C. M. M.; Mezari, B.; Hessel, V.; Hulshof, L. A.; Hensen, E. J. M.; Wheatley, A. E. H.; Schouten, J. C. Novel Cu-based catalysts supported on TiO_2 films for Ullmann SnAr-type C-O coupling reactions. *Chem. Eur. J*. **2012,** *18,* 1800.
35. Babu, B. V.; Munawar, S. A. Differential evolution strategies for optimal design of shell-and-tube heat exchangers. *Chem. Eng. Sci.* **2007**, *62,* 3720.
36. Rebrov, E. V.; Ismagilov, I. Z.; Ekatpure, R. P.; Croon, M. H. J. M. de.; Schouten, J. C. Header Design for Flow Equalization in Microstructured Reactors. *AIChE J*. **2007,** *53*, 28.
37. Fogler, H. S. Elements of chemical reaction engineering *(4th edition)*, Pearson Education International: United States, 2006.
38. Janssen, L. P. B. M; Warmoeskerken, M. M. C. G. Transport Phenomena Data companion *(3rd edition),* Delft university press: Delft, 2001.
39. Wilke, C. R.; Chang, P. Correlation of diffusion coefficients in dilute solutions. *AIChE J.* **1955**, *1*, 264.

7

Scale-up of microwave assisted flow synthesis by transient processing through monomode cavities in series

This chapter will be submitted as:
Patil, N. G.; Benaskar, F.; Rebrov, E. V.; Meuldijk, J.; Hulshof, L. A.; Hessel, V.; Schouten, J. C. Scale-up of microwave assisted flow synthesis by transient processing through cavities in series, *Org. Process Res. Dev.* 2012, *In preparation*.

Abstract

In this chapter, a new scale-up concept for microwave assisted flow processing is presented where modular scale-up is achieved by implementing microwave cavities in series. The scale-up concept is demonstrated for case studies of a packed-bed reactor and a wall-coated tubular reactor. With known kinetics and reaction temperature, a packed-bed reactor gave a conversion of 99 % with highest production rate of 170 kg_{prod}/kg_{cat}·hr for esterification of acetic acid and ethanol catalyzed by ion exchange resin in 18 cavities. A similar approach for a multi component reaction of benzadehyde, piperidine and phenylacetylene catalyzed by a thin Cu film in a wall-coated tubular reactor gave 99 % conversion with the highest production rate of 7740 kg_{prod}/kg_{cat}·hr in 28 cavities. In both cases, pseudo first order reaction rate with respect to the limiting reactant, yielded a typical rise in conversion and production rate. In a packed-bed reactor-heat exchanger operated at a temperature between 343 and 348 K, the conversion in the esterification reaction increased from 22 % to 88 % when the number of cavities was increased from one to eight. The experimental conversions matched the predictions of a packed bed reactor model within 5 %. The production capacity in flow reactors, restricted to smaller sizes due to a limited microwave penetration depth and dominated mainly by the reaction kinetics, was increased by modular scale-up with implementation of the microwave multi-cavity assembly.

7.1. Introduction

Since the last two decades microwave heating has been studied as a promising tool for process intensification.[1-4] The possibility of heating at the locus of the reaction, *i.e.* the catalyst surface, makes it a special intensification tool.[5-6] Direct heating of the catalyst surface, where the reaction occurs, allows higher reaction rates at lower bulk liquid temperatures. This avoids not only large energy input but also excessive heating of the reactants which are sometimes lost due to coke formation.[7-8] The inherently safe (immediate shut down of the energy supply) and efficient nature of the operation makes microwave heating attractive for industrial application.[9-10] However, efficient microwave heating is severely limited by the penetration depth of the microwaves.[11] The penetration depth, being typically in the millimeter range (*e.g.* 13 mm for water), limits uniform heating of the entire reaction mixture. This un-predictive nature of heating makes application for large scale batch processes difficult.

One of the options is to switch from batch operation to flow processing at the early stages in process development. However, replicating standardized batch procedures in continuous reactors not only leads to questionable underperformance but also jeopardizes the application of microwave heating in general.[12-16] The idea of scaling very small batch volumes (5 ml) by replication in flow reactors (liters per min) almost never works.[17,18] The reasons are simple. Firstly, microwave heating is selective in nature and often this characteristic is not explicitly understood for most of the case studies. Secondly, in almost all of the case studies, the process is initially developed in monomode type microwave cavities and then transferred to larger multimode microwave cavities for scaling up. However, our previous studies suggest that process performance is strongly dependent on the microwave equipment type. As a consequence, a specific microwave integrated reactor design is necessary for optimal performance.[9,19]

One of the suitable approaches for scaling microwave assisted flow processing is numbering-up.[20-21] Scaling up by numbering-up can be achieved by parallelization of tubular structured reactors with a channel diameter in the millimeter range. Multiple (parallelized) smaller reactors ensure high throughput while taking the

penetration depth limitation into account. The throughput in the case of flow processing, however, is controlled by the kinetics of the conducted chemical reaction. More specifically, the kinetics of the reaction defines the flow rates through reactors needed for characterizing and optimizing the reactor performance at measurable conversions. This ultimately controls the production rate of a specific reactor type and hence the throughput of the process. In our previous work, we have already shown that, once optimized, the flow reactor concept can be scaled out by parallelization, leading to an increased throughput.[21]

Another possibility for scale-up is numbering-up microwave cavities in series.[22] This approach, particularly with applicator type monomode cavities, permits optimization of the energy use in an individual cavity.[5] Once optimized, the microwave cavity and the flow reactor can be placed in series to increase the productivity of the process. Additional improvement in the overall energy efficiency is obvious by using a single main waveguide (single magnetron), thus minimizing the multiple grid to applicator losses (conversion of electrical power into microwave power).

In this chapter, the above mentioned concept of modular scale-up is presented where energy utilization and reactor performance are optimized at a cavity level and then scaled out by transient operation through cavities in series. The productivity increase with each additional cavity in series is determined for two different types of reactors, *i.e.* a packed-bed reactor and a wall-coated reactor. Two different chemical processes, an esterification of acetic acid and ethanol catalyzed by ion exchange resin (in a packed-bed reactor) and a multi component reaction of benzadehyde, piperidine and phenylacetylene catalyzed by a thin Cu film (in a wall-coated tubular reactor) with previously quantified kinetics,[5,14] are used for estimation of the productivity. The theoretically predicted productivities are then validated for the former reaction in the case of a packed-bed reactor.

7.2 Theoretical determination of productivity

The productivity increase with each additional cavity in series is determined for two different types of catalytic reactors, *i.e.* a packed-bed reactor and a wall-coated reactor. The following sub-sections give the details of the steps followed for these calculations.

7.2.1 Esterification reaction in a packed-bed reactor

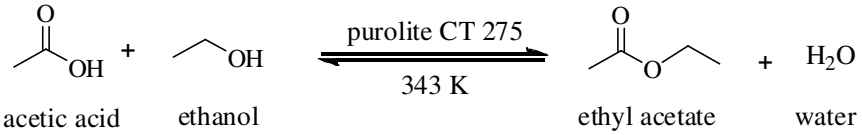

Scheme 7.1: Esterification of acetic acid and ethanol over a solid ion-exchange catalyst to produce ethyl acetate.

Esterification of ethanol and acetic acid to produce ethyl acetate over a packed-bed of strong acid ion-exchange resin (Purolite CT 275) is used as a model reaction (Scheme 7.1). The productivity increase with each consecutive cavity is predicted with known reaction kinetics as well as the dependence of the productivity on the reactor length, catalyst volume, and the reaction temperature. Since the catalyst in this case is confined in a packed-bed of predefined length, the differential form of a packed-bed reactor equation (Eq. 7.1) is solved.

$$F_V dC_A = r_A^{'} = k_{(T)}^{v} C_A dW \tag{7.1}$$

Solving the differential equation (Eq. 7.1) lead to:

$$X = \left(1 - \left(\exp\left(\frac{k^v}{F_v} W\right)\right)^{-1}\right) 100\% \tag{7.2}$$

Using equation 7.2, the increase in conversion with an increased amount of the catalyst (W) can be predicted. The reaction rate constant (k^V) is volumetric in nature and it is dependent on the catalyst volume as well as on the reactor volume (Eq. 7.3).

$$k^V = \frac{k_{obs} V_R}{V_{cat}} \left[\frac{1}{s}\right] \tag{7.3}$$

The observed reaction rate constant (k_{obs}) depends on the temperature through the Arrhenius equation (Eq. 7.4).

$$k_{obs}(T) = k_0 e^{-\frac{E_a}{RT}} \tag{7.4}$$

The reactor volume is

$$V_R = \pi r^2 l \tag{7.5}$$

and catalyst volume is

$$V_{cat} = \frac{W}{\rho_{cat}} \tag{7.6}$$

The length of the reactor (l) and weight of the catalyst (W) increased with each subsequent cavity in the series. The influence of increased reactor length and the catalyst weight, however, vanishes in the calculations of the volumetric reaction rate constant (k^V, Eq. 7.3). Therefore, the conversion and consequently, the productivity increase could be mapped with each additional cavity in series for a packed-bed reactor by using the following equation:

$$X = \left\{1 - \left[\exp\left(\frac{k_0 e^{-E_a/RT} V_R W}{V_{cat} F_V} N\right)\right]^{-1}\right\} 100\% \tag{7.7}$$

where, N is the number of cavities in series. Note that, for equally sized reactor, $V_r W / V_{cat} F_V$ is the same for each cavity-reactor combination. The kinetic experiments to determine the activation energy (E_a) and the frequency factor (k_0) are reported in chapter 4, appendix 4.C.

Table 7.1: Values of the parameters in Eq. 7.7 used for the calculation of the conversion and the production rate

Parameter	Value
k_0	$2.65 \cdot 10^5$ s^{-1}
E_a	$50.5 \cdot 10^3$ J/mol
r	$1.5 \cdot 10^{-3}$ m
l	$75 \cdot 10^{-3}$ m
W	$3 \cdot 10^{-4}$ kg
ρ_{cat}	770 kg/m^3
F_V	$1.67 \cdot 10^{-6}$ m^3/s
T	348 K

The values of parameters in Eq. 7.7, collected in Table 7.1, with an applied reaction temperature of 348 K are used to calculate the conversion (*X*) as a function of the number of cavities (*N*).

7.2.2 Multi component reaction in a wall-coated tubular reactor

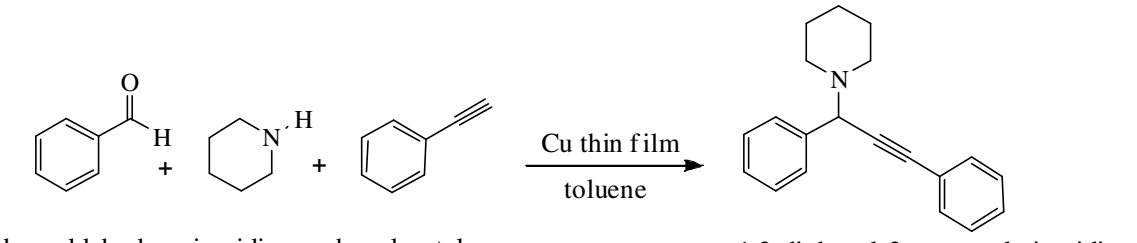

Scheme 7.2: Multi component reaction of benzaldehyde, piperidine and phenylacetylene over a Cu thin film to produce 1,3-diphenyl-2-propynyl piperidine

The multi component reaction of benzaldehyde, piperidine and phenylacetylene to produce 1,3-diphenyl-2-propynyl piperidine over a thin Cu film (Scheme 7.2) was used as the model reaction in the tubular reactor. The productivity increase in the wall-coated reactor with each consecutive cavity is predicted through known reaction kinetics and its dependence on the reactor length as well as the reaction temperature. Since the catalyst in this case is Cu deposited on the inner tube wall, the differential form of the plug flow reactor equation modified for the surface reaction (Eq. 7.8) is used.

$$-F_V dC_A = k' a_{Cu} C_A dx \tag{7.8}$$

Solution of Eq. 7.8 for the surface reaction on the wall of a tubular reactor (see chapter 6, appendix 6.A for the derivation) gives:

$$\ln\left(\frac{1}{1-X}\right) = \frac{k_0 e^{-Ea/RT}}{(1-\varepsilon)} \frac{d_P}{6} \frac{a_{film} \pi d_R \delta l}{F_V} \tag{7.9}$$

The only parameter that changes with each consecutive cavity in this case is the reactor length (*l*). Therefore, the conversion and, consequently, the productivity are mapped with each additional cavity in series for a wall-coated reactor by using Equation 7.10:

$$X = \left\{ 1 - \left[\exp\left(N \frac{k_0 e^{-Ea/RT}}{(1-\varepsilon)} \frac{d_P}{6} \frac{a_{film} \pi d_R \delta l}{F_V} \right) \right]^{-1} \right\} \tag{7.10}$$

where, N is the number of cavities in series. The kinetic experiments to determine the activation energy (E_a) and the frequency factor (k_0) are reported in chapter 6, appendix 6.C.

Table 7.2: Values of the parameters in Eq. 7.10 used for the calculation of the conversion and the production rate

Parameter	Value
k_0	$1.42 \cdot 10^3$ s^{-1}
E_a	$51.7 \cdot 10^3$ J/mol
$(1-\varepsilon)$	0.07 m^3_{cat}/m^3_R
d_P	$5 \cdot 10^{-5}$ m
a_{film}	$8.92 \cdot 10^6$ m^2_{cat}/m^3_{cat}
d_R	$2 \cdot 10^{-3}$ m
δ	$3.5 \cdot 10^{-7}$ m
l	$75 \cdot 10^{-3}$ m
F_V	$1.7 \cdot 10^{-9}$ m^3/s
T	477.3 K

The values of the parameters in Eq. 7.10, collected in Table 7.2, are used together with an applied catalyst surface temperature of 477.3 K (see chapter 6) for calculating the conversion (X) as a function of the number of cavities (N).

For both case studies, *i.e.* for the packed-bed reactor and the wall-coated tubular reactor, the conversion is translated into the production rate, see Equation 7.11.

$$P = \frac{X C_A F_V Mw}{W} 3600 \tag{7.11}$$

7.3 Experimental section

Predictions of conversion and production rate with each consecutive cavity were validated for the ethyl acetate formation in a packed-bed reactor (Scheme 7.1). Figure 7.1 schematically illustrates the packed-bed reactor-heat exchanger assembly. The liquids, *i.e.* the reaction mixture and the coolant (toluene, anhydrous, 99.8 wt%, Sigma-Aldrich), enter the microwave cavity first while flowing through

the integrated reactor-heat exchanger. Here, the reaction mixture is heated directly by the microwaves and the excess of the microwave energy is transferred to the coolant by convective heat transfer. Co-current flow of the microwave transparent coolant is used to avoid overheating of the reaction mixture and to minimize the heat loss to the exterior of the microwave cavity by providing a heated jacket. In chapter 4, optimization of the reactor-heat exchanger size and the length of the catalyst bed are discussed.

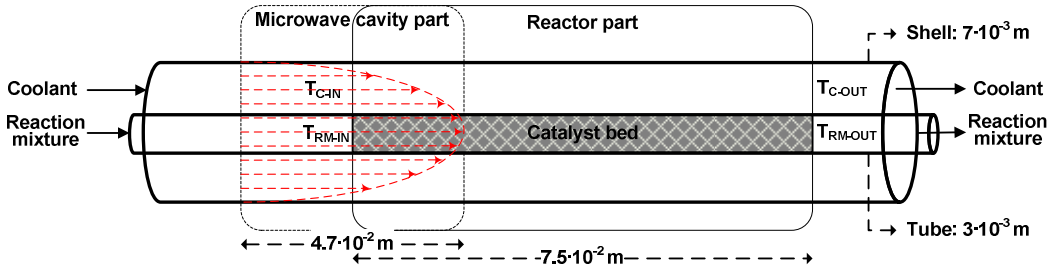

Figure 7.1: Schematic view of the packed-bed reactor-heat exchanger assembly used in the flow experiments of the esterification reaction. Red lines signify the microwave field pattern over the assembly.

7.3.1 Equipment

7.3.1.1 Microwave setup

The microwave setup consists of a single mode microwave waveguide operating at a frequency of 2.45 GHz with adjustable power settings up to 2 kW (Figure 7.2). Four parallel cavities are co-axially coupled with the main waveguide at equal distances to extract the same amount of microwave energy in each of the cavities. The concept of using a main waveguide with a single magnetron (as discussed in chapter 2) is to minimize the grid to applicator losses (conversion of electrical power into microwave power), while providing the possibility of a modular scale-up. Focusing of the resonating microwaves in the cavity as well as in the main waveguide is possible over the inserted reactor (packed-bed in this case, see Figure 7.1) by tuning the cavity with the help of short circuit and 3 stub tuner (Figure 7.2). Focusing of the microwaves allows getting the microwave field maxima on the reactor assembly as shown schematically in Figures 1 and 2. Focusing assures maximum microwave absorption by the reactor assembly and minimum losses to the dead load at the isolator of the cavity. The reflected power is recorded by using

a detector diode on an isolator. This allowed calculation of the microwave power available in the cavity with an accuracy of 90%. Process control and data acquisition were performed via the LABVIEW program.

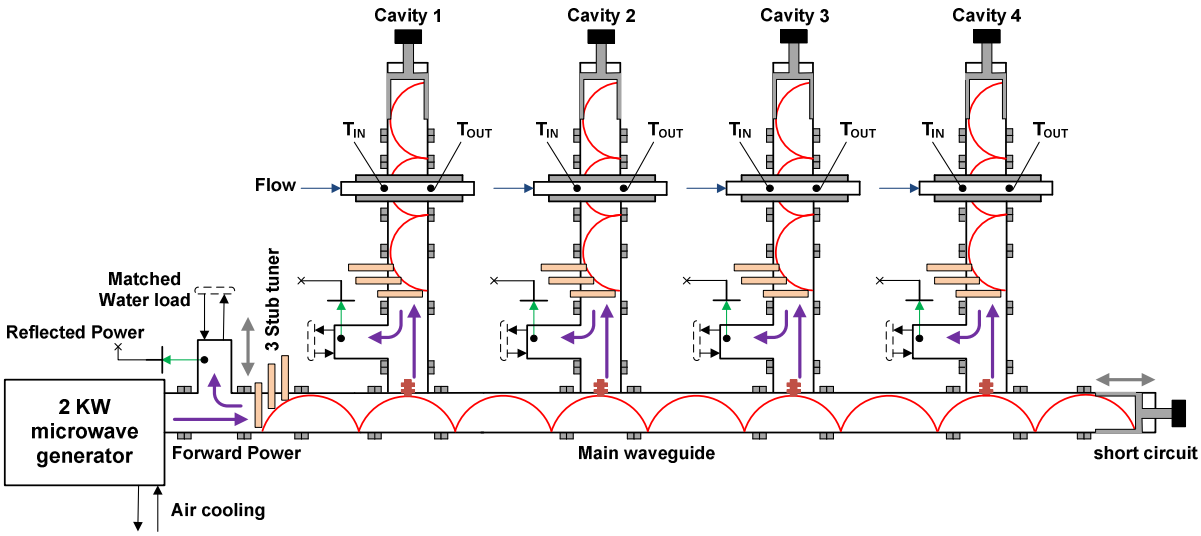

Figure 7.2: Schematic view of the microwave setup with an electric field pattern (red lines) in the setup. Arrows signify flow of energy (purple), signals (green), and liquids (blue), and movement of stub tuner, short circuit (grey). Actual load (reactor) opening diameter: $1.4 \cdot 10^{-2}$ m. Manufacturer: Fricke und Mallah GMbH, Germany.

7.3.1.2 Pumps

Two Gilson HPLC pumps (flow range: $8.33 \cdot 10^{-9}$ to $2.5 \cdot 10^{-6}$ m^3/s) were used to supply the reaction mixture and the coolant to the inner (reactor) tube and to the shell, of the reactor-heat exchanger assembly, respectively.

7.3.2 Experimental procedures

The heterogeneously catalyzed esterification (Scheme 7.1) of acetic acid (99.8%, Sigma Aldrich) and ethanol (99.8%, Sigma Aldrich) is conducted in a packed-bed reactor-heat exchanger assembly (Figure 7.1). 5-Fold excess of ethanol is used in order to increase the conversion for this equilibrium-limited reaction and to maintain a pseudo first-order reaction rate with respect to the acetic acid concentration. The reaction mixture and coolant are pumped through the assembly at the flow rates of $1.67 \cdot 10^{-6}$ m^3/s and $8.35 \cdot 10^{-7}$ m^3/s, respectively. The catalyst, a strong acid ion-exchange resin (CT 275, Purolite®) with average particle diameter of $7.5 \cdot 10^{-4}$ m, is dried for 2 days at room temperature before use. The catalyst bed is packed over a predefined length of $7.5 \cdot 10^{-2}$ m (Figure 7.1). The reaction mixture

temperature is maintained between 343 and 348 K by tuning each cavity independently. Tuning of the cavity allowed controlling the amount of microwave power supplies to each cavity and, consequently, permitted control over the reaction mixture temperature. The unique feature of independent tuning of each cavity is possible due to our novel microwave setup design.

The reaction mixture, flowing through the microwave cavity, gets heated to the desired reaction temperature and entered the catalyst bed for actual reaction before leaving the system towards the collection vessel. Samples are taken over time (every 5 min) and analyzed by gas chromatography (GC) to determine the conversion. The samples for GC analysis are diluted with methyl isobutyl ketone (99.8%, Sigma Aldrich) at a dilution weight ratio of 1:10. Lowering the original concentration of the reaction components allowed precise determination of the concentrations. From the GC-results, the conversion of acetic acid, the limiting reactant, is calculated over time. In multi-cavity experiments, the consecutive cavity is added only after achieving both steady state temperatures and conversion in the previous cavity. Thus, the experiment is started at the first cavity where a steady state is meanwhile achieved and then the outlets of the cavity are connected to the inlets of the second cavity. In a similar manner after achieving a steady state in second cavity, the outlets are connected to the third and then to the fourth cavity.

7.4 Results and Discussion

Increase in production rate with each consecutive cavity was predicted for two cases, *i.e.* using a packed-bed reactor and using a wall-coated tubular reactor. The validation experiments were performed only for the esterification reaction case using a packed-bed reactor. The following sub-sections deal with a discussion on the obtained results in detail.

7.4.1 Packed-bed reactor

Conversion of acetic acid (limiting reactant) for the esterification reaction was calculated with the kinetic parameters (Table 7.1) and the reaction temperature of 348 K by using Eq. 7.7 (section 7.2.1). Figure 7.3 (solid line) shows the dependence of conversion on the number of individual cavities employed in series. The production rate of ethyl acetate (Figure 7.3, dotted line) was calculated from conversion using Eq. 7.11 (section 7.2) assuming an equal amount of catalyst in each cavity (*i.e.* $W = 3 \cdot 10^{-4}$ kg).

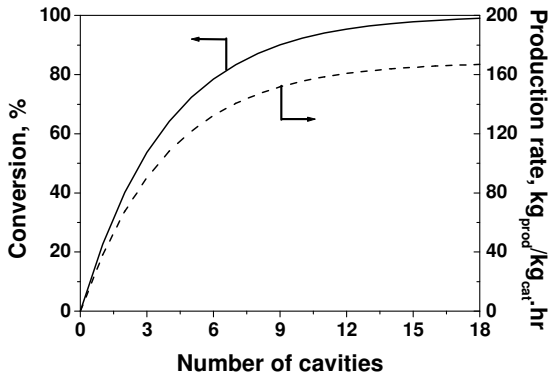

Figure 7.3: Predicted conversion of acetic acid (solid line) and production rate of ethyl acetate (dotted line) for the esterification reaction (Scheme 7.1) in a packed-bed reactor as a function of the number of cavities.

A steep increase of the conversion as well as the production rate was observed for $0 < N < 8$ which lateron flattened out for $N \geq 8$. This is typical for a pseudo first order dependency of the reaction rate on the concentration of limiting reactant (acetic acid). Theoretically, at around 18 cavities, the conversion reached almost 99 % and the production rate at this conversion extrapolated to around 170 kg_{prod}/kg_{cat}.hr.

7.4.2 Wall-coated tubular reactor

Similarly, conversion of phenylacetylene for the multi component reaction (Scheme 7.2) was calculated the known kinetic parameters (Table 7.2) and the catalyst surface temperature of 477.3 K, by using Eq. 7.10 (section 7.2.2). Figure 7.4 shows the dependence of the conversion on the number of cavities employed in series. The production rate was calculated by Eq. 7.11 (section 7.2) based on the known catalyst amount needed per reactor (*i.e.* $W = 2 \cdot 10^{-6}$ kg/reactor tube with six reactor tubes in parallel) in each cavity (Figure 7.4, dotted line). Similar to the packed-bed reactor case, the multi component reaction is first order with respect to phenylacetylene in the wall-coated tubular reactor. Therefore, both the conversion as well as the production rate were seen to be increasing steeply at the beginning ($0 < N < 10$) and then both flattened out in the latter part for $N \geq 10$.

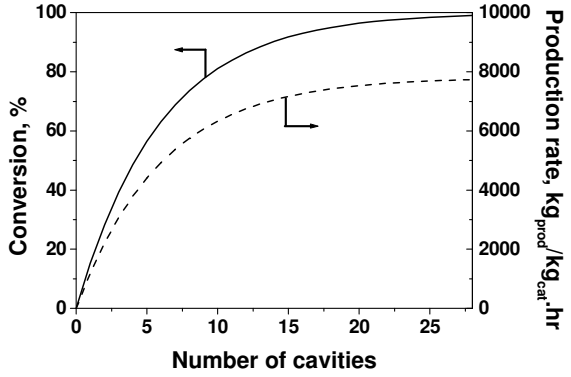

Figure 7.4: Predicted conversion of phenylacetylene (solid line) and the production rate of 1,3-diphenyl-2-propynyl piperidine (dotted) for the multi component reaction (Scheme 7.2) in a wall-coated tubular reactor as a function of the number of cavities.

At around 28 theoretical cavities, the conversion reached almost 99 % and the production rate at this conversion extrapolated to around 7740 kg_{prod}/kg_{cat}·hr. The production rate obtained for the wall-coated tubular reactor at a lower reaction mixture flow rate was a factor of 50 higher than the production rate obtained in the case of a packed-bed reactor for the esterification reaction. It should be noted that, the flow rate of the multi component reaction mixture in the wall-coated reactor ($1.67 \cdot 10^{-7}$ m^3/s) was a factor of 10 lower than for the esterification reaction in the packed-bed reactor ($1.67 \cdot 10^{-6}$ m^3/s). This is majorly due to selective heating of the catalyst film which permits conversion calculation at high temperatures (100 K

higher than the bulk) otherwise impossible to achieve with bulk liquid heating (see chapter 6). Thus, catalyst activity increased by selective heating is a key issue for process intensification by using microwaves and milli-reactors.

It is important to note here that in both cases *i.e.* a packed bed reactor and a wall-coated reactor, the theoretical conversion of 90 % is achieved in 8 and 13 cavities in series, respectively. These are less than half the number of cavities needed to reach 99 % conversion in both cases. Thus, it is more practical to exploit another ways such as increasing reactant concentration or reaction temperature to reach complete conversion. The approach of modular scale-up, *i.e.* utilization of cavities in series and independent operation through each consecutive cavity provides such a possibility. While the approach of recycling[23] having conceptual similarity of conversion enhancement cannot provide such as a possibility. This particular feature makes the concept of modular scale-up more attractive.

7.4.3 Experimental validation for the packed-bed reactor

Next, the conversion and, consequently, the production rate were validated in the multi-cavity experiments for the case of the esterification reaction in a packed-bed reactor, *i.e.* reaction of acetic acid with excess of ethanol over a packed-bed of strong acid ion-exchange resin (Scheme 7.1). Figure 7.5 shows the steady state temperature and the steady state conversion obtained in each consecutive cavity. The reaction mixture temperature was maintained between 343 and 348 K at an average applied microwave power of 32 W in each cavity (Figure 7.5). The steady state conversion increased logarithmically from 22 % in the first cavity to 65 % in the fourth cavity. The steady state conversions of 38 % and 55 % were obtained in the second and the third cavity, respectively.

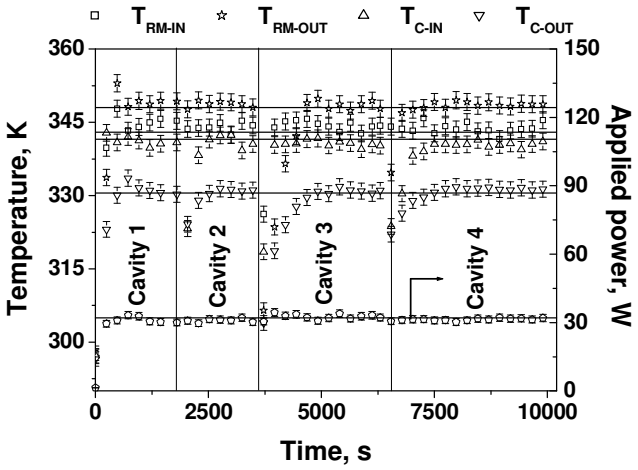

(a)

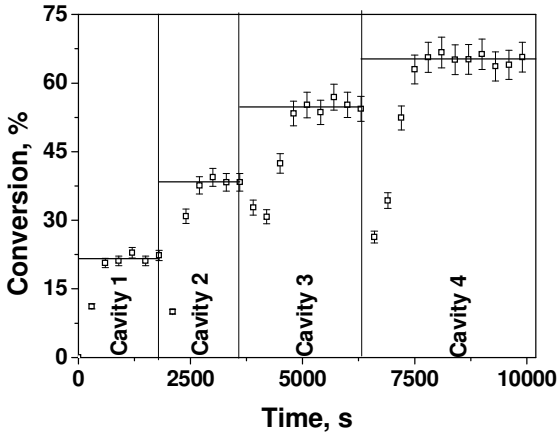

(b)

Figure 7.5: a) Temperature-time history of a packed-bed reactor-heat exchanger assembly (□: reactant inlet temperature, ☆: reactant outlet temperature, △: coolant inlet temperature, ▽: coolant outlet temperature, ⬠: applied microwave power). b) Conversion of acetic acid over time. Horizontal lines in both graphs demonstrate steady state. Flow rates of the reaction mixture and the coolant were $1.67 \cdot 10^{-6}$ and $0.835 \cdot 10^{-6}$ m^3/s, respectively. RM: reaction mixture; C: coolant.

Each time when the product stream of a stabilized cavity was connected as feed to the next cavity in series, approach to a new steady state was longer. Similar to the conversion, time required to reach a steady state increased linearly from 300 s in the first cavity to 1200 s in the fourth cavity. The time required to reach a steady state was 600 s and 900 s for cavity 2 and cavity 3, respectively. This was mainly due to shut down of the setup (*i.e.* pumps and microwave power) before the product stream of the stabilized cavity was connected as feed stream to the next cavity in series. Thus, the time required to reach a steady state, although constant, added up

linearly with each consecutive cavity. The thermal heat flux to the surrounding coolant flow amounted up to 20% of the total energy input to the packed-bed reactor-heat exchanger assembly.

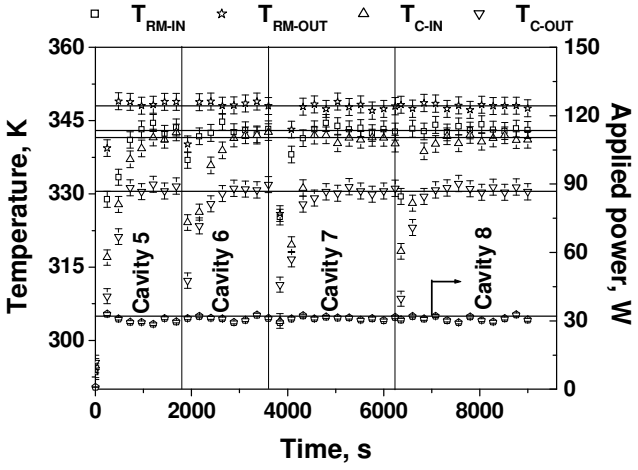

(a)

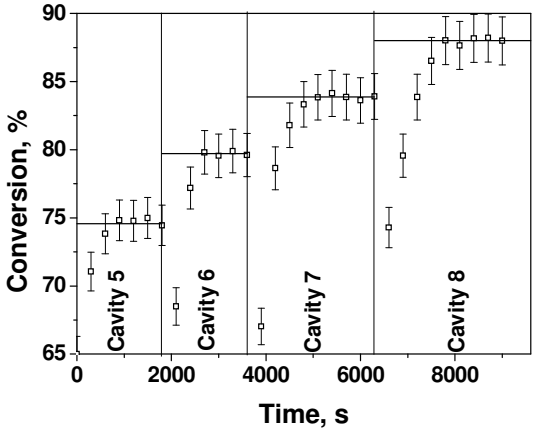

(b)

Figure 7.6: a) Temperature-time history of a packed-bed reactor-heat exchanger assembly (□: reactant inlet temperature, ☆: reactant outlet temperature, △: coolant inlet temperature, ▽: coolant outlet temperature, ⬠: applied microwave power), b) Conversion of acetic acid over time. Horizontal lines in both the graphs demonstrate steady state. Flow rates of the reaction mixture and the coolant were $1.67 \cdot 10^{-6}$ and $0.835 \cdot 10^{-6}$ m^3/s, respectively. RM: reaction mixture; C: coolant.

To see the influence of additional cavities in a series (from five to eight), the next set of experiments began with a reaction mixture composition corresponding to 65 % conversion. Similar to previous observations, the reaction mixture temperature was maintained between 343 and 348 K at an average applied microwave power of 32 W in each cavity (Figure 7.6). However, the increase of the steady state

conversion with stepwise addition of cavities in series was lower in this case (Figure 7.6). It increased from 75 % in the fifth cavity to 88 % in the eighth cavity. The steady state conversions of 80 % and 84 % were obtained in the sixth and the seventh cavity, respectively. The production rate was then calculated for the obtained steady state conversion in each cavity by using Eq. 7.11 (section 7.2). Finally, the experimental results for the conversion as well as for the production rate were compared with the predictions (Figure 7.7).

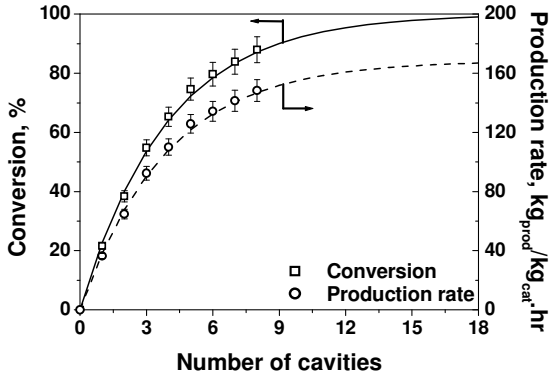

Figure 7.7: Experimental validation of the predicted conversion of acetic acid and the production rate of the ethyl acetate for the esterification reaction in the packed-bed reactor as a function of the number of cavities in series. Symbols: experimental results, lines: theoretical predictions. Model reaction: esterification of acetic acid and ethanol over a strong acid ion-exchange resin to produce ethyl acetate (Scheme 7.1).

The experimentally obtained conversions matched well with the model predictions (error < 5%) for all number of cavities. Further validation by following the same strategy, *i.e.* beginning next set of experiments at reaction mixture composition corresponding with 90 % conversion, was not possible due to high experimental error which is comparable with the theoretically predicted change in the conversion (see prediction in Figure 7.7 for cavity number 9 onwards). The linearity in predictions based on global reaction kinetics and identical behavior of each additional cavity-reactor combination, however, does not require further validation. Therefore, it can be concluded that increasing the production capacity of the flow reactors is possible by increasing the number of microwave cavities in series. Each cavity must be independently tuned to the process requirements without disturbing the microwave field pattern either in neighboring cavities or in the main waveguide.

7.5 Conclusions

A concept of modular scale-up for microwave assisted flow processing has been demonstrated where utilization of cavities in series and transient operation through each consecutive cavity increased the production rate. Two cases, *i.e.* an esterification of acetic acid and ethanol catalyzed by ion exchange resin in a packed-bed reactor and a multi component reaction of benzadehyde, piperidine and phenylacetylene catalyzed by Cu-thin in a wall-coated tubular reactor were used to predict an increase in the conversion and, consequently, the production rate with the use of microwave cavities in series. For the case of esterification reaction in a packed-bed reactor, around 18 cavities in series gave a theoretical conversion of 99 % with extrapolation to the production rate of 170 kg_{prod}/kg_{cat}·hr. In contrast, the case of multi component reaction in a wall-coated tubular reactor, a theoretical conversion of 99 % with extrapolation to the production rate of 7740 kg_{prod}/kg_{cat}·hr was obtained in around 28 cavities. Validation experiments were performed for the case of esterefication reaction in a packed-bed reactor-heat exchanger assembly at stable reaction temperatures between 343 and 348 K. The steady state conversion rose from 22 % in the first cavity to 88 % in the eighth cavity used in series. The experimentally obtained results matched the predictions well within a 5 % of error margin. Thus, an increase of production capacity in flow reactors proved to be possible by implementing microwave cavities in series. This was possible due to our microwave setup design which permitted the independent tuning of each cavity to process requirements without disturbing the microwave field pattern either in neighboring cavities or in the main waveguide. In conclusion, we have provided proof of concept for modular scale-up at minimized grid to applicator losses by utilization of cavities in series over a main waveguide connected to single microwave generator.

Nomenclature

Symbol	Description
a_{film}	surface area per unit volume of the copper film, m^2_{cat}/m^3_{cat}
a_{Cu}	surface area per unit reactor length of the copper film, m^2_{cat}/m_R
C_A	instantaneous concentration of limiting component A, mol/m^3_R

d_p	particle diameter of the powdered copper catalyst, m_{cat}
d_R	reactor tube diameter, m_R
E_a	activation energy, J/mol
F_V	volumetric flow rate, m^3/s
k_{obs}	observed reaction rate constant, $m^3_{cat}/m^3_R.s$
k^V	volumetric reaction rate constant, 1/s
k'	surface reaction rate constant, $(m^3_R/m^2_{cat}.s)$
k_0	pre-exponential factor in Arrhenius equation, (s^{-1})
l	reactor length, m_R
Mw	molecular weight, g/mol
N	number of cavities
P	production rate, $kg_{prod}/kg_{cat}.hr$
R	gas constant, 8.314 J/mol.K
r	radius of the reactor, m_R
r_A	reaction rate, $mol/m^3_R.s$
T	temperature, K
V_{cat}	catalyst volume, m^3_{cat}
V_R	reactor volume, m^3_R
W	catalyst weight, kg_{cat}
x	differential reactor length, m_R
X	conversion of phenylacetylene

Greek symbols

$1-\varepsilon$	catalyst volume fraction
δ	catalyst film thickness, m
ρ_{cat}	catalyst density, kg/m^3

References

1. Gerven T. Van.; Stankiewicz, A. Structure, energy, synergy, time - The fundamentals of process intensification. *Ind. Eng. Chem. Res.* **2009**, *48*, 2465.
2. Hessel, V. Novel Process Windows – Gate to Maximizing Process Intensification via Flow Chemistry, *Chem. Eng. Technol.* **2009,** *32*, 1655.
3. Stankiewicz, A. On the Applications of Alternative Energy Forms and Transfer Mechanisms in Microprocessing Systems, *Ind. Eng. Chem. Res.* **2007,** *46,* 4232.
4. Roberge, D. M.; Ducry, L.; Bieler, N.; Cretton, P.; Zimmermann, B. Microreactor Technology: A Revolution for the Fine Chemical and Pharmaceutical Industries? *Chem. Eng. Technol.* **2005,** *28,* 318.
5. Shore, G.; Morin, S.; Organ, M. G. Catalysis in Capillaries by Pd Thin Films Using Microwave-Assisted Continuous-Flow Organic Synthesis (MACOS). *Angew. Chem.* **2006**, *118*, 2827.
6. Shore, G.; Yoo, W. -J.; Li, C. -J.; Organ, M. G. Propargyl Amine Synthesis Catalysed by Gold and Copper Thin Films by Using Microwave-Assisted Continuous-Flow Organic Synthesis (MACOS). *Chem. Eur. J.* **2010,** *16,* 126.
7. He, P.; Haswell, S. J.; Fletcher, P. D. I. Efficiency, monitoring and control of microwave heating within a continuous flow capillary reactor. *Sens. Actuators B.* **2005**, *105*, 516.

8. Benaskar, F.; Hessel, V.; Krtschil, U.; Lo□b, P.; Stark, A. Intensification of the Capillary-Based Kolbe–Schmitt Synthesis from Resorcinol by Reactive Ionic Liquids, Microwave Heating, or a Combination Thereof. *Org. Process Res. Dev.* **2009**, *13*, 970.
9. Patil, N. G.; Hermans, A. I. G.; Benaskar, F.; Rebrov, E. V.; Meuldijk, J.; Hulshof, L. A.; Hessel, V.; Schouten, J. C.; Energy efficient and controlled flow processing under microwave heating by using a milli reactor-heat exchanger. *AIChE J.* 2011, *Accepted*, DOI 10.1002/aic.13713.
10. Roberge, D. M.; Gottsponer, M.; Eyholzer, M.; Kockmann, N.; Industrial design, scale-up and use of microreactors, *Chimica oggi.* **2009,** *27,* 4.
11. Damm, M.; Glasnov, N. T.; Kappe, O. C. Translating high-temperature microwave chemistry to scalable continuous flow processes. *Org. Process Res. Dev.* **2010**, 14, 215.
12. Moseley, J. D.; Lawton, S. J. Initial results from a commercial continuous flow microwave reactor for scale-up. *Chem. Today*. **2007**, *25*, 16.
13. Bergamelli, F.; Iannelli, M.; Marafie, J. A.; Moseley, J. D. A Commercial Continuous Flow Microwave Reactor Evaluated for Scale-Up. *Org. Process Res. Dev*. **2010**, *14*, 926.
14. Bierbaum, R.; Nuchter, M.; Ondruschka, B. Microwave–assisted reaction engineering: Microwave apparatus at mini plant scale with online analysis. *Chem. Eng. Technol.* **2005**, *28*, 427.
15. Leadbeater, N. E. Microwave heating as a tool for sustainable chemistry. CRC press Taylor and Francis group. 2010.
16. Kremsner, J. M.; Stadler, A.; Kappe, C. O. The Scale-Up of microwave-Assisted Organic Synthesis. *Top Curr Chem*. **2006**, *266*, 233.
17. Roberts, A. B.; Strauss, R. C. Towards rapid, 'green' predictable microwave-assisted synthesis. *Acc. Chem. Res.* **2005,** *38*, 653.
18. Chemat, F.; Esveld, E.; Poux, M.; Di-Martino, L. J. The role of selective heating in the microwave activation of heterogeneous catalysis reactions using a continuous microwave reactor. *J. microwave power EE.* **1998,** *33,* 88.
19. Patil, N. G.; Rebrov, E. V.; Esveld, E.; Eränen, K.; Benaskar, F.; Meuldijk, J.; Mikkola, J. -P.; Hessel, V.; Hulshof, L. A.; Murzin, D.Y.; Schouten, J. C. Effect of the load size on the efficiency of microwave heating under stop flow and continuous flow conditions. *J. of Microwave Power EE*. 2012, *accepted*.
20. Comer E.; Organ, M. G. A Microcapillary System for Simultaneous, Parallel Microwave-Assisted Synthesis, *Chem. Eur. J.* **2005**, *11*, 7223.
21. Patil, N. G.; Benaskar, F.; Rebrov, E. V.; Meuldijk, J.; Hulshof, L. A.; Hessel, V.; Schouten, J. C. Continuous multi-tubular milli-reactor with a Cu thin film for microwave assisted fine chemical synthesis. *Ind. Eng. Chem. Res.* **2012**, *submitted / in press.*
22. Matsuzawa, M.; Togashi, S.; Hasebe, S.; Basic Examination of a Pilot Plant for Continuous Flow Microwave-Assisted Chemical Reaction Combined with Microreactors. *J. Thermal Sci. Tech*. **2011,** *6*, 69.
23. Strauss, C. R. On Scale Up of Organic Reactions in Closed Vessel Microwave Systems. Org. Process Res. Dev. **2009,** *13,* 915.

8

Conclusions and outlook

8.1 Conclusions

This thesis describes the generic chemical engineering aspects of microwave assisted continuous-flow production of fine chemicals in milli-tubular reactors. Process intensification by using microwave heating was investigated for the enhancement of productivity as compared to conventionally heated reactor systems applied nowadays. The role of microwaves as either a volumetric or a selective heating source was, therefore, exploited. A microwave setup and a continuously-operated milli reactor-heat exchanger combination were designed and built to demonstrate that efficient, controlled, uniform, and sustainable production of fine chemicals at kilogram/day scales is feasible.

In a stepwise approach, state-of-the-art multi- and mono-mode microwave cavities were tested for efficient and uniform heating of process streams. Applying monomode microwave cavities proved to be essentially superior to multimode cavities by providing better heating efficiencies. Additionally, the heating rate and the heating efficiency showed dependence either on the position and/or the geometry of the sample, *i.e.* reaction mixture. State-of-the-art microwave cavities also lacked in providing important functionalities, such as a predictable electric field pattern, tuning capacity, detailed energy distribution and possibilities for a modular scale-up. These shortcomings and the requirements of a continuous operation resulted in the specific design of a monomode microwave setup (Figure 9, chapter 2). The realized microwave setup allowed proper formulation of

complete energy balances with efficient and uniform heating as well as a modular scale-up, thus resolving the aforementioned handicaps.

The effect of the load diameter and the loss tangent ($tan\,\delta$) on the heating efficiency of the liquid medium (*i.e.* solvent) was determined in a monomode microwave cavity under stop-flow (*i.e.* stagnant liquid) and continuous-flow conditions. Under stop-flow conditions, the highest heating efficiency (70 %) was observed at the load diameter equal to and above the half wavelength of the electromagnetic field in the liquid medium. It decreased at higher temperatures due to a decreasing heating rate and a monotonous drop in loss tangent with increasing temperature. The heating efficiency at continuous-flow conditions increased linearly with the load diameter. However, microwave leakage above the propagation diameter (also known as half wavelength) restricted the highest load diameters usable in continuous operation.

Based on these findings, a milli reactor-heat exchanger was developed for energy efficient and controlled continuous operation under microwave heating. The reactor was particularly designed with a focus on using microwave heating as a volumetric heating source, *i.e.* bulk liquid heating. Gratifyingly, co-current flow of a microwave transparent solvent (coolant) permitted heat integration, resulting in extended reactor lengths and high heating efficiencies (96 %). The temperature of the reaction mixture went through a maximum (hot spot) in the microwave cavity part of the reactor. The temperature of the hot spot was limited by convective heat-transfer to the coolant.

Detailed modeling study with coupled electromagnetic and hydrodynamic phenomena in the reactor-heat exchanger showed that the stagnancy in the flow of the microwave absorbing fluid (reactant) resulted in a temperature distribution. The stagnant layer formation caused either by any insertion of system components (such as fiber optic sensors) or at the reactor walls, yielded higher temperatures and lower microwave energy dissipation regions. The coolant flow, unless used as a heated jacket to minimize heat losses, was found to be ineffective in controlling final (outlet) temperatures of the reactant. Additionally, a buoyancy effect (as a result of

gravitational forces) was visible for a horizontal arrangement of the reactor-heat exchanger assembly at millimeter sizes.

Subsequently, process intensification by selective heating of a structured catalyst was demonstrated in a Cu-thin film coated multi-tubular milli-reactor/heat exchanger (MTMR, Figure 1, chapter 6). The Cu film played a dual role by providing uniform microwave absorption and improving the production rate. Extraction of excessive heat by counter-current flow of a microwave transparent coolant (toluene) reduced copper leaching and improved the steady performance of the coated reactor tubes. The temperature of the copper surface in the reactor tubes was found to be at least 100 K higher than the bulk temperature of the reaction mixture. The temperature deviation in the multiple reactor tubes of the MTMR in terms of the kinetically determined reaction temperature was not more than 8.0 ± 0.5 K. The obtained throughput in the MTMR (6 parallel tubes) was slightly lower (93 %) than expected as a result of minor flow and temperature distributions. It was demonstrated that the numbering up approach by parallelization of multiple milli-reactor tubes can successfully be implemented in scaling up microwave assisted fine chemicals synthesis and commercially interesting production rates can be obtained.

Finally, a new concept of a modular scale-up for microwave assisted flow synthesis has been demonstrated. Transient operation through each cavity and utilization of cavities in series increased the production rate. Additionally, known kinetics allowed estimation of the production rate for each additional cavity in the series. Principally, independent tuning of each cavity to the process requirements without disturbing the microwave field pattern either in neighboring cavities or in the main waveguide permitted the modular scale-up. This approach of scale-up is possible at minimized grid to applicator losses by utilization of cavities in series over a main waveguide connected to single microwave generator.

Scale-up with each of the investigated numbering up approaches was successful. However, as an overall conclusion it is worthwhile to note that application of microwaves as a process intensification tool, especially in the case of organic synthesis, is more attractive for liquid-solid reactions, where the solid is the

selectively (microwave) heated catalyst. Targeting direct and selective heating of the catalytically active surface, *i.e.* the locus of the reaction, results in elevated reaction temperatures and, therefore, in high reaction rates with limited bulk liquid heating.

8.2 Outlook

For organic synthesis, intensifying application of microwaves is unquestionably at the locus of the reaction *i.e.* catalyst surface. Therefore, based on the results of the investigations reported in this thesis, the following activities are suggested to be considered in future research.

The influence of the catalyst film thickness on its sustainable use, also as a microwave absorbing component, is a key issue, particularly to ensure a long lifetime of wall coated reactor tubes in a multi-tubular reactor. Controlled utilization of arching in metal films/particles under microwave irradiation is interesting even in cases where use of metals is not necessary as catalyst (Kappe *et al. Chem. Open.* **2012,** *1,* 39.). Another important issue is the physical insight into microwave-metal interactions especially for liquid-solid reaction. Understanding and tuning of these interactions should help in improving the process performance and sustainability. Lastly, the extension of current work, *i.e.* selective heating of the catalyst, to more traditional supported catalytic systems, in particular of the transition metals which are abundantly used as catalysts in organic synthesis, can be explored for various organic reactions.

List of publications

Journal Publications

- Patil, N.G.; Benaskar, F.; Rebrov, E.V.; Meuldijk, J.; Hulshof, L.A.; Hessel, V.; Schouten, J.C. (2012). Microwave setup design for continuous fine-chemicals synthesis. *Chemical Engineering Technology*, submitted.
- Patil, N.G.; Esveld, D.C.; Benaskar, F.; Rebrov, E.V.; Meuldijk, J.; Hulshof, L.A.; Hessel, V.; Schouten, J.C. (2012). Microwave assisted flow synthesis: coupling of electromagnetic and hydrodynamic phenomena. *AIChE Journal: Chemical Engineering Research and Development*, submitted.
- Patil, N.G.; Benaskar, F.; Rebrov, E.V.; Meuldijk, J.; Hulshof, L.A.; Hessel, V.; Schouten, J.C. (2012). Scale up of microwave assisted flow synthesis by transient processing through cavities in series, *Organic Process Research & Development*, submitted.
- Benaskar, F.; Patil, N.G.; Engels, V.; Rebrov, E.; Meuldijk, J.; Hulshof, L.A.; Hessel, V.; Wheatley, A.E.H.; Schouten, J.C. (2012). Microwave-assisted Cu-catalysed Ullmann synthesis in a continuous-flow milli-plant. *Chemical Engineering Journal*, submitted.
- Benaskar, F.; Patil, N.G.; Rebrov, E.; Ben-Abdelmoumen, A.; Meuldijk, J.; Hulshof, L.A.; Hessel, V.; Schouten, J.C. (2012). Micro/milli-flow processing combined with selective catalyst microwave heating in the Cu-catalyzed Ullman etherification reactions: a micro^2-process.*ChemSusChem*, submitted.
- Patil, N.G.; Benaskar, F.; Rebrov, E.V.; Meuldijk, J.; Hulshof, L.A.; Hessel, V. & Schouten J.C. (2012). Continuous multi-tubular milli-reactor with a Cu thin film for microwave assisted fine-chemicals synthesis, *Industrial and Engineering Chemistry Research*, submitted.
- Patil, N.G.; Hermans, A.I.G.; Benaskar, F.; Rebrov, E.; Meuldijk, J.; Hulshof, L.A.; Hessel, V.; Schouten, J.C. (2011). Energy efficient and controlled flow processing under microwave heating by using a milli reactor-heat exchanger, *AIChE Journal: Chemical Engineering Research and Development*, DOI 10.1002/aic.13713.
- Patil, N.G.; Rebrov, E.V.; Eränen, K.; Benaskar, F.; Meuldijk, J.; Mikkola, J.-P.; Hessel, V.; Hulshof, L.A.; Murzin, D.Y.; Schouten, J.C. (2011). Effect of the load size on the efficiency of microwave heating under stop flow and continuous flow conditions, *Journal of Microwave Power and Electromagnetic Energy*, 46(2), 83-92.

- Benaskar, F.; Patil, N.G.; Engels, V.; Rebrov, E.V.; Meuldijk, J.; Hessel, V.; Hulshof, L.A.; Wheatley, A.E.H.; Schouten, J.C. (2012). A kinetic study on the Cu(0)-catalyzed Ullmann SnAr-type C-O coupling of potassium phenolate and 4-chloropyridine, *Dalton Transactions*, submitted.
- Benaskar, F.; Ben-Abdelmoumen, A.; Patil, N.G.; Rebrov, E.V.; Meuldijk, J.; Hessel, V.; Hulshof, L.A.; Krtschil, U.; Schouten, J.C. (2012). Cost analysis of a continuously operated fine chemicals production plant at 10 kg/day using a combination of microprocessing and microwave heating, *Journal of Flow Chemistry*, 1(2), 74-89.
- Benaskar, F.; Engels, V.; Rebrov, E.V.; Patil, N.G.; Meuldijk, J.; Thüne, P.C.; Magusin, P.C.M.M.; Mezari, B.; Hessel, V.; Hulshof, L.A.; Hensen, E.J.M.; Wheatley, A.E.H.; Schouten, J.C. (2012). Novel Cu-based catalysts supported on TiO_2 films for Ullmann SnAr-type C-O coupling reactions, *Chemistry - A European Journal*, 18, 1800-1810.
- Engels, V.; Benaskar, F.; Patil, N.G.; Rebrov, E.V.; Hessel, V.; Hulshof, L.A.; Jefferson, D.A.; Vekemans, J.A.J.M.; Karwal, S.; Schouten, J.C.; Wheatley, A.E.H. (2010). Cu-based nanoalloys in the base-free Ullmann heterocyle-aryl ether synthesis, *Organic Process Research & Development*, 14(3), 644-649.
- Benaskar, F.; Engels, V.; Patil, N.G.; Rebrov, E.V.; Meuldijk, J.; Hessel, V.; Hulshof, L.A.; Jefferson, D.A.; Schouten, J.C.; Wheatley, A.E.H. (2010). Copper(0) in the Ullmann heterocycle-aryl ether synthesis of 4-phenoxypyridine using multimode microwave heating, *Tetrahedron Letters*, 51(2), 248-251.
- Patil, N.G.; Roy, D.; Chaudhari, A.S.; and Chaudhari, R.V. (2007). Kinetics of reductive alkylation of *p*-phenylenediamine with methyl ethyl ketone using 3% Pt/Al_2O_3 catalyst in a slurry reactor, *Industrial and Engineering Chemistry Research*, 46 (10), 3243 -3254.

Patent

- Bruijn, R.; Schaaf, J. van der; Patil, N.G.; Schouten, J.C. (2010). Process for preparing monodispersed emulsions, Patent no WO2010031709 (A1).

Oral Presentations

- Patil, N.G.; Esveld, E.; Benaskar, F.; Rebrov, E.V.; Hulshof, L.A.; Meuldijk, J.; Hessel, V.; Schouten, J.C. (2012). Microwave assisted flow processing: Coupling of electromagnetic and hydrodynamic phenomena. *AICHE Annual meeting*, 28th Oct - 2nd Nov 2012, Pittsburgh, USA.

- Benaskar, F.; Rebrov, E.V.; Patil, N.G.; Meuldijk, J.; Hulshof, L.A.; Hessel, V.; Schouten, J.C. (2012). Process intensification in a microwave heated fine-chemical milli-plant at large scale operation. *22nd International Symposium on Chemical Reaction and Engineering (ISCRE-22),* 2-5 Sept 2012, Maastricht, Nederlands.
- Benaskar, F.; Patil, N.G.; Rebrov, E.V.; Meuldijk, J.; Hulshof, L.A.; Hessel, V.; Schouten, J.C. (2012). Micro-process technology combined with selective catalyst microwave heating in Cu-catalyzed reactions for fine-chemicals synthesis: a micro^2 process. *20th International Congress of Chemical and Process Engineering (CHISA 2012)*, 25-29 Aug 2012, Prague, Czech Republic.
- Patil, N.G.; Benaskar, F.; Meuldijk, J.; Rebrov, E.V.; Hulshof, L.A.; Hessel, V.; Schouten, J.C. (2012). Cu thin films for enhanced microwave assisted flow synthesis of fine chemicals at industrial scale. *Netherlands Catalysis and Chemistry Conference (NCCC XIII)*, 5-7 Mar 2012, Noordwijkerhout, Netherlands.
- Benaskar, F.; Rebrov, E.V.; Engels, V.; Patil, N.G.; Hessel, V.; Hulshof, L.A.; Meuldijk, J.; Wheatley, A.E.H.; Schouten, J.C.(2012). A novel continuous process for copper catalyzed Ullmann-type C-O coupling under microwave heating. *Microwave & Flow Chemistry Conference,* 28 Feb - 2 Mar 2012, Lanzarote, Spain.
- Patil, N.G.; Benaskar, F.; Rebrov, E.V.; Meuldijk, J.; Hulshof, L.A.; Hessel, V.; Schouten, J.C. (2012). Design of a continuous multi-tubular milli-reactor with a Cu thin film for microwave assisted fine-chemical synthesis at industrial scale. *12th International Conference on Microreaction Technology (IMRET-12),* 20 - 22 Feb 2012, Lyon, France.
- Patil, N.G.; Hermans, A.I.G.; Rebrov, E.V.; Meuldijk, J.; Hulshof, L.A.; Hessel, V.; Schouten, J.C. (2011). Efficient and controlled flow processing under microwave heating by using a milli reactor-heat exchanger. *Netherlands Process Technology symposium (NPS-11)*, 24-26 Oct 2011, Arnhem, Netherlands.
- Patil, N.G.; Hermans, A.I.G.; Rebrov, E.V.; Meuldijk, J.; Hulshof, L.A.; Hessel, V.; Schouten, J.C. (2011). Optimization of energy use for flow processing under microwave heating by using integrated reactor - heat exchanger. *European Process Intensification Conference*, 20-23 Jun 2011, Manchester, UK.
- Patil, N.G.; Rebrov, E.V.; Esveld, E.; Meuldijk, J.; Hessel, V.; Hulshof, L.A.; Schouten, J.C. (2009). Development of microwave heated micro-heat exchanger for continuous operations. *IMM Young Scientists Workshop*, 19-20 Nov 2009, Mainz, Germany.

Poster Presentations

- Patil, N.G.; Benaskar, F.; Rebrov, E.V.; Meuldijk, J.; Hulshof, L.A.; Hessel, V.; Schouten, J.C. (2012). Scale-up of microwave assisted flow processes for fine chemical synthesis. *22nd International Symposium on Chemical Reaction and Engineering (ISCRE 22)*, 2-5 Sept 2012, Maastricht, Netherlands.
- Patil, N.G.; Hermans, A.I.G.; Rebrov, E.V.; Benaskar, F.; Meuldijk, J.; Hulshof, L.A.; Hessel, V.; Schouten, J.C. (2012). Microwave heating in a continuous flow reactor heat exchanger. *Microwave & Flow Chemistry Conference*, 28 Feb - 2 Mar 2012, Lanzarote, Spain.
- Benaskar, F.; Ben-Abdelmoumen, A.; Patil, N.G.; Meuldijk, J.; Rebrov, E.V.; Hessel, V.; Hulshof, L.A.; Schouten, J.C.(2012). Process intensification using a microwave heated micro plant in the Ullmann type C-O coupling for production scale operation. *12th International Conference on Microreactor Technology (IMRET-12)*, 20 - 22 Feb 2012, Lyon, France.
- Patil, N.G.; Meuldijk, J.; Rebrov, E.V.; Hulshof, L.A.; Hessel, V.; Schouten, J.C. (2011). Microwave heating: An alternative to conventional heating in fine chemical synthesis. Simon Stevin Leering 2011, *STW annual congress*, 6th Oct 2011, Nieuwegein, Netherlands.
- Patil, N.G.; Rebrov, E.V.; Esveld, E.; Meuldijk, J.; Hessel, V.; Hulshof, L.A.; Schouten, J.C. (2010). Optimization of heating efficiency under Monomode microwave heating for organic synthesis in microchannel reactors. *Netherlands Process Technology symposium (NPS-10)*, 25-27 Oct 2010, Veldhoven, Netherlands.
- Patil, N.G.; Rebrov, E.V.; Esveld, E.; Meuldijk, J.; Hessel, V.; Hulshof, L.A.; Schouten, J.C. (2009). Development of a continuous-flow microwave-heated micro-heat exchanger. *Netherlands Process Technology Symposium (NPS-9)*, 26-28 Oct 2009, Veldhoven, Netherlands**.**

Acknowledgements

At last, I reached to a point where the dream appears to be fulfilling. Of course this dream of completing PhD could not have been achieved without the help of many people. Therefore, I would like to take this opportunity to express my gratitude to everybody who helped me during my doctoral candidature.

My first and foremost thanks go to Professor Jaap Schouten. Dear Jaap, thank you very much for giving me this opportunity. I remember, after reading the MEMFiCs proposal, first thing I said to you was “I don’t know anything about microwaves”. I must say you believed in me more than I did at that time. Jaap, I learned a perfectionist approach and professionalism from you during these four years. I am highly obliged to you for all the help.

I am deeply thankful to all my supervisors Professor Evgeny Rebrov, Professor Jan Meuldijk, Professor Bert Hulshof and Professor Volker Hessel.

Dear Evgeny, I had many fruitful discussions with you at the beginning of the project. According to me, they laid the foundation of my PhD work. I learned the trick of starting with quick and dirty for preliminary estimations from you. I thank you also for being available and involved even after moving to Belfast as a full professor.

Dear Jan, you took over the reins from Evgeny. Your supportive and caring nature helped me move comfortably over each and every trouble I encountered during the project. Your critical look at the results has certainly improved the quality of my thesis. I cannot imagine completing this thesis without our weekly meetings where you encouraged and guided me to be optimal in result production as well as in writing.

Dear Bert, thank you very much for your help during my PhD. The timely success of this project has to be credited to your constant check of everything during this project. I also enjoyed learning managerial skills from you.

Dear Volker, unfortunately we could not work more closely during my PhD due to your part-time work at TU/e and other responsibilities. Nevertheless, I am grateful for all prolific discussions we had, during the project and several progress meetings.

The work done during this project would not have been possible without the help of the technical staff of SCR. I deeply appreciate Anton, Carlo and Erik for their help in building the microwave setup and the safety measures around it. Erik, I really admire your attitude of careful listening and being available upon request. This has made the experimental stint during the PhD project extremely comfortable and easy going. The team of analytical experts

also played an important role during my experimental work. I remember, I could count on Peter, Marlies and Carlo for their help with the analysis. I would also like to thank Denise, for taking care of all the administrative responsibilities and solving all my bureaucratic troubles.

I take this opportunity to also thank Professor Dimitri Murzin, Abo Academy Turku, Erik Esveld, Wageningen UR, and Professor Andrzej Stankiewicz, Delft University of Technology for fruitful collaborations and permissions to work in their laboratories. I also want to acknowledge Bastiaan for his help to get me started with microwave flow synthesis and patiently answering my stupid questions at the beginning.

My stay at SCR was cheerful and fun-filled. I thank all the SCR PhD's for that. Thank you guys and lately (lot of) girls for the great time together during SCR events, borrels, and NPS late night parties. Faysal, it was fun working with you as PhD's in the MEMFiCs project, thanks for all your help. Lida, Serdar and Slavisa: I am thankful to you for bearing with me during the time we shared the office and the comfortable atmosphere in the office. Lida, I hope you will find listening and caring office mates like me and Serdar in future. Serdar, my friend, I hope you have found better doctors in Turkey and/or facing less physical troubles back home. Slavisa, I was busy trying to finish my thesis when you joined our office, so I think, we have spent very little relaxed time together in the office. Thank you for bearing with my quietness filled with typing noises.

Many people contributed in making my social life in Eindhoven a wonderful experience. I thank all my friends from the university, Eindhoven cricket club and supposedly called Eindhoven Marathi Mandal. I had a great time with you all.

Finally, I would like to thank my family for their support and confidence which has provided me courage to come to Europe and successfully accomplish the dream of getting doctorate. I thank my wife and my life, Snehal who has equally bared the philosophical burden of my PhD. I dedicate this thesis to my family especially to Snehal who has stood by me in my endeavors.

Narendra Patil

31st July 2012

About the Author

Narendra G. Patil was born on 8th August 1981 in Bhokane, India. He obtained his Bachelor's degree in Chemical Engineering in 2003 at Mumbai University, India. He worked as a research assistant from 2003 till 2006 in the department of Homogeneous Catalysis at the National Chemical Laboratory, Pune, India. This work focused on reaction kinetics, optimization and reactor modeling of three phase catalytic reactors. In 2006, he joined the MSc program in the department of Chemical Engineering and Chemistry (specialization Process Engineering) at the Eindhoven University of Technology (TU/e), the Netherlands. His master's thesis work was about the production of multiple emulsions in micro-channels. After completion of the MSc program (Cum Laude) in 2008, he started with his PhD project in the Laboratory of Chemical Reactor Engineering (SCR) of the Eindhoven University of Technology (TU/e) under the supervision of prof.dr.ir. J.C. Schouten, prof.dr. J. Meuldijk, prof.dr. L.A. Hulshof, and prof.dr. E.V. Rebrov. The goal of his PhD project was to design, develop, and validate an integrated microwave microreactor system for (fine) chemical production.